

VELOCities of CEpheids (VELOCE)

II. Systematic Search for Spectroscopic Binary Cepheids

Shreeya S. Shetye^{1,3*}, Giordano Viviani^{1**}, Richard I. Anderson^{1***}, Nami Mowlavi², Laurent Eyer², Nancy R. Evans⁴, and László Szabados⁵

¹ Institute of Physics, École Polytechnique Fédérale de Lausanne (EPFL), Observatoire de Sauverny, 1290 Versoix, Switzerland

² Département d'Astronomie, Université de Genève, Chemin Pegasi 51, 1290 Versoix, Switzerland

³ Instituut voor Sterrenkunde, KU Leuven, Celestijnenlaan 200D bus 2401, Leuven, 3001, Belgium

⁴ Smithsonian Astrophysical Observatory, MS 4, 60 Garden St., Cambridge, MA 02138, USA

⁵ Konkoly Observatory, HUN-REN Research Centre for Astronomy and Earth Sciences, MTA Centre of Excellence, Konkoly Thege Miklós út 15-17, H-1121 Budapest, Hungary

Received May 31, 2024; accepted date here

ABSTRACT

Classical Cepheids provide valuable insights into the evolution of stellar multiplicity among intermediate-mass stars. Here, we present a systematic investigation of single-lined spectroscopic binaries (SB1) based on high-precision velocities measured by the VELOCities of CEpheids (VELOCE) project. We detected 76 (29%) SB1 systems among the 258 Milky Way Cepheids in the first VELOCE data release, 32 (43%) of which were not previously known to be SB1 systems. We determined 30 precise and 3 tentative orbital solutions, 18 (53%) of which are reported for the first time. This large set of Cepheid orbits provides a detailed view of the eccentricity e and orbital period P_{orb} distribution among evolved intermediate-mass stars, ranging from $e \in [0.0, 0.8]$ and $P_{\text{orb}} \in [240, 9000]$ d. Orbital motion on timescales exceeding the 11 yr VELOCE baseline was investigated using a template fitting technique applied to literature data. Particularly interesting objects include a) R Cru, the Cepheid with the shortest orbital period in the Milky Way (240 d), b) ASAS J103158-5814.7, a short-period overtone Cepheid exhibiting time-dependent pulsation amplitudes as well as orbital motion, c) 17 triple systems with outer visual companions, among other interesting objects. Most VELOCE Cepheids (21/23) that exhibit evidence for a companion based on *Gaia* proper motion anomaly are also spectroscopic binaries, whereas the remaining do not exhibit significant ($> 3\sigma$) orbital RV variations. *Gaia* quality flags, notably the Renormalized Unit Weight Error (RUWE), do not allow to reliably identify Cepheid binaries, although statistically the average RUWE of SB1 Cepheids is slightly higher than that of non-SB1 Cepheids. Comparison with *Gaia* photometric amplitudes in G -, Bp , and Rp also does not allow to identify spectroscopic binaries among the full VELOCE sample, indicating that the photometric amplitudes in this wavelength range are not sufficiently informative of companion stars.

Key words. Stars: variables: Cepheids – binaries: visual – Stars: oscillations – distance scale

1. Introduction

Classical Cepheids (henceforth: Cepheids) are evolved, luminous, intermediate-mass ($\sim 3 - 11 M_{\odot}$), radially pulsating stars. For more than a century, Cepheids have been crucial calibrators of the extragalactic distance scale (Hertzsprung 1913) thanks to the famous period-luminosity relation (PLR or Leavitt Law, Leavitt & Pickering 1912). The unceasing interest in Cepheids is not only due to their cosmological relevance, but also because these are crucial populations to understand stellar physics and are important tracers in galactic studies (Luck & Lambert 2011; Genovali et al. 2014; Poggio et al. 2021; Kovtyukh et al. 2022, and references therein).

Given the importance of Cepheids as distance tracers, many astrophysical effects have been explored as potential biases of the Leavitt law, including multiplicity (e.g.

Mochejska et al. 2000; Kiss & Bedding 2005). For certain individual Cepheids, light contributed by companions can indeed affect distance estimates, the most extreme cases of this kind include V1334 Cyg in the Milky Way (Gallenne et al. 2018) and a sample of Cepheids with double-lined spectroscopic companions in the Large Magellanic Cloud (Pilecki et al. 2021, which are indeed selected using their Leavitt law outlier nature). However, Anderson & Riess (2018) showed that statistically speaking, Cepheid companions cannot bias the extragalactic distance scale or the Hubble constant measured therefrom. A similar result was recently obtained using population synthesis (Karczmarek et al. 2022). However, orbital motion on timescales of up to several years may affect the accuracy of parallax measurements of Cepheids (Anderson et al. 2015, 2016a; Benedict et al. 2022).

Parallaxes of Cepheids provided by the third data release (DR3) of the ESA mission *Gaia* do not yet account for orbital motion due to companions. However, this is expected to be available in future data releases, and DR3

* e-mail: shreeya.shetye@kuleuven.be

** e-mail: giordano.viviani@epfl.ch

*** e-mail: richard.anderson@epfl.ch

already provided a large number of non-variable stars with non-single star solutions (Gaia Collaboration et al. 2022). Combining astrometric and radial velocity data to determine orbits is particularly useful because it allows to measure the total mass of a system (e.g. Gallenne et al. 2019) and thus provides key information for constraining stellar models in the context of the mass discrepancy problem (e.g. Caputo et al. 2005; Anderson et al. 2016c).

In the past few decades, numerous complementary techniques are used for the detection of Cepheid binarity/multiplicity. Direct spectroscopic identification of low-mass companions at any separation is possible using X-ray and ultraviolet (UV) observations (Evans 1992; Evans et al. 2013, 2022). The detection of orbital motion through radial velocity (RV) variations is effective to a wide range of companion masses and spectral types, however, it necessitates long temporal baselines (Evans et al. 2015; Anderson et al. 2016a). Conversely, photometric binary detection methods, such as those using photometric amplitudes (Coulson & Caldwell 1985; Klagyivik & Szabados 2009) or photometric colors and ratios of amplitudes of different colors (Gieren 1985), require confirmation of the binary detection through subsequent spectroscopic investigations. Cepheid companions can also be detected using optical long-baseline interferometry, if the contrast and angular separation between the Cepheid and its companion are sufficiently small (Gallenne et al. 2014a, 2015, 2016, 2019).

Gaia proper motions have been introduced as indicators of multiplicity (Kervella et al. 2019a,b, 2022). While proper motion analysis is a powerful tool to detect resolved companions, it cannot be applied to the brightest stars that saturate the *Gaia* detectors. Furthermore, *Gaia* astrometric quality flags like the reduced χ^2 statistic are used as indicators of binarity assuming that the orbital motion leads to a photocentre wobble (Belokurov et al. 2020; Stassun & Torres 2021). In fact, several cuts on *Gaia* quality flags like the RUWE and astrometric excess noise have been defined to filter the potentially multiple systems (Gaia Collaboration et al. 2022). However, these cuts are established using stars where astrometric processing is simpler than in high-amplitude chromatically variable stars, such as classical Cepheids. It remains unclear if the same cuts can be applied to Cepheids, which are brighter than most stars used for calibrating *Gaia* systematics (cf. Khan et al. (2023) and references therein), and whose variability can cause excess noise in astrometric measurements.

The traditional approach of RV variations provides an unambiguous detection of a binary companion and helps constrain the orbital parameters. Dedicated RV monitoring campaigns have unraveled the orbital elements distribution of Cepheids (e.g., Evans et al. 2015; Szabados 2003). Low-mass companions such as the one of δ Cep (Anderson et al. 2015) or companions of fainter Cepheids ($m_V > 8$ mag) require significant observational effort and precision to be detected, and this can only be achieved by long-term RV monitoring.

The VELOCities of CEpheids (VELOCE) project provides unprecedented RV time series of classical Cepheids (Anderson et al. (2024); Paper I henceforth). Taking advantage of the 11-year baseline of VELOCE, here we report the results of a systematic study of single-lined spectroscopic binaries (SB1). Where the data allow it, we provide estimates of orbital periods, or describe the orbital motion using different methods. The paper is structured as follows. The observa-

tions and data analysis are presented in Section 2, in Section 3 we describe the different methods we used to analyze the SB1 Cepheids, followed by results in Section 4, which is divided into sub-sections for results from each method used to describe the binary. In Section 5, we present the correlation between derived orbital parameters and compare our results with the *Gaia* binarity indicators. We briefly discuss and summarize this work in Section 6. The RV data as well as any fitted models, including orbital solutions and polynomial trends, used here are made publicly available as part of Paper I. In the Appendix, we have presented supporting figures (Sections A, B, C, E) and tables (Sections D, F).

2. Sample selection and available data

VELOCE comprises of precise Cepheid RV time-series data collected from both hemispheres using the high-resolution spectrographs *Coralie* (Queloz et al. 2001) and *Hermes* (Raskin et al. 2011). We used a minimum of 30 RV measurements per star, extending to up to 300 RV measurements for some cases. These observations cover a temporal baseline of nearly eleven years. Most of the VELOCE observations targeted signal-to-noise ratios (SNRs) of at least 20, more commonly between 25 to 30, per pixel near 5500 Å. With such SNR we have typical RV uncertainties in the order of 50 ms⁻¹. A detailed description of the observations and the RV data can be found in Paper I.

We identify SB1 candidates from 258 classical Cepheids observed by the VELOCE project (cf. Paper I for details) via time-variable pulsation-averaged velocities, v_γ . Orbital motion in Cepheids introduces Doppler shifts on timescales of typically one year or longer that are mostly well separated from the pulsational timescales (of order days to months). Using VELOCE data, orbital motion can be detected in several different ways, depending on the availability and quality of the measurements (Section 3). The cleanest examples in our sample are Cepheids where clear, and possibly repeating, variations of v_γ are discernible by eye in the pulsation (Fourier series) fit residuals. Such cases generally have orbital semi-amplitudes of several km s⁻¹ and orbital periods of ≤ 3 yr.

While the selection function of Cepheids in VELOCE is rather complex, cf. Paper I, we consider VELOCE neither particularly biased towards the detection of SB1 systems, nor against it. For example, VELOCE initially specifically targeted Cepheids with no prior RV information and Cepheids residing near star clusters (Anderson et al. 2013). Later, Cepheids bright and nearby enough to measure interferometric radii were added (e.g. Anderson et al. 2016b; Breiterfeldt et al. 2016), and long-period Cepheids were targeted specifically for their use in distance ladder calibration (Anderson et al. 2016a). VELOCE also followed Cepheids with the goal of detecting modulated variability (e.g. Anderson 2014, 2016, 2019, 2020). Of course, stars found to exhibit orbital motion were followed up with the goal of characterizing orbits. However, only few stars were added to specifically search for suspected orbital signals.

Table 1 contains the list of stars considered in the present paper, ordered by whether their nature as spectroscopic binary was first reported here, was previously discussed in the literature. In Figure 1, we present the on-sky distribution of the sample SB1 Cepheids and the range in *Gaia* *G* mag that they span.

Table 1: Sample of binary Cepheids and candidates from the literature considered here.

Cepheid	<i>Gaia</i> DR3 source ID	$\langle m_V \rangle$ (mag)	<i>Gaia</i> (m_G) (mag)	P_{puls} (d)	Status	References	Evidence	Triple?
Newly discovered spectroscopic binary Cepheids								
AQ Pup	5597379741549105280	8.54	8.32	30.1965	Susp	R1	Trend	Y
ASAS J064540+0330.4				3.0147	New		Orbit	Y
ASAS J064553+1003.8	3350719221309022720	10.78	10.44	2.6801	New		Trend	
ASAS J084951–4627.2	5329675052782690944	11.03	10.85	3.7889	New		Orbit	
ASAS J100814–5856.6	5258280842214814336	11.48	11.40	3.7665	New		Orbit	
ASAS J103158–5814.7	5351436724362450304	11.06	11.08	1.1192	New		Trend	
ASAS J155847–5341.8	5980814424369504256	9.99	9.45	2.8075	New		Trend	
ASAS J174108–2328.5	4116471792510901248	9.55	8.86	3.7797	New		Trend	
ASAS J174603–3528.1	4041107790775862272	10.94	10.31	2.5724	New		Orbit	
β Dor	4757601523650165120	3.76	3.59	9.8427	New		RVTF-Yes	
DR Vel	5313887130948758016	9.25	8.94	11.1995	New		Trend	
FO Car	5241780677399802624	10.96	10.35	10.3569	New		Orbit	Y
GX Car	5257664497238811776	9.42	9.09	7.1969	New		Orbit	
IT Car	5337191279937200256	7.9	7.82	7.5330	New		Orbit	
MY Pup	5506374096132016512	5.65	5.47	5.6941	New		Orbit	
NT Pup	5537860123428416640		11.56	15.5603	New		Orbit	
OX Cam	473293889810320128	10.81	10.06	5.0655	New		Trend	
RY Sco	4041690364529590144	7.51	7.49	20.3267	New		Trend	Y
RY Vel	5355057622307185280	7.86	7.88	28.1742	New		Trend	
SX Vel	5329838158460391296	8.33	8.12	9.5507	New		Trend	
SZ Aql	4267549637851481344	7.92	8.20	17.1409	New		RVTF-Yes	
V0391 Nor	5881995546318024704	8.99	8.66	4.3733	New		Trend	
V0402 Cyg	2060021625508894592	9.87	9.52	4.3649	New		RVTF-Yes	Y
V0407 Cas	2012787293154800896		11.47	4.5661	New		Orbit	Y
V0492 Cyg	2058874388200159872		11.56	7.5780	New		Trend	
V0659 Cen	5868451040512196224	6.49	6.47	5.6240	Susp	R2	Orbit	Y
V0827 Cas	430814876547869440	11.57	10.74	3.1986	New		Trend	Y
V1162 Aql	4190143160245024256	7.81	7.59	5.3762	New		Trend	
V1803 Aql	4319018739208020096	10.35	9.39	8.6281	New		Trend	
V2475 Cyg	2055881689337758336		11.41	11.5557	New		Trend	
VZ Pup	5600052040150252800	10.15	9.34	23.1743	New		Orbit	
X Cyg	1870258975238302208	6.47	6.20	16.3866	New		RVTF-Yes	
First orbital solutions for literature SB1 Cepheids								
BP Cir	5877460679352962048	7.52	7.33	2.3981	Known	R4	Orbit	
FN Vel	5307761545524640256	10.25	9.85	5.3242	Known	VELOCE, R5, R6	Orbit	
MU Cep	2200018111723748224	12.3	11.64	3.7678	Known	VELOCE, R6	Orbit	
R Cru	6054935874795049216	6.42	6.58	5.8257	Known	R7	Orbit	
R Mus	5855468247702904704	6.33	6.23	7.5103	Known	R3	Orbit	
VY Per	459035766618689280	11.32	10.47	5.5319	Known	R24	Orbit	
Literature SB1 confirmed by VELOCE								
α UMi		2.02		3.9720	Known	VELOCE, R32	Orbit ¹	
AD Pup	5614312705966204288	9.99	9.63	13.5976	Susp	R9	Trend	
AH Vel	5519380081746387328	5.76	5.59	4.2272	Known	R3	Trend	
AQ Car	5254662177677566464	8.84	8.64	9.7696	Susp	VELOCE, R10	Trend	
AW Per	174489098011145216	7.51	7.09	6.4638	Known	R11	Trend	Y
AX Cir	5873984023533350400	5.96	5.66	5.2734	Known	R4	Orbit	
CD Cyg	2058374144759464064	8.35	8.59	17.0762	Known	VELOCE, R10	RVTF-Yes	
δ Cep	2200153454733285248	3.75	3.85	5.3663	Known	VELOCE, R12	Orbit	
DL Cas	428620663657823232	8.63	8.58	8.0009	Known	R13, R14	Orbit	
η Aql	4240272953377646592	3.8	3.75	7.1768	Known	R15	RVTF-Yes	
FF Aql	4514145288240593408	5.38	5.17	4.4710	Known	R16	Orbit	Y
FR Car	5337764640889249536	9.64	9.33	10.7169	Known	R17	Trend	
KN Cen	5864135319959353600	9.86	9.24	34.0273	Known	VELOCE, R10	Trend	
LR TrA	5824226655600824704	7.8	7.59	2.4283	Known	R7	Trend	
RS Ori	3368698813404804352	8.42	8.19	7.5669	Known	R18	RVTF-Yes	
RV Sco	6026412893938675712	6.61	6.77	6.0613	Susp	R19	Trend	Y
RW Cam	473043922712140928	8.72	8.23	16.4157	Known	R2	Trend	
RX Aur	200708636406382720	7.62	7.36	11.6248	Known	R20	Trend	
S Mus	5855852527008107008	8.33	5.88	9.6600	Known	R16	Orbit	
S Sge	1820309639468685824	5.36	5.46	8.3821	Known	R20	Orbit	Y
SS CMa	5616601820448126336	9.84	9.56	12.3525	Known	VELOCE, R10	RVTF-Yes	
SU Cyg	2031776202613700480	6.44	6.80	3.8458	Known	R21	Orbit	
SY Nor	5884729035255064064	9.77	9.04	12.6452	Known	R2, R14	Orbit	
SZ Cyg	2071433765909167232	9.37	8.95	15.1096	Known	VELOCE, R10	RVTF-Yes	
T Mon	3324535073449061504	5.98	6.12	27.0355	Known	R13, R20	Trend	
TX Mon	3106349738382214144	10.67	10.60	8.7021	Known	R8	Orbit	

Continued on next page

¹ We refer the reader to [Anderson \(2019\)](#) for the detailed orbital solution of α UMi using VELOCE data.

Table 1 – Continued from previous page

Cepheid	<i>Gaia</i> DR3 source ID	$\langle m_V \rangle$ (mag)	<i>Gaia</i> $\langle m_G \rangle$ (mag)	P_{puls} (d)	Status	References	Evidence	Triple?
U Vul	1825621002188696448	7.16	6.70	7.9907	Known	R17	Orbit	
UX Per	506699870563323264	11.26	11.41	4.5657	Known	R8	Trend	Y
UZ Sct	4104869264724284544	10.91	10.36	14.7475	Susp	R22	Trend	Y
V0340 Ara	5937099633141128448	10.03	9.74	20.8155	Known	R7	RVTF-Yes	
V0916 Aql	4313179507891570304	10.86	10.06	13.4436	Known	R33	RVTF-Yes	
V1334 Cyg	1964855904803120640	5.88	5.72	3.3325	Known	R23	Orbit	Y
VY Sgr	4094007532908816896	11.36	10.50	13.5585	Known	R22	RVTF-Yes	
W Sgr	4050309195613114624	4.69	4.59	7.5951	Known	R16	Orbit	Y
XX Cen	5871922507947292032	7.3	7.62	10.9520	Known	R13	Orbit	
XZ Car	5338036117182452096	8.67	8.31	16.6521	Susp	VELOCE, R10	Trend	
YZ Car	5255254711361371520	8.24	8.39	18.1696	Known	R10, R16	Orbit	
Z Lac	2007201567928631296	8.57	8.19	10.8859	Known	R13	Orbit	Y
Literature SB1 not confirmed by VELOCE								
AA Gem	3430067092837622272	9.91	9.39	11.3037	Known	R8	RVTF-No	
AN Aur	201574982848108416	10.21	10.01	10.2885	Known	R25	RVTF-No	
AV Sgr	4069645924308096512	11.49	10.24	15.3294	Known	R17	RVTF-No	
BB Sgr	4085919765884068736	6.69	6.58	6.6371	Susp	R26	RVTF-No	
BG Cru	6058439910929477120	5.53	5.27	3.3425	Known	R7	RVTF-No	
BG Vel	5324034867356093056	7.69	7.22	6.9239	Susp	VELOCE, R31	RVTF-No	
CS Ori	3330259852538068608	11.29	11.26	3.8891	Known	R8	RVTF-No	
FN Aql	4269036830424588800	7.96	8.01	9.4814	Known	R27	RVTF-No	
RT Aur	3435571660360952704	5.55	5.34	3.7284	Susp	R28	RVTF-No	
RU Sct	4258436301367796480	8.82	8.71	19.7076	Known	R17	RVTF-No	
RZ Vel	5523162573544337408	7.26	6.85	20.4020	Known	VELOCE, R31	RVTF-No	
S Nor	5835124087174043136	6.49	6.18	9.7547	Known	R1	RVTF-No	
SV Per	203496585576324224	8.86	8.70	11.1294	Known	R2	RVTF-No	
TY Sct	4256744187345732224	11	9.90	11.0538	Known	R22	RVTF-No	
TZ Mon	3112475495616980992		10.51	7.4282	Known	R17	RVTF-No	
U Sgr	4092905375639902464	6.68	6.43	6.7453	Known	R14	RVTF-No	
VW Cen	5864955727424819200	10.36	9.85	15.0368	Known	R17	RVTF-No	
VY Car	5351161399793209984	6.87	7.34	18.8824	Susp	VELOCE, R10	RVTF-No	
WZ Sgr	4094784475310672128	7.45	7.68	21.8494	Known	R30	RVTF-No	
X Lac	2004036486267748352	8.42	8.12	5.4454	Known	R20	RVTF-No	
X Pup	5620098679741674496	8.46	8.35	25.9697	Susp	VELOCE, R10	RVTF-No	
XX Aur	5238808628736339584	9.42	9.08	15.7052	Known	R30	RVTF-No	
YZ Aur	188724234539584256	10.24	9.88	18.1943	Known	R8	RVTF-No	
YZ Sgr	4099189015819292800	7.02	7.01	9.5539	Known	R17	RVTF-No	

Notes. Identifiers and magnitudes were compiled from SIMBAD, *Gaia* mean G-band magnitudes from the *Gaia* archive, and pulsation periods from Paper I. Column ‘Status’ indicates whether a star’s SB1 nature was newly discovered (‘New’), or previously known or suspected (‘Known’ or ‘Susp’). Stars listed as ‘Susp’ among newly discovered SB1 systems were considered tentative previously. References to previous studies are abbreviated using alphanumeric codes as follows. R1: Evans & Udalski (1994), R2: Evans (1994), R3: Lloyd Evans (1982), R4: Petterson et al. (2004), R5: Kovtyukh et al. (2015), R6: Anderson (2013), R7: Szabados (2003), R8: Szabados & Pont (1998), R9: Szabados et al. (2013b), R10: Anderson et al. (2016a), R11: Griffin (2016), R12: Anderson et al. (2015), R13: Evans (1995), R14: Bersier et al. (1994), R15: Evans (1991), R16: Gallenne et al. (2019), R17: Szabados (1996), R18: Evans et al. (1990), R19: Evans (1992), R20: Gorynya et al. (1996a), R21: Wahlgren & Evans (1998), R22: Pont et al. (1994), R23: Gallenne et al. (2013), R24: Szabados (1992), R25: Madore (1977), R26: Gieren (1982), R27: Szabados et al. (2014), R28: Turner et al. (2007), R29: Russo et al. (1981), R30: Bersier (2002), R31: Szabados et al. (2013a), R32: Anderson (2019), R33: Gorynya et al. (1996b). The stars with ‘VELOCE’ in the ‘References’ column are cases where VELOCE data was previously used to establish the binarity or the orbit. Column ‘Evidence’ states whether we determine a combined model for orbit and pulsation (‘Orbit’), determine a trend in the pulsation residuals (‘Trend’), or whether template fitting involving literature RV data indicates a time-variable v_γ (‘RVTF-Yes’) or not (‘RVTF-No’). The last column ‘Triple?’ indicates whether the star is likely part of a triple system, usually involving a visually resolved companion.

3. Data treatment/Methods

3.1. RV curve models adopted

In most Cepheids, the RV variability due to pulsation dominates the RV time series with pulsational peak-to-peak amplitudes typically ranging from $20 - 70 \text{ km s}^{-1}$. It is customary to model the pulsational variability using a Fourier series with a number of harmonics adapted to match the complexity of the RV variability. Paper I describes this process for all Cepheid RV curves in VELOCE. In short, the RV signal due to pulsation is modeled as:

$$v_r(t) = v_\gamma + \sum_n a_n \cos(2n\pi\phi) + b_n \sin(2n\pi\phi), \quad (1)$$

where n represents the order of the harmonic, t is time (in heliocentric Julian Date) and $\phi = (t - E)/P_{\text{puls}}$ is the pulsation phase with epoch² E and the pulsation period, P_{puls} . As described in Paper I, the optimal model is determined by fitting each RV time series using up to 20 Fourier harmonics and then performing model comparisons using the F-test and the Bayesian Information Criterion (BIC).

The key evidence for the spectroscopic binary nature presented here is a long-term modulation of $v_\gamma = v_\gamma(t)$, typically on timescales $> 1 \text{ yr}$ and much longer than the pulsation period. We thus identify binaries by the correlated fit residuals they produce (Eq. 1). Orbital motion is then either modeled using a Keplerian orbit or approximated via linear, quadratic, or even higher order polynomials if the orbit is not sufficiently sampled to determine the full orbital solution.

As noted by Anderson (2014), Cepheids can exhibit modulated RV curves that can be misinterpreted as showing evidence of orbital motion. We note that all targets discussed here are bona fide spectroscopic binaries as identified by the absence of modulated line shape variability (Anderson 2016), although a few of the binaries presented here also show additionally modulated spectral variability. A detailed description of modulated RV variability of VELOCE Cepheids will be presented in future work.

3.2. Keplerian fitting

In the case of spectroscopic binaries, $v_\gamma = v_\gamma(t)$ in Eq. 1 varies with time. The degree to which such variation can be used to infer the orbital elements depends largely on the sampling, baseline, and precision. Depending on these factors, we employed two methods for fitting Keplerian orbits to the data.

When fitting pulsational variability and orbital motion simultaneously, we fitted the Fourier series (Eq. 1) and a Keplerian model simultaneously using the non-linear least squares routine `leastsq` available in `scipy.optimize` (Virtanen et al. 2020). Following e.g. Hilditch (2001), the orbital motion is represented as:

$$v_\gamma(t) = v_{\gamma,0} + K [\cos(\omega + \theta) + e \cos \omega], \quad (2)$$

where ω denotes argument of periastron, K semi-amplitude (in km s^{-1}), e eccentricity, θ true anomaly, and $v_{\gamma,0}$ the systemic RV relative to the solar system barycenter. We note

² Defined for all VELOCE stars such that $\phi = 0$ coincides with v_γ on the steeper descending branch of the RV curve close to the mean observing date.

that v_γ (without subscript 0) refers to the pulsation averaged velocity (cf. Paper I), which coincides with $v_{\gamma,0}$ if an orbital solution is determined or if the star does not have a companion. The uncertainties on the parameters are determined using the covariance matrix returned by the fitting routine, which incorporates statistical information on the reliability of the parameters estimated. Two examples of combined Fourier series plus Keplerian orbits for classical Cepheids are illustrated in Figures 2 and 3.

To understand and mitigate any dependence of our results on starting values, as well as to avoid convergence to a local minimum, we also implemented a Markov Chain Monte Carlo (MCMC) method for determining Keplerian orbits. The MCMC fits further allow to explore the posterior distribution of the orbital parameters to identify possible correlations and to rigorously quantify uncertainties (e.g. Ford 2005, 2006). However, we have not yet implemented an MCMC fit to simultaneously model pulsational and orbital variations; this is foreseen for future work. Thus, all MCMC orbital solutions presented here use template fitting residuals of VELOCE (c.f. Section 5.1 of Paper I for more details) as well as literature radial velocity data, where pulsational variability has been removed (cf. Section 3.4). The MCMC orbits presented in this work utilize an extended baseline, achieved through the combination of VELOCE with literature datasets (V+L).

After testing different orbital parameterizations, we found that the following implementation converged the fastest (cf. also Fulton et al. 2018):

$$\mathbf{x} = (v_{\gamma,0}, \ln P_{\text{orb}}, \ln K, e, \omega, \phi_0) \quad (3)$$

where ϕ_0 is the orbital phase to the next pericenter passage at $t = E$. We opted for a uniform prior for all parameters, and set sharp boundaries far away from possible solutions so that they would not alter the posterior distribution. Initial guesses were obtained by computing the Maximum A Posteriori (MAP)³ probability estimates from a grid of starting values of the parameters. The resulting orbits allowed us to visualize the possible different sets of parameters that could explain our data and have a sense of the stability of each solution by counting how many grid points converged to the same orbital parameters. We then chose the best parameters as the initial guess for our MCMC (an example of MCMC orbital fitting is provided in Figure 4).

We used the MCMC implementation provided by the python package `emcee` (Foreman-Mackey et al. 2013) and, as suggested by the authors, used the autocorrelation time, τ_{ACT} , to determine whether the chain was sufficiently long. In particular, the convergence criterion consisted of the following inequalities:

$$\langle \tau_{ACT} \rangle < N_{\text{iteration}}/60 \quad (4)$$

$$\frac{\Delta \tau_{ACT}}{\tau_{ACT}} < 0.01 \quad (5)$$

After running the MCMC, we visually inspected the resulting posterior distributions to check the absence of significantly non-gaussian distributions (Figure 5). We also verified that the mean and standard deviation were compatible

³ In the case of uniform priors, the MAP method coincides with the more known Maximum Likelihood Estimate (MLE) method.

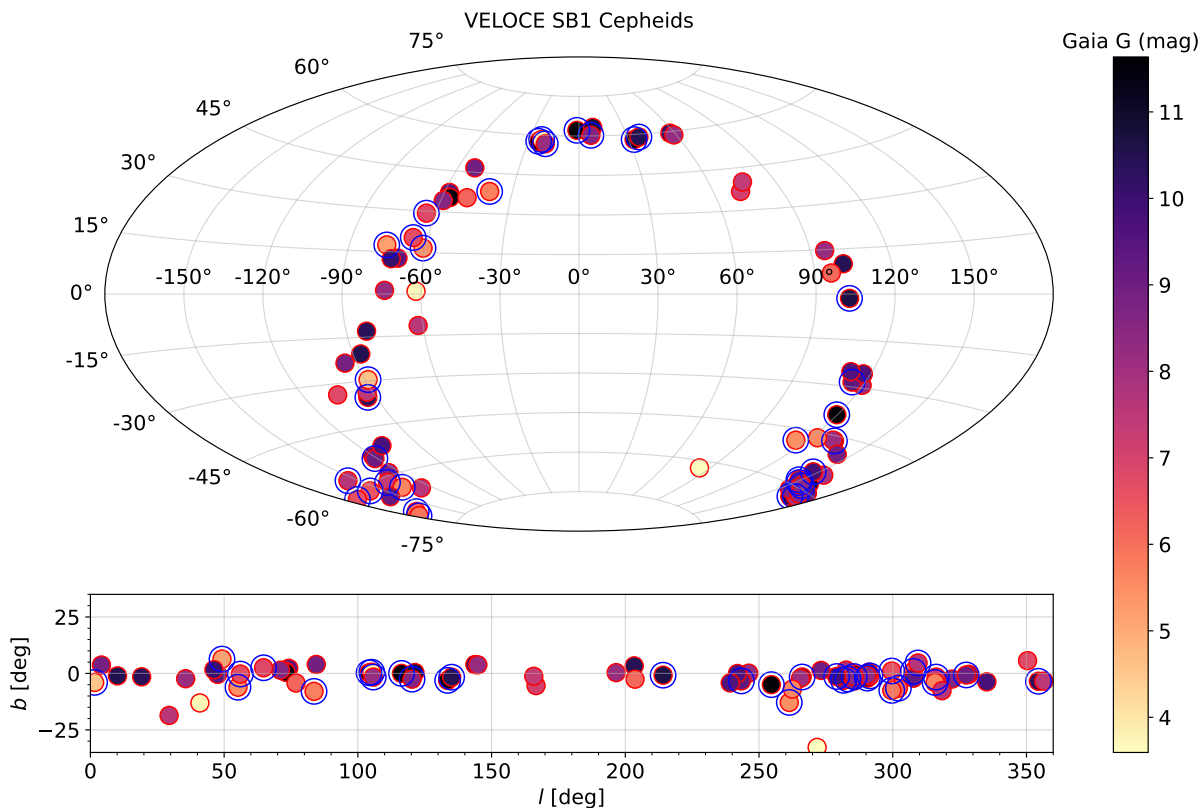


Fig. 1: Location of the sample SB1 Cepheids on the sky in equatorial (Top panel) and in galactic (Bottom panel) coordinate system. The symbols are color coded in the *Gaia* G magnitude. The symbols surrounded with blue circles are systems for which we provide an orbital solution in the current work.

with the 16th, 50th, and 84th percentiles. We use the mean and standard deviation as the final results for the orbital estimates and its uncertainties. Finally, we also investigated circular orbits in a few cases where e was either very small or not significantly detected. In this case:

$$\mathbf{x} = (v_{\gamma,0}, \ln P_{\text{orb}}, \ln K, \phi_0), \quad (6)$$

whereby ϕ_0 represents the orbital phase to the next outgoing node at $t = E$.

Using orbital elements, we calculate the projected semi-major axis as:

$$a \sin i \text{ [au]} = \frac{1}{2\pi G} K P_{\text{orb}} \sqrt{1 - e^2} \quad (7)$$

and the mass function as

$$f_{\text{mass}} \text{ [M}_{\odot}] = \frac{1}{2\pi G} K^3 P_{\text{orb}} (1 - e^2)^{\frac{3}{2}}, \quad (8)$$

where G denotes the gravitational constant and the mass of the Sun was assumed to be $M_{\odot} = 1.98840987 \cdot 10^{30}$ kg (as used in `astropy.constants`).

3.3. Orbital trends represented using polynomials

Cepheids whose pulsation residuals computed using Eq. 1 indicated the presence of incompletely sampled orbital motion were modeled using the sum of Eq. 1 and a low-order

polynomial of the form:

$$v_{\text{trend}}(t) = \sum_{k=1, \dots, i} p_k \cdot (t - E)^k. \quad (9)$$

The polynomial degree i adopted depends on the structure observed in the pulsation residuals (e.g., linear or non-linear) and the overall $v_{\gamma(t)}$ variation over the VELOCE temporal baseline. We prioritized low values of i , typically < 3 , and sought to obtain a reasonably close fit to the data. Additional data are required to determine full orbital solutions in these cases. Please note that in the present study, Fourier+polynomial fitting was exclusively employed for incompletely sampled orbits within VELOCE. This differs from the approach in Paper 1, where polynomials were utilized to represent modulated variability of any origin.

We note that $v_{\text{trend}}(t)$ represents the change of the pulsation averaged velocity $v_{\gamma}(t)$ over time, so that v_{γ} in Eq. 1 becomes the pulsation-averaged velocity near the midpoint of the RV time-series. Introducing such polynomials allows to faithfully recover the pulsational variability and to partially quantify the orbital motion already sampled by the available data. However, it should be noted that in this case v_{γ} is specific to the time-series and not generally valid for the star. Specifically, v_{γ} then does not refer to the center of mass line-of-sight velocity of the system with respect to the Sun.

3.4. RV template fitting (RVTF)

We investigated variations of v_γ over timescales exceeding the VELOCE baseline using RV datasets from the literature. To this end, we adopted the literature RV zero-point differences from Paper I and the RV template fitting (RVTF) approach developed in Anderson et al. (2016a); Anderson (2019). In this approach, the pulsational RV curve is assumed to be fully characterized by the high-quality pulsation fits obtained in Paper I using VELOCE data of each star. The template fitting technique then fits the VELOCE pulsation models to the available literature data while solving for two parameters, an offset in $v_\gamma(t)$ with respect to VELOCE, and a phase shift $\Delta\phi$. While the former is required to investigate binarity, the latter allows to efficiently deal with pulsation periods changing over the course of several decades without having to assume a functional form for such period changes (cf. Section 5.2 of Paper 1).

In Paper I, we developed a semi-automated approach for clustering the available data sets using a Kernel Density Estimation algorithm whose bandwidth was varied according to data availability and quality. For binaries, we double checked the most appropriate bandwidth to use to avoid fitting data exhibiting significant variations of v_γ as one epoch. Furthermore, we visually inspected all template fits to make sure they covered a sufficiently broad range in phase to be informative. Template fits restricted to an insufficiently narrow range in phase were discarded. For each clustered template fit and per literature reference, we obtained the mean date, range of dates, fit parameters Δv_γ , $\Delta\phi$, their uncertainties, as well as the time-series epoch residuals (denoted as ϵv_γ henceforth).

To investigate the significance of orbital signatures, we calculated the SNR between velocity offset and square-summed uncertainties as follows:

$$\text{SNR}_{\text{SB1}} = \frac{|\Delta v_\gamma|}{\sqrt{(\sigma_v)^2 + (\sigma_{v_\gamma})^2}}, \quad (10)$$

where Δv_γ is the difference between the zero-point-corrected⁴ v_γ obtained by template fitting and the pulsation averaged velocity from Paper I. σ_v denotes the uncertainty on v_γ , and σ_{v_γ} is the uncertainty on the instrumental zero-point correction v_γ . Using Eq. 10, we searched for stars exhibiting deviations of more than $\text{SNR}_{\text{SB1}} > 3$ and rejected any spurious v_γ variations among closely neighboring cluster sets following visual inspection, cf. Section 4.3.

Where feasible, we determined full orbital solutions using our MCMC algorithm (cf. Section 3.2) using the ϵv_γ from template fitting as input. In practice, this often worked better than trying to fit a combined Fourier series and Keplerian model, since period changes could be effectively removed using the template fitting algorithm. The v_γ and ϵv_γ of literature datasets used in the orbital fits with MCMC algorithm and in the RVTF analysis are included in the VELOCE data files published as part of Paper 1.

Please note that a thorough analysis comparing *Gaia* DR3 RVs with VELOCE RVs was performed in Paper I. The main arguments against including *Gaia* data in the current work were as follows: Firstly, their temporal baselines mostly overlapped with existing data, and no significant

⁴ These zero-points were established based on stars with stable v_γ , more details can be found in Section 5.2 of Paper 1.

improvements in orbital coverage were identified. Secondly, we observed that certain stars displayed temporal trends in *Gaia* radial velocities (RVs) over timescales where VELOCE RVs showed no variations in pulsation-averaged velocity. However, a clear pattern regarding when and for which stars this occurred could not be discerned. In light of these disparities, *Gaia* RVs were omitted as a literature source for the spectroscopic binary search employing the method described above. With extended baselines, increased observation frequency, and improved data processing, future data releases with *Gaia* DR4 and DR5 are poised to excel in detecting SB1 systems and refining orbital solutions.

4. Results

This section describes the results of our systematic search for spectroscopic binary Cepheids using VELOCE data. An overview of the results is presented in Table 2. Tables 3 and 4 list orbital parameters for 18 Cepheids whose orbital parameters are being reported for the first time and 15 Cepheids whose orbits had previously been reported in the literature, respectively. Overall, we identified 76 bona fide SB1 Cepheids and 14 additional SB1 candidates in the VELOCE sample. 32 of these are reported as SB1 systems for the first time. Unless otherwise specified, we here discuss only bona fide SB1 Cepheids.

We first discuss fully determined orbits in Section 4.1. Sections 4.2 and 4.3 present Cepheids with incompletely sampled orbits represented by polynomials and investigated using template fitting, respectively. We discuss the spectroscopic binary fraction in Section 4.4 and provide brief notes on individual Cepheids in Section 4.5.

4.1. Full orbital solutions

This section presents the results obtained by fitting full orbital solutions to the RV time-series. We determined complete orbital solutions for 33 stars (including 3 tentative orbital fits). Section 4.1.1 begins with results based on VELOCE data alone, followed by results based on combined VELOCE and (zero-point offset-corrected) literature RVs in Section 4.1.2. Tables 3 and 4 distinguish these solution types using the tags ‘V’ and ‘V+L’, respectively.

4.1.1. Orbits from VELOCE data alone (V)

Thanks to the high RV precision and data homogeneity, orbits derived using VELOCE data alone are typically very accurate. However, the available 11 yr baseline is not always sufficient to sample orbits fully, and occasional gaps in the time series may unfortunately coincide with particularly important orbital phases, preventing a definitive determination of all orbital parameters. All systems presented here were fitted using the combined Fourier series plus Keplerian model, which simultaneously solves for pulsational and orbital variability. The resulting orbital periods range from 237 to approximately 4000 days, that is, the baseline available from VELOCE DR1.

Figures 2 and 3 illustrate two examples of combined Fourier series plus Keplerian orbits for the naked-eye prototype of classical Cepheids, δ Cephei, and the faint southern target NT Puppis, cf. Section 4.5 for additional details. All other combined fits are illustrated in Appendix B.

Table 2: An overview of the results from the current work.

Total SB1 detections	76
No. of new SB1 detections	32
No. of orbits	33 (15 (New) + 15 (Known) + 3 (Tentative))
No. of stars fitted with polynomial	30 (16 (New) + 14 (Known))
No. of stars with RVTF-Yes	12 (4 (New) + 8 (Known))
No. of stars with RVTF-No	24

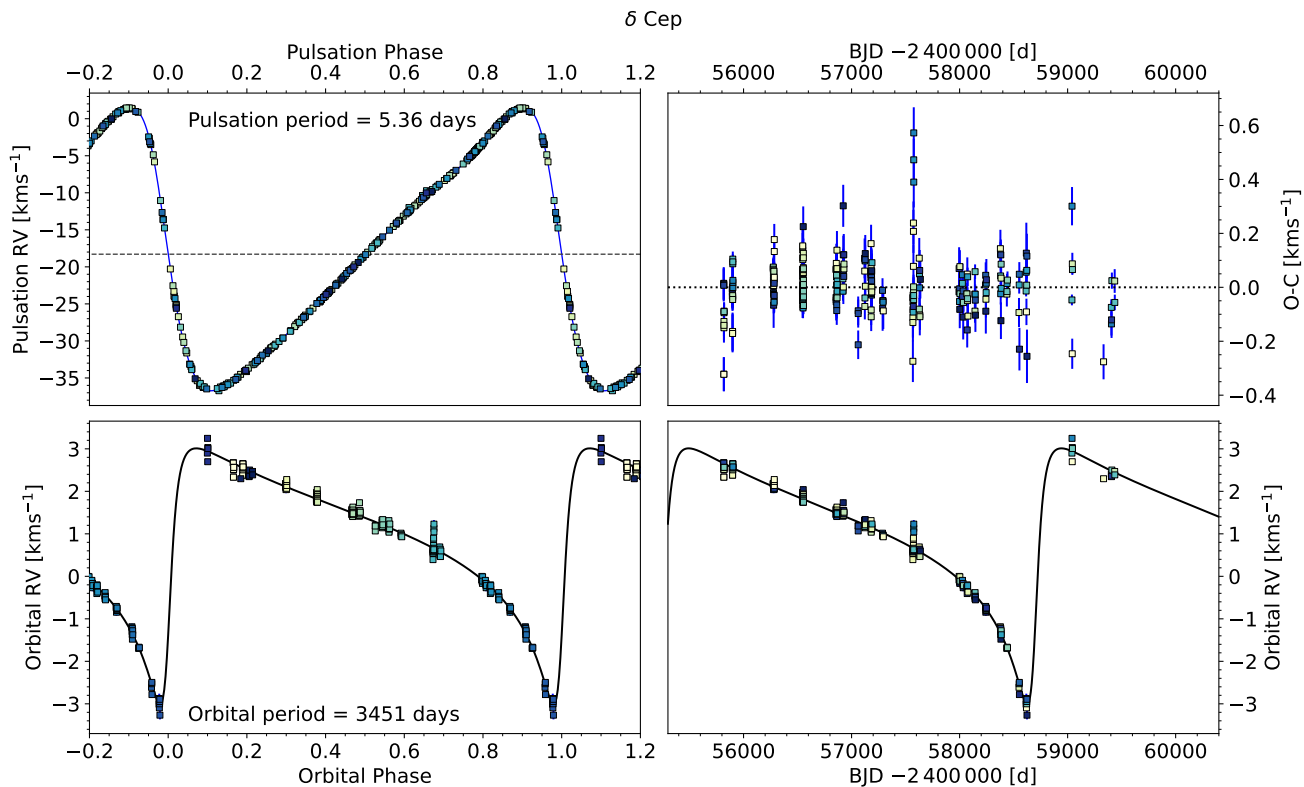


Fig. 2: Pulsation and orbital fit of the naked-eye Cepheid prototype δ Cephei. Left top: pulsation RV variability where the systemic velocity, $v_{\gamma,0}$ is indicated by a dashed line. Right top: residuals after fitting the Fourier series and Keplerian orbit against observation date. Left bottom: phase-folded orbital RV variation against orbital phase. Right bottom: orbital RV variation versus the observation date.

The choice of starting values for model fit parameters, notably P_{orb} and e , can impact the determination of orbital solution. We therefore adopted reasonable starting values estimated by inspecting the Fourier series fit residuals. Where starting values could influence the result, we cross-checked the results using the MCMC template fitting algorithm, cf. Section 3.2. For most stars, however, the data set sampled the orbital cycles sufficiently well to allow an initial guess close to the correct orbital period.

The best fit orbital parameters obtained here generally agree with previous orbital solutions published in the literature despite improved uncertainties. However, we obtain significantly different orbital periods for six Cepheids δ Cep (cf. Figure 2), AX Cir, MU Cep, V1334 Cyg, W Sgr, and XX Cen. These stars, among others, are discussed in detail in Section 4.5.

4.1.2. Orbits from VELOCE and literature data (V+L)

We determined orbital solutions using combined VELOCE and literature data using our MCMC algorithm applied to the template fitting epoch residuals; such fits are labeled as ‘V+L’ in Tables 3 and 4. Orbits of five newly discovered binaries (FO Car, MY Pup, R Cru, VY Per, and VZ Pup) and nine previously known binaries (DL Cas, FF Aql, S Mus, S Sge, SY Nor, TX Mon, U Vul, V1334 Cyg, and YZ Car) were obtained using VELOCE data alone as well as in combination with literature RVs. The ‘V’ and ‘V+L’ orbits for 12 of these 14 agree within the uncertainties, although ‘V+L’ orbits tend to have lower uncertainties, mostly due to better orbital sampling. The exceptions are MY Pup and VZ Pup. The VELOCE baseline only marginally covers the orbital period of MY Pup, hence, incorporating literature data results in a modification of the period. The P_{orb} of VZ Pup differs by 2.4σ between ‘V’ and ‘V+L’ orbits due to the P_{orb} being on the order of the available VELOCE baseline. The ‘V+L’

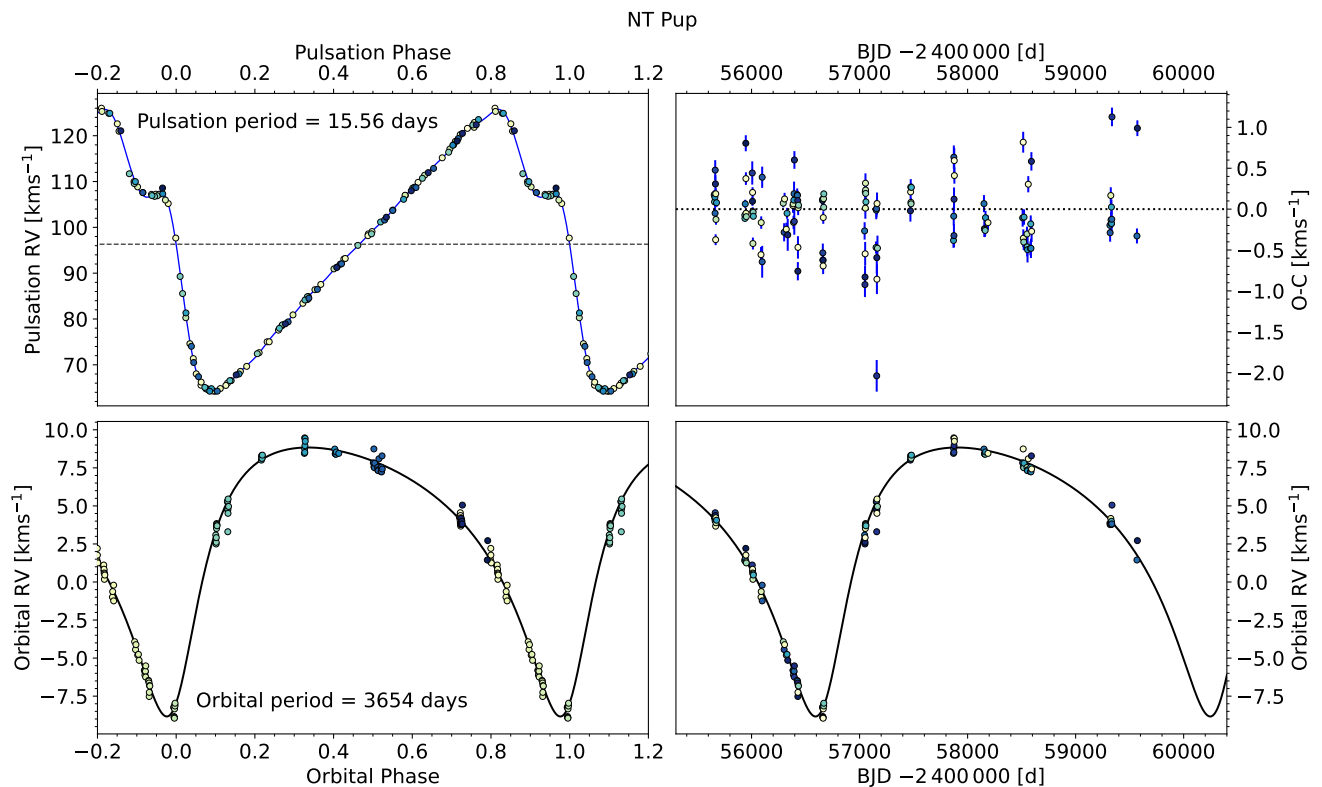


Fig. 3: Pulsation and orbital fit of one of the faintest binaries in our sample, NT Puppis. Figure description is same as Figure 2.

result is thus clearly preferred, hence, whenever available we use ‘V+L’ orbital estimates in any sample descriptions presented here. Lastly, for two stars, AX Cir and SU Cyg, we could only obtain a combined fit using VELOCE and literature data. In the case of AX Cir (Figure C.1), due to its very long orbital period and for SU Cyg (Figure C.11) due to the incomplete sampling of orbital phase with VELOCE data alone.

4.1.3. ‘Tentative’ orbits using VELOCE and literature data

We determined first tentative orbital solutions for three stars: BP Cir, R Mus, and V0659 Cen. We consider these orbits ‘tentative’ because the literature data were not sufficiently constraining, while the VELOCE data alone were not sufficient to sample a full orbit. Additional observations are required to ascertain the true orbital solutions for these stars. Please note that the uncertainties associated with the orbital parameters of the ‘tentative orbits’ listed in Table 3 may not accurately reflect the limitations arising from the insufficient sampling of these long orbits. The stated uncertainties are formal uncertainties on the model given the data. However, in cases of poor or incomplete orbital sampling, it is possible that the true orbital period is outside the range of these formal errors. This is why we present these cases separately as ‘tentative’.

4.2. Incompletely sampled orbits modeled as polynomial trends

We represented 16 newly detected SB1 systems and 14 previously reported SB1 systems using a combined Fourier series plus polynomial trend. Table 5 quantifies the measured range of the orbital RV variation, A_{p2p} , over the temporal baseline (denoted by ΔT_{p2p}), which is the baseline of the observations over which the A_{p2p} was calculated. Among the 30 systems examined with Fourier plus polynomial fit, 15 Cepheids exhibit non-linear trends. Among the 15 stars with linear trends, 5 demonstrate a decreasing trend in v_γ , whereas the remaining 10 feature increasing v_γ . Additional observations are required to determine these orbits.

Figure 6 presents the distribution of A_{p2p} versus ΔT_{p2p} and the pulsation period. A clear trend of increasing A_{p2p} as we extend to longer temporal baselines is visible. For a fixed value of K , this trend arises because longer baselines increasingly sample the full (albeit incomplete) peak-to-peak variation of the orbit. However, there is significant dispersion in the value of K at fixed P_{orb} due to different inclinations and mass ratio. The smallest trends of between 0.2 - 0.35 km s^{-1} are found for V1162 Aql, DR Vel, FR Car and SX Vel (over $\sim 1.8, 4.5, 5.8$ and 5.9 yrs respectively). By comparison, the smallest K among completely solved orbits is 0.67 km s^{-1} (MY Pup, 5.7 yr). At the long timescale limit, we find $A_{p2p} = 1.2 \text{ km s}^{-1}$ variation for T Mon over the course of nearly 10.5 yr. By comparison, the lowest $K = 2.1 \text{ km s}^{-1}$ for a completed orbit and a similar P_{orb} of 11 yr is found for VZ Pup.

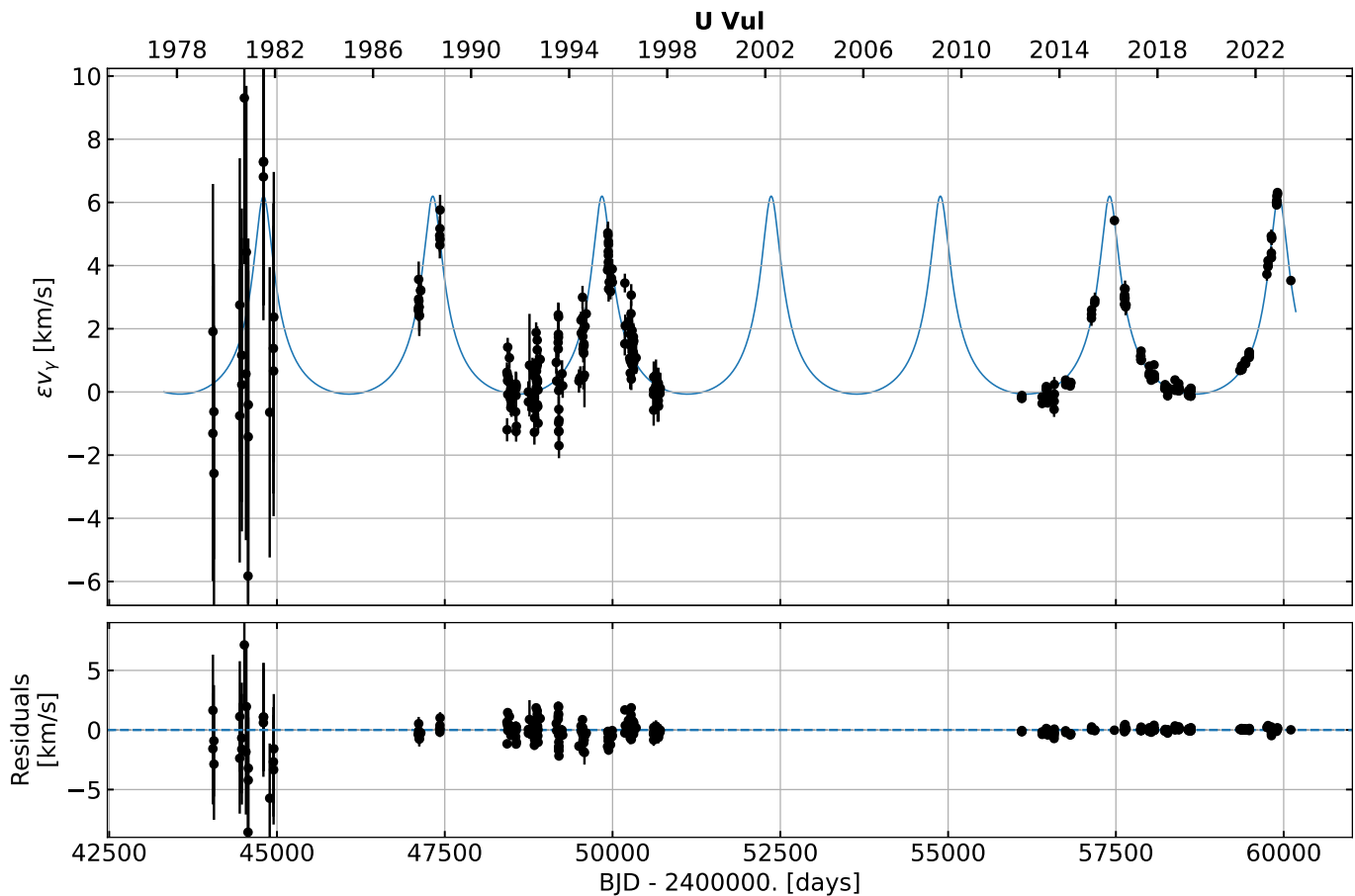


Fig. 4: The orbit of U Vul determined by fitting v_γ epoch residuals of literature and VЕLOCE data.

4.3. Template fitting for stars without orbital signatures in VЕLOCE data

Paper I presented a list of SB1 Cepheids exhibiting time-variable average velocities detected using VЕLOCE data alone. SB1 Cepheids with very long P_{orb} could, however, remain undetected based on VЕLOCE data alone. Hence, we investigated the temporal stability of v_γ for all Cepheids in VЕLOCE using the well-defined RV templates from Section 3.4. To this end, we computed SNR_{SB1} (Eq. 10) and considered a star a likely binary if any template fit resulted in a $3\text{-}\sigma$ deviation ($\text{SNR}_{\text{SB1}} > 3$) from a constant value of v_γ .

Applying this method to 174 bona fide VЕLOCE Cepheids with available literature data resulted in the discovery of four additional SB1 candidates: β Dor, SZ Aql, V0402 Cyg, and X Cyg, cf. Figure 7. All four exhibit visually convincing trends in v_γ on the order of $1 - 3 \text{ km s}^{-1}$ on timescales exceeding $15\,000 - 20\,000 \text{ d}$.

Additionally, we found 8 bona fide SB1 Cepheids (CD Cyg, η Aql, RS Ori, SS CMa, SZ Cyg, V0340 Ara, V0916 Aql and VY Sgr) among a sample of 32 SB1 candidates previously reported in the literature (Szabados 2003) where the available baseline of VЕLOCE data alone was insufficient to detect orbital motion. Figure 8 illustrates these cases. CD Cyg and SS CMa were already discussed as potential SB1s from the RVTF analysis of Anderson et al. (2016a) using VЕLOCE data. Here, we confirm that the deviations in v_γ indicate of binarity.

For the remaining 24 Cepheids among the 32 candidates, we could not confirm unambiguous orbital motion despite large overlaps in the data used. Ten of these 24 Cepheids do not exhibit a $\text{SNR}_{\text{SB1}} > 3$, over a temporal baseline of $10\,000 - 20\,000$ days. For the remaining 14 cases, individual v_γ variations are found, although they should be considered spurious variations because closely neighboring v_γ estimates clearly show the absence of a trend at these epochs. In Appendix Figure E.1, we present all these ‘non-SB1’ cases and we have tagged these stars with ‘RVTF-No’ in the ‘Binarity’ column of Table 1.

Given the high accuracy of the VЕLOCE template fitting procedure, which effectively removes any pulsational variability and period variations, and since instrumental zero-point differences have been corrected using non-binary Cepheids (cf. Paper I), we conclude that these 24 Cepheids should not be considered spectroscopic binaries.

4.4. SB1 fraction among VЕLOCE Cepheids

The 76 bona-fide SB1 Cepheids detected as part of VЕLOCE yield a lower limit to the spectroscopic binary fraction of $29.6 \pm 3.4\%$ that is fully consistent with the result by Evans et al. (2015) of $29 \pm 8\%$ based on the 40 brightest Cepheids. If all 14 SB1 candidates from Paper I should be confirmed to be bona-fide SB1 systems, then the VЕLOCE binary fraction would increase to $\sim 35\%$.

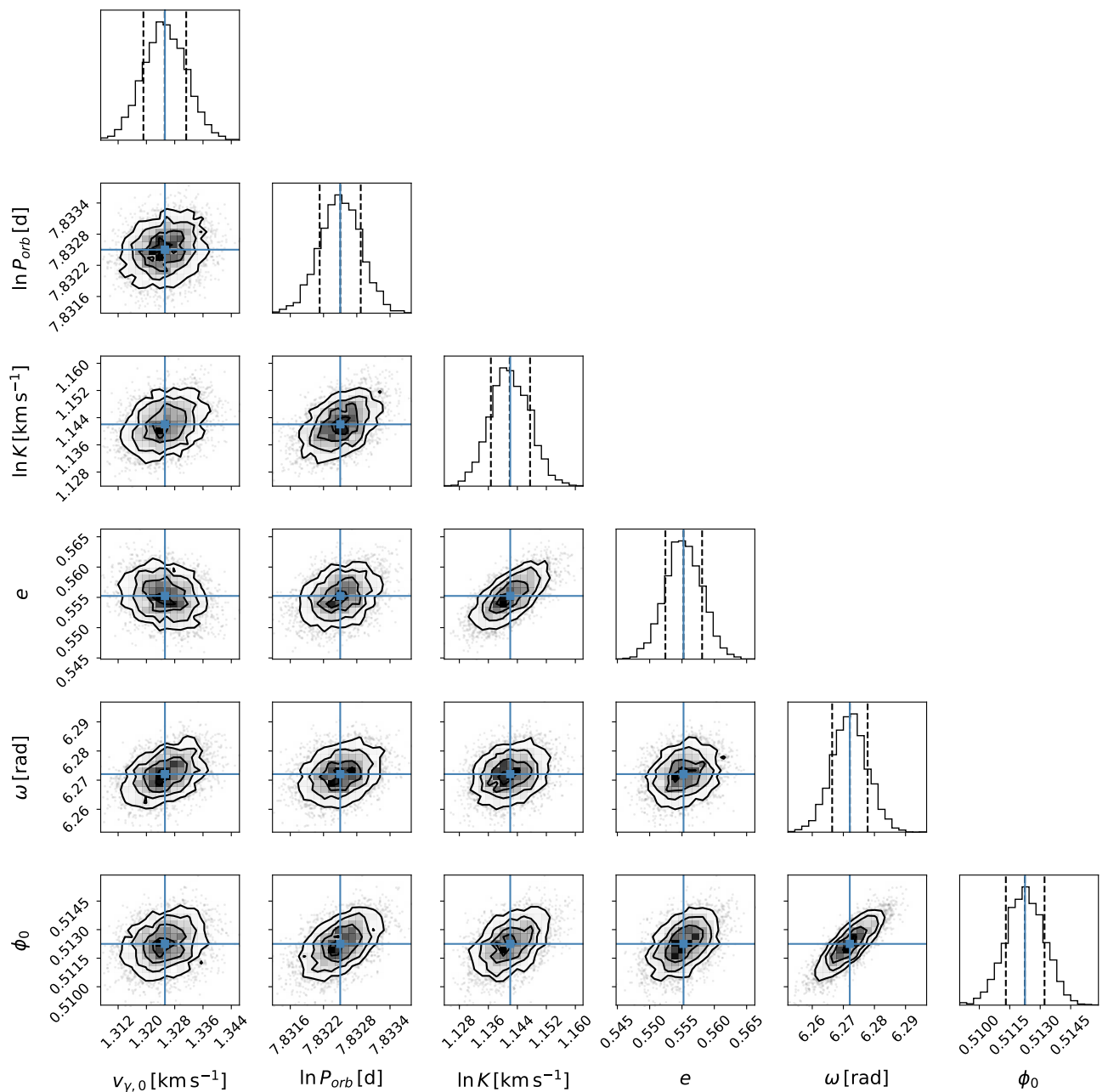


Fig. 5: Joint posterior distributions derived from the MCMC sampling for U Vul. The histograms show marginalized posterior distributions of the parameters.

Using the subset of Cepheids with fully determined orbital solutions from Tables 3 and 4 and assuming that all non-determined orbits have very long orbital periods, we find a lower limit to the fraction of SB1 Cepheids with orbital periods of less than 10 yr of $15.2 \pm 2.4\%$, slightly lower albeit consistent with the reported $20 \pm 6\%$ from Evans et al. (2015). Although our stringent template-based investigation (Section 4.3) questioned the veracity of the SB1 nature of 24 Cepheids for which such evidence had been previously discussed (cf. references in Szabados 2003), the fraction of SB1 systems among Cepheids we determined remains similar because we also identified new SB1 systems. However,

the more accurate determination of time-variable v_γ alongside detailed zero-point corrections affords much greater confidence in the determination of the SB1 nature of individual Cepheids. Of course, the SB1 fraction of Cepheids is merely a lower limit of the total fraction of Cepheids with companions due to the possibility of very large separations, unfavourable inclinations, and extreme mass ratios.

Figure 9 illustrates the magnitude distribution of newly discovered and detected SB1 Cepheids alongside the distribution of binary systems reported in the online compilation by Szabados (2003), as well as the distribution of magnitudes for which orbits were determined here. To ensure con-

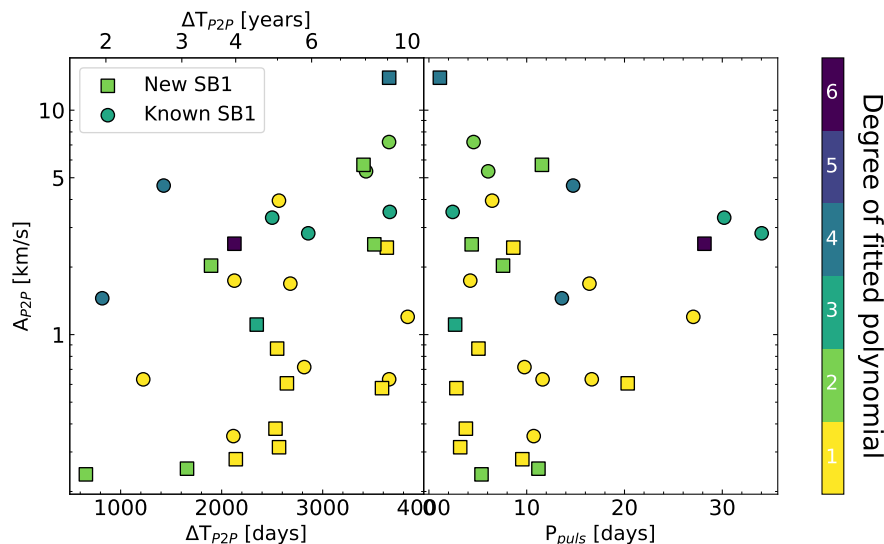


Fig. 6: The distribution of A_{p2p} , maximum amplitude variation in v_γ , for the stars in our sample where we could fit a polynomial to the v_γ trend (see Section 3.3 for details). In the left panel, we have the A_{p2p} vs the baseline in time over which it was calculated and in the right panel, the same against the pulsation period. The newly discovered SB1s from our sample are plotted in filled squares, while the literature-known SB1s are plotted in filled circles. The color bar represents the degree of polynomial fitted in the Fourier+Polynomial model.

sistency in the comparison, we have exclusively included the bona-fide SB1 binaries from Szabados (2003) in Figure 9. Therefore, other types of binaries (such as photometric, visual, etc.) from their catalog are not accounted for in this analysis. Please note that Figure 9 does not include 24 systems that are not detected as SB1 in our study.

As the right panel of Figure 9 shows, we here double the number of orbital solutions for Cepheids fainter than ~ 8 -th magnitude, and there are only 14 Cepheids with known orbital solutions that are not included in this work (one Cepheid among these 14, namely T Mon has incompletely sampled orbit in this study). Conversely, we determine the first orbital solutions for 18 Cepheids, most of which fainter than ≥ 8 th magnitude.

4.5. Notes on individual binaries

We have presented evidence of the SB1 nature of 76 Milky Way Cepheids on timescales spanning up to 40 years, including 32 stars whose SB1 nature was not previously known. The following provides additional background for specific stars of interest, notably if our results disagree with previous studies. We note that several Cepheids were first reported to be SB1 systems based on early VELOCE results, such as FN Vel and MU Cep (Anderson 2013), BG Vel and RZ Vel (Szabados et al. 2013a), δ Cep (Anderson et al. 2015), and AQ Car, CD Cyg, KN Cen, SS CMa, SZ Cyg, XZ Car, VY Car and X Pup (Anderson et al. 2016a). Anderson et al. (2016a) noticed tentative evidence of v_γ variations in VY Car, AQ Car, SZ Cyg and X Pup. However, they ultimately deemed these findings inconclusive due to imprecise data in the literature and the occasional substantial fluctuations in pulsational variability. In the current work we successfully detect these v_γ variations for SZ Cyg (when VELOCE data is combined with zero-point corrected literature datasets, see Figure 8) and AQ Car (cf. Table 5, Figure 10). Nevertheless, in the case of VY Car and X Pup, the

v_γ values, when adjusted for zero-point, do not reveal any consistent variation indicative of binarity (see Figure E.1).

α UMi (Polaris) was one of the first Cepheids whose nature as an SB1 system was realized (Moore 1929), and much literature exists on this star. Polaris was extensively studied using pre-2019 VELOCE data by Anderson (2019), who determined a full orbital solution and studied the stability of RV amplitudes as well as the presence of additional periodic signals. Given the very long ~ 30 -year orbital period, we did not update the orbital solution here and instead refer to the aforementioned publication as well as Torres (2023) for orbital parameters.

δ Cephei is the archetype of classical Cepheids and was discovered to be an SB1 system using an earlier subset of VELOCE data. Anderson et al. (2015) estimated an orbit with $P_{\text{orb}}=2201^{+5.73}_{-6.31}$ d, $K = 1.5^{+0.239}_{-0.080}$ km s $^{-1}$, and $e = 0.647^{+0.038}_{-0.021}$ by combining new RV data with RV measurements from the literature. A main difficulty of this approach was the correction of zero-point differences for datasets with short (~ 1 yr) baselines. Here, we report a correction to the orbital solution, with $P_{\text{orb}}=3450.9 \pm 19.6$ d, $K = 3.01 \pm 0.02$ km s $^{-1}$, and $e = 0.745 \pm 0.006$, based purely on VELOCE data and hence not subject to the uncertainties associated with literature zero-point offsets. This updated orbit of δ Cep was already presented at the 2022 RR Lyr-Cep conference in La Palma (Shetye 2022). It agrees reasonably well with the results recently presented by Nardetto et al. (2024) based on a combination of High Accuracy Radial velocity Planet Searcher for the Northern hemisphere (HARPS-N) data and existing literature. Their estimated orbital period of 3401.8 d and eccentricity of 0.71 differ by $2-\sigma$ and $1.7-\sigma$ from ours. These small differences may result from their use of a heterogeneous dataset, or the better coverage of the periastron passage by the HARPS-N data. As Figure 2 shows, the

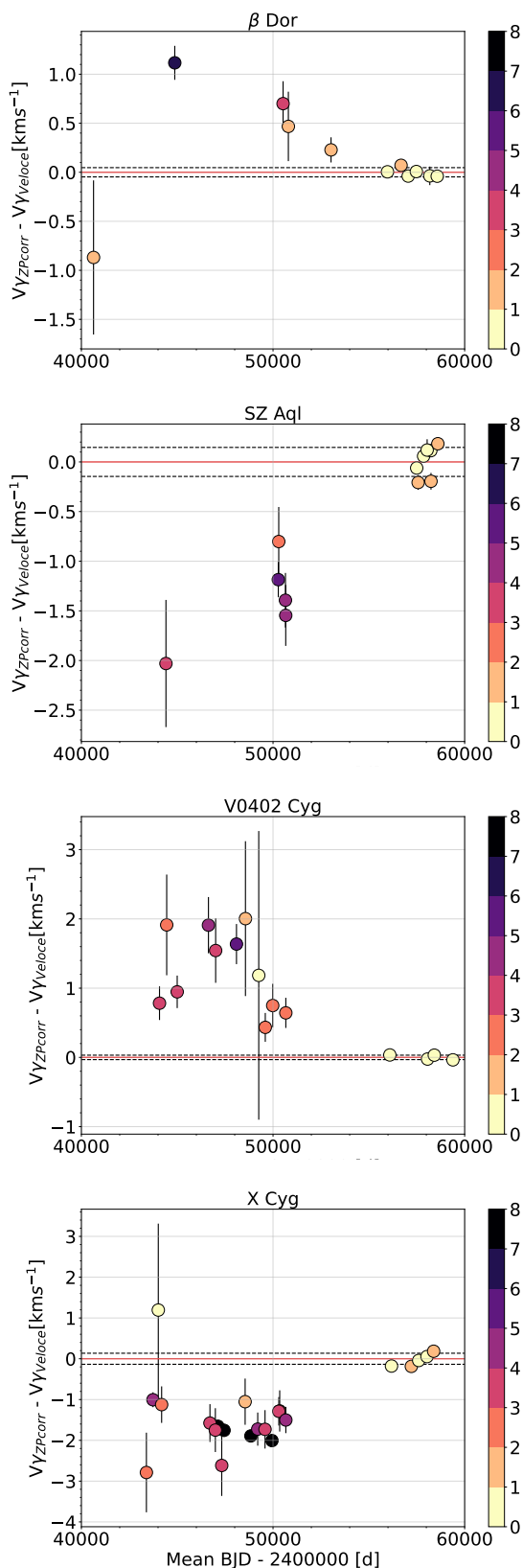


Fig. 7: Zero-point corrected Δv_γ for new SB1s detected through RVTF. The dotted lines mark the standard deviation of the $v_{\gamma, \text{VELOCE}}$. This figure only includes stars where we have a $3\text{-}\sigma$ detection through our analysis. The color bar represents the SNR_{SB1} of the various v_γ measurements where the SNR_{SB1} was calculated as described in the text.

orbit is now completely sampled and contained within the VELOCE baseline (3620 d). Importantly, the extreme ends of the orbital velocity have been observed and tightly constrain e and K . Unfortunately, including literature data for a ‘V+L’ orbit does not improve the orbital solution due to the same issues that affected the prior analysis. Extending the baseline with future *Hermes* observations will further improve the orbital period. We note that the mass function and the high brightness contrast imply the companion to be a low-mass star, possibly a white dwarf (Gallenne et al. 2016). A similar deduction was made in the recent X-ray study of Cepheids by Evans et al. (2022). A companion of G spectral type or later would be expected to be detected in X-rays, which puts a lower limit on the mass of the companion. Finally, we note that the single-star astrometric solution provided in *Gaia* DR3 clearly indicates poor fit quality⁵. It thus appears likely that *Gaia*’s next data release could deliver an astrometric orbital solution, as predicted by Anderson et al. (2015).

η Aql was recently studied by Benedict et al. (2022) using spectroscopic, photometric and astrometric (from the Hubble Space Telescope’s Fine Guidance Sensor) observations, including unpublished VELOCE data. No significant variations in the RV residuals were detected after removing the Cepheid pulsational RV signature, leading Benedict et al. (2022) to conclude that either η Aql has a very long orbital period (longer than their baseline of ~ 38 years) or that it has a face-on orbit. We considered an extended temporal baseline by including RV data from Lloyd Evans (1980), Barnes et al. (1987), and Wilson et al. (1989) and detect a $3\text{-}\sigma$ variation in the Δv_γ (Figure 8). If the older datasets are to be believed despite large RV uncertainties of $\sim 1 \text{ km s}^{-1}$, then η Aql is indeed an SB1 Cepheid with a very long orbit of more than 50 years. Verifying whether this spectroscopic companion corresponds to the one identified in the UV imaging and spectra of η Aql by Evans et al. (2013), at a separation of 180 au, necessitates a follow-up of the long orbital period.

AQ Car was reported to show tentative signs of time-variable v_γ using an earlier set of VELOCE and literature data. In Paper I, we confirmed the SB1 nature of this star. Although weak, $\sim 0.7 \text{ km s}^{-1}$, the signal is clearly present in the VELOCE data thanks to the baseline of ~ 4 yr. Although literature datasets appear imprecise to usefully inform the v_γ variations (cf. Figure 10), in actuality, the fluctuations observed in the literature data surpass a $3\text{-}\sigma$ threshold. As σ is calculated using VELOCE data under the assumption of no orbital motion, consequently, the deviations from a stable v_γ are consistently underestimated in this scenario.

AQ Pup was reported to have a photometric companion (Evans & Udalski 1994) that was not previously confirmed spectroscopically (Vinko 1991). Here, we report low-amplitude v_γ variations ($\sim 3.3 \text{ km s}^{-1}$) on a timescale of 2500 days. Whether this signature corresponds to the photometric companion remains unclear.

⁵ Specifically, the *Gaia* DR3 astrometric parameters `astrometric_gof_al`= 31, `astrometric_chi2_al`= 41802, `astrometric_excess_noise`= 1.23, `astrometric_gof_noise_sig`= 1777, and `RUWE`= 2.7 all indicate the presence of unmodeled signal.

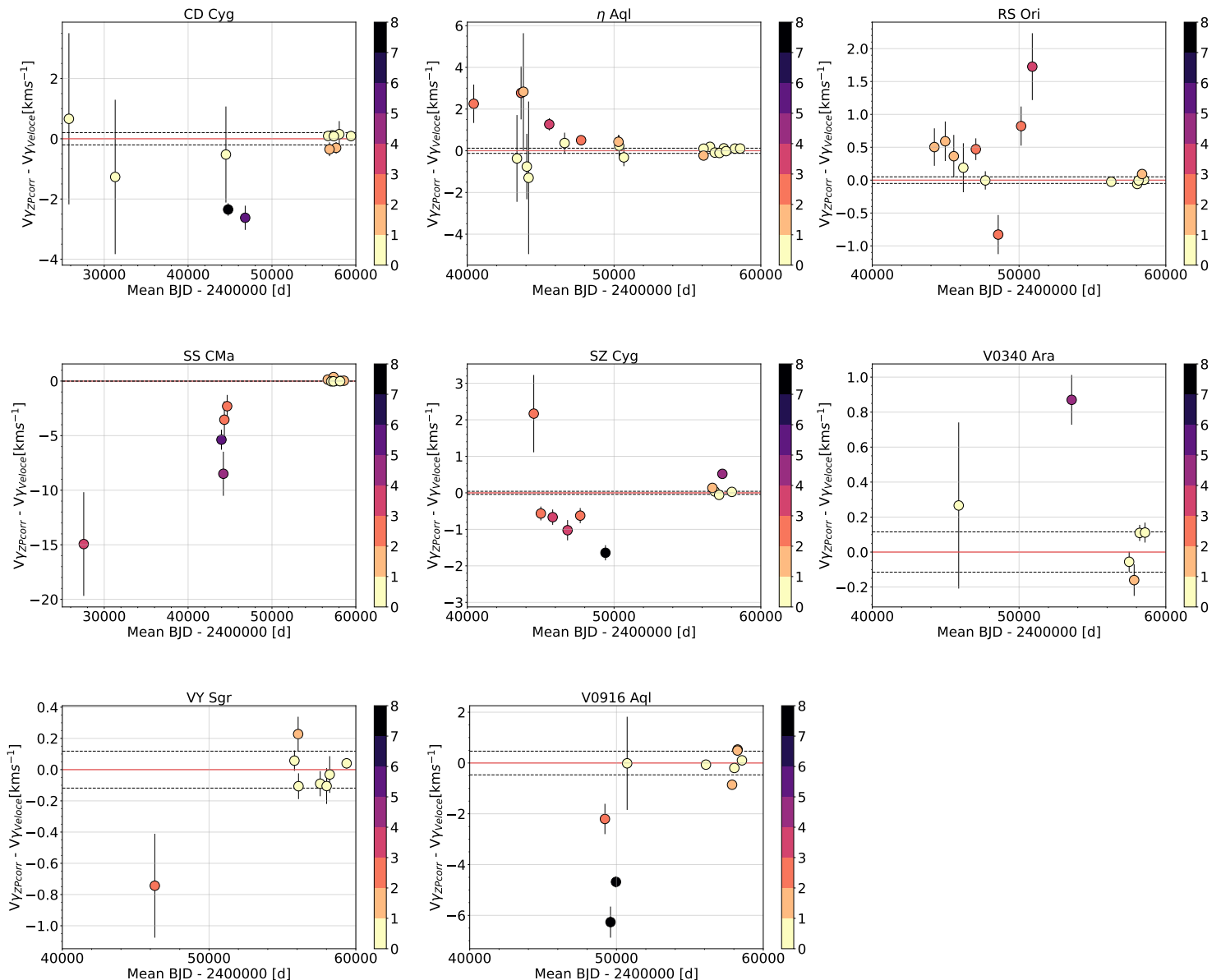


Fig. 8: Literature-known SB1 candidates detected through RVTF. The figure description is same as Figure 7.

ASAS J064540+0330.4 - We present the first orbital fit for ASAS J064540+0330.4 with a P_{orb} of 901.18 ± 2.81 days and an eccentricity of 0.44 ± 0.01 . As shown in Figure B.1, the pulsational residuals indicate additional signals beyond the orbital ones. It is important to note that further observational follow-up is necessary to sample the orbital phase better and establish this orbit more firmly.

ASAS J103158-5814.7 (GDR3 5351436724362450304) is a particularly interesting star, cf. Figure 11 and Paper I. It exhibits three signals at once: very short-period overtone pulsation (classified as first overtone by Gaia DR3 SOS, $P_{\text{puls}} = 1.11936$ d), high-amplitude orbital motion exceeding 13 km s^{-1} , cf. Table 5, and strongly modulated pulsation amplitudes reminiscent of the “Blazhko” Cepheid V0473 Lyrae (Burki et al. 1982; Molnár et al. 2017). At present, the orbital variations do not allow the estimation of an orbital period and we will thus continue monitoring

this intriguing star. Unfortunately, this star was not included in the list of Cepheids with time-series RV data in *Gaia* DR3.

AX Cir is a known SB1 and its orbit was first derived by Peterson et al. (2004). Our P_{orb} estimate of ~ 6285 days differs by 5% ($10\text{-}\sigma$) from that of Peterson et al. (2004). While our combined dataset, comprising VELOCE and literature data, incompletely samples orbital phases, we obtain an eccentricity that is in total agreement with the previously reported orbital eccentricity for AX Cir.

FN Vel was discovered to be an SB1 by Anderson (2013) who provided a first orbital solution. Kovtyukh et al. (2015) showed evidence for the companion using the Ca H & K lines. Here, we provide an updated orbital solution.

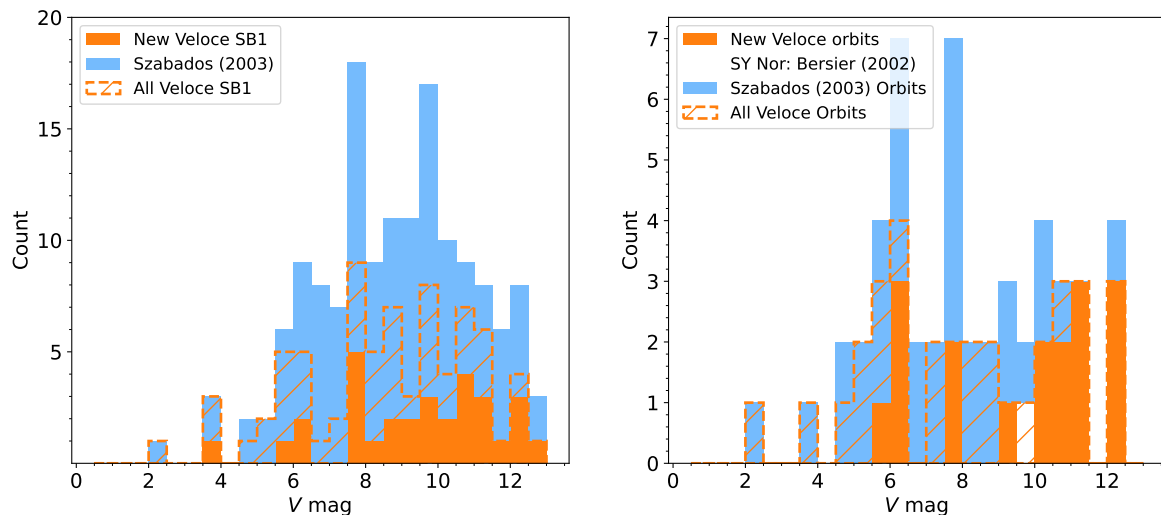


Fig. 9: Stacked histogram presenting the new VELOCE SB1 detections (left panel) and the new VELOCE orbits (right panel) along with the same from Szabados (2003). SY Nor’s orbit is provided by us as well as Bersier (2002); however, it is missing in the Szabados (2003) database.

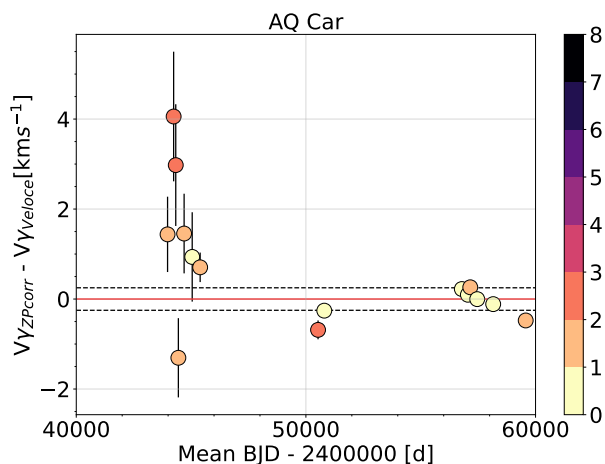


Fig. 10: Temporal variation of v_γ for AQ Car based on RVTF. The data points after BJD > 56000 are from VELOCE.

BP Cir is known to host a hot main-sequence companion (Arellano-Ferro & Madore 1985; Evans et al. 1992) based on IUE spectroscopy. Petterson et al. (2004) reported v_γ variations exceeding 5 km s^{-1} and that the star could possibly have a long orbital period. Using VELOCE alone we have v_γ variations of $\sim 2 \text{ km s}^{-1}$, however, when we combined VELOCE with literature datasets from Petterson et al. (2004) and Borgniet et al. (2019) we found v_γ variations of $\sim 4 \text{ km s}^{-1}$ at a temporal baseline of 9000 days. We estimated BP Cir’s orbital period using VELOCE and literature datasets, and found a tentative solution with $P_{\text{orb}} \sim 4300$ days and $e \sim 0.8$, cf. Figure C.2. Nevertheless, due to limitations in the available data, we are unable to definitively determine whether a period of 4300 days or twice that duration provides a more accurate representation.

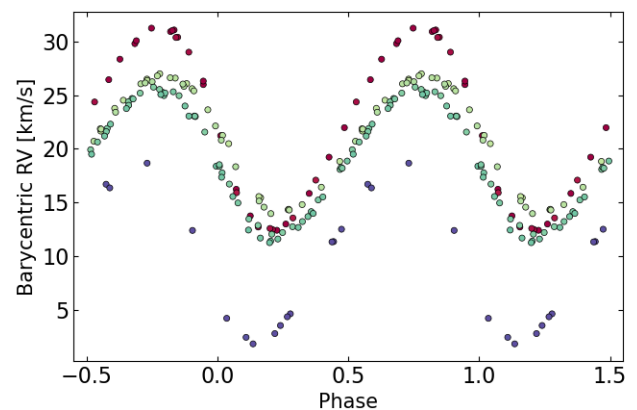


Fig. 11: Phase-folded Coralie RV of ASASJ103158-5814.7, same star that exhibits orbital motion, variable amplitude and a variable pulsation period.

FO Car’s observations began in March 2016, and we find a Keplerian orbit of $P_{\text{orb}} \sim 1660$ d. To the best of our knowledge, no previous publication⁶ has presented the case of FO Car. However, the online database of binary Cepheids (Szabados 2003) lists it as a spectroscopic binary, crediting Szabados & Berdnikov (2003 in preparation). Russo et al. (1981) found photometric evidence for a companion using a phase shift technique involving optical and UV data. Based on the visual companion identified during the spectroscopic observations (cf. Figure A.1) we consider this as the most likely source of the phase shift. Given the angular separation, the visual companion is clearly not the cause of the 4.5 yr orbit, and hence, FO Car is a triple system composed

⁶ Zhou 2010 credited Szabados 1996 with detecting such evidence. Although FO Car is not listed in this publication, FR Car is, and we surmise a typo in Zhou 2010.

of the Cepheid with an inner spectroscopic and outer visual companion.

MU Cep - The spectroscopic binarity of MU Cep (not to be confused with the much brighter red supergiant μ Cep) was discovered by Anderson (2013). Here we present an updated orbital solution, cf. Table 3, illustrated in Figure B.11. The previously reported $P_{orb} \sim 1500 \pm 350$ d exceeded the observational baseline. Thanks to continued follow-up of this faint star ($\langle m_V \rangle = 12.3$ mag), we have achieved nearly complete coverage of MU Cep's orbital phase and obtain tight orbital constraints, with $P_{orb} = 2028 \pm 2.7$ d.

R Cru is listed as an SB1 in the database by Szabados (2003), which credits unpublished work by L. Szabados and D. Bersier with this discovery. More recently, Evans et al. (2020) reported a visual companion of R Cru at a separation of 1.9 arcseconds based on Hubble Space Telescope (HST) imaging. We have acquired nearly 7 yr worth of very high-precision RV data for this bright Cepheid. The data clearly reveal low-amplitude orbital motion with $P_{orb} \sim 238$ d (cf. Figure B.13), rendering R Cru the Cepheid with the shortest orbital period in the Milky Way. The template fitting routine further finds evidence for non-linear period changes (see Figure 15 of Paper I), cf. also Csörnyei et al. (2022). The relative semimajor axis of $a_{rel} > 274R_{\odot}$ implies that the Cepheid and its companion are not in contact, assuming a Cepheid radius of $47R_{\odot}$ computed using a P-R relation (Anderson et al. 2016c) and a nearly circular orbit. For a Cepheid mass of around $5M_{\odot}$ and a $2M_{\odot}$ A2 companion (upper limit from the IUE spectrum, Evans 1992), the mass function for a circular orbit yields a minimum inclination of > 3.3 deg, improving slightly over the limit from the mass function alone (1.6 deg). For the range of inclinations $3.3 - 90$ deg, and assuming a $5M_{\odot}$ Cepheid, we thus find the allowed mass range for the companion to be between $0.09 - 2.0 M_{\odot}$.

RV Sco - Proust et al. (1981) list RV Sco as a visual multiple system, with a non-variable companion of $m_V \sim 13$ mag at a separation of 6.0 arcseconds. Evans (1992) did not detect any photometric companion for RV Sco within their IUE spectral analysis. Szabados (1989) suspected its binarity through its variable γ -velocity. Here, we confirm the finding as we detected significant ($A_{p2p} \sim 5.3$ km s $^{-1}$) amplitude variation in RV resulting into a $4\text{-}\sigma$ detection of binarity. RV Sco is therefore a triple (SB1 + visual companion) system.

RY Sco is listed as a visual binary in Szabados (2003), with references to Proust et al. (1981); Evans & Udalski (1994). We here detect the stars's SB1 nature for the first time, with very low-amplitude orbital RV variations of ~ 0.6 km s $^{-1}$. Combining VELOCE with literature datasets and extending to longer baseline, we notice a v_{γ} variation of ~ 2.5 km s $^{-1}$ on a timescale of 41 years. RY Sco is thus most likely a triple system with both a visual and a spectroscopic companions.

RZ Vel was reported to be an SB1 Cepheid by Szabados et al. (2013a). Szabados et al. (2013a) used a subset of VELOCE data (between BJD 2455650 - 2456400). We extended

this VELOCE baseline to BJD 2459600 and combined it with literature datasets from Lloyd Evans (1980); Coulson & Caldwell (1985); Bersier (2002); Borgniet et al. (2019). Although, data from Bersier (2002) was also included in Szabados et al. (2013a), we do not detect $3\text{-}\sigma$ v_{γ} variations for this or any other recent dataset after the year 2000.

S Mus was first identified as a binary using photometric observations (Lloyd Evans 1968). A first orbital solution was presented by Lloyd Evans (1982), with several others since. In particular, Petterson et al. (2004) provided a precise update to this solution, and Binnenfeld et al. (2022) determined the periodicity using partial periodograms directly computed from the spectra rather than RV measurements. We gathered 78 high-precision Coralie RVs over a total baseline of 6.3 yr. These data alone yield an orbital solution in agreement (to within 1 day) with Petterson et al. (2004) and Gallenne et al. (2019), cf. Table 4. As shown by Evans et al. (2015, 2020), the companion is an X-ray active B3V star.

S Nor was detected as an SB1 by Szabados (1989), where they estimated tentative orbital periods of 3300 or 6500 days. Groenewegen (2008) modeled S Nor's RV data using a circular orbit with a fixed P_{orb} of 3600 days and concluded that more RV data are needed to better determine this orbit. Here, we do not find this orbital estimate to be consistent with VELOCE data. We do not detect any v_{γ} variations with VELOCE data alone, however, when VELOCE is combined with literature datasets we do obtain a $3\text{-}\sigma$ detection for the oldest RV datasets (Figure E.1). However, the only cluster that exceeds $3\text{-}\sigma$ is based on only three observations and the uncertainty of this particular cluster is likely underestimated. Consequently, we doubt the validity of the only $>3\text{-}\sigma$ outlier and cannot consider the star a bonafide binary. Nevertheless, if the RVTF results are taken at face value, then the orbit would have to be significantly eccentric. Lastly, Figure E.1 indicates that a potential orbit clearly has high eccentricity.

SU Cyg is a solitary case wherein the pulsation model was derived using a combination of VELOCE data and zero-point corrected RV data from Borgniet et al. (2019). While VELOCE data provided strong constraints on the orbit, they were insufficient on their own to create a satisfactory Fourier series model. To address this, we included the Borgniet et al. (2019) measurements to formulate the RV template. This template was then used to compute ϵv_{γ} , as listed in the appendix Table F.1. Finally, employing the MCMC method, we obtained the 'V+L' orbit of SU Cyg with P_{orb} of $\sim 548 \pm 0.1$ d and eccentricity of $\sim 0.34 \pm 0.005$ (Figure C.11). These orbital estimates are in agreement with $\Delta P_{orb} < 1$ d (all orbital elements within $3\text{-}\sigma$ difference) the ones in the literature from Evans (1988); Imbert (1984); Groenewegen (2008).

TX Mon was first reported as an SB1 by Szabados & Pont (1998), who estimated a short $P_{orb} \approx 470 \pm 30$ d. We here confirm the SB1 nature of the star and determine the orbit, albeit at much longer $P_{orb} = 1607 \pm 1$ d, with $K = 11.9 \pm 0.04$ km s $^{-1}$.

V0659 Cen is host to a hot B6.0V companion detected directly using IUE UV spectroscopy (Evans 1994). V0659 Cen also has a high X-ray flux potentially originating from its companion (Evans et al. 2022). Here we present the first RV evidence of the Cepheid’s orbital motion with a peak-to-peak RV variation of $\geq 5 \text{ km s}^{-1}$. Combining VELOCE and literature data, we estimate a preliminary orbital period $P_{\text{orb}} \sim 9300 \pm 130 \text{ d}$ with mild eccentricity ($e = 0.32$). We designate this orbit as ‘tentative’ due to the ambiguity regarding whether the orbital period is approximately 6000 or 9000 days. It should be emphasized that the current uncertainties, which are around 100 days, do not account for this ambiguity. Additional *HST* UV spectroscopy will be particularly valuable to measure the mass of the Cepheid (Evans et al. in prep.).

V1334 Cyg is among the few sample cases where there is a disagreement between ‘V’ and ‘V+L’ estimates, specifically of 0.8% ($3\text{-}\sigma$) in P_{orb} for V1334 Cyg. Even after combining the VELOCE and literature datasets, constraints on the ascending part and extremities of the orbital phase remain limited. As the literature dataset from Gorynya et al. (1992) and Borgniet et al. (2019) add extra constraints on the descending branch of the orbital phase, we prefer the ‘V+L’ orbital estimate for V1334 Cyg. Furthermore, both ‘V’ and ‘V+L’ orbital estimates are in 0.5% ($3\text{-}\sigma$) disagreement with the ones from Gallenne et al. (2018) and $3\text{-}\sigma$ and $2\text{-}\sigma$, respectively, with the ones from Evans (2000). This maybe attributed to the aforementioned poor sampling at some orbital phases. Future observations, with overall improved sampling will help to elucidate the discrepancy. Lastly, Gallenne et al. (2018) demonstrated that *Gaia* DR2 parallax is off by $3.6\text{-}\sigma$ compared to the orbital parallax determined from the visual orbit + RVs of both components. This could be another reason for the discrepancy between our orbital parameters and the ones from Gallenne et al. (2018).

VY Car was considered a tentative SB1 candidate by Anderson et al. (2016a). Despite improved treatment of instrumental zero-point offsets, the orbital signal has neither disappeared nor clarified. We note that Figure E.1 suggests a trend with time. However, none of the epochs deviate from the average by more than $3\text{-}\sigma$. Hence, VY Car remains an unconfirmed SB1 candidate with a potentially very long orbital period.

VY Per was reported to exhibit v_γ variations exceeding 5 km s^{-1} by Szabados (1992) over a baseline of two years. We confirm the SB1 nature of this star and obtain a tentative orbital solution, with a $P_{\text{orb}} \sim 806 \text{ d}$ and $e \sim 0.4$ (cf. Figure B.21). Additionally, the MCMC (V+L) orbital estimate is presented in Table 3 and Figure C.17. This MCMC indicates that the true orbital period could be a multiple of 805 d. Unfortunately, the result remains ambiguous due to the sampling of the data, which also does not include the orbit’s descending branch.

W Sgr’s P_{orb} using VELOCE data differs by $6\text{-}\sigma$, $20\text{-}\sigma$ and $18\text{-}\sigma$ from that of Babel et al. (1989), Petterson et al. (2004), and Gallenne et al. (2019) respectively. We would

like to note that in our work the eccentricity is not sufficiently constrained (Figure B.23), hence, the orbit is probably more eccentric and shorter than our model as well as the P_{orb} is potentially more uncertain than the fit suggests. Unfortunately, the current dataset does not provide sufficient information for a more accurate fit, and additional observations will be necessary. In light of these considerations, we emphasize that Petterson et al. (2004) currently offer a more reliable orbital solution.

X Cyg was reported to exhibit an orbital signal via the light time travel effect by Szatmary (1990), who estimated $P_{\text{orb}} \approx 55 \text{ yr}$. Evans et al. (2015) and Hintz et al. (2021) did not detect long-term v_γ variations based on $\sim 11\text{-year}$ baselines. We here identify X Cyg’s v_γ variations using much longer temporal baselines of $\sim 40 \text{ yrs}$ by combining VELOCE data with the literature (Barnes et al. 1987; Wilson et al. 1989; Kiss 1998; Barnes et al. 2005; Gorynya et al. 1992; Storm et al. 2004; Bersier et al. 1994; Borgniet et al. 2019). We thus find a total v_γ difference of $\sim 3 \text{ km s}^{-1}$ and a lower limit of 40 yr on P_{orb} , consistent with Szatmary (1990).

X Pup was mentioned by Anderson et al. (2016a) to exhibit tentative signs of time-variable v_γ based on a difference between VELOCE data and the literature. However, the improved corrections of RV zero-points from VELOCE-I together with the clustered RVTF analysis do not reveal a significant signature of orbital motion, cf. Figure E.1.

XX Cen - Groenewegen (2008) determined an orbital solution with $P_{\text{orb}} = 924 \pm 1.1 \text{ d}$ and $K = 4.47 \pm 0.28 \text{ km s}^{-1}$, and e fixed to 0. We find a significantly different orbit for XX Cen based on VELOCE data alone and determine an orbital solution with $P_{\text{orb}} = 722.44 \pm 0.42 \text{ d}$, $K = 5.4 \pm 0.03 \text{ km s}^{-1}$, that is significantly eccentric with $e = 0.295 \pm 0.004$.

5. Sample analysis

5.1. Correlations among orbital elements

Figure 12 shows the correlation between different orbital elements (ω , K , e , and $a \sin i$) with P_{orb} for all orbital solutions reported here. This includes first-time orbital estimates of 18 stars and 15 VELOCE orbital estimates for Cepheids with literature-known orbits. Newly discovered SB1 systems populate the full range of orbital parameters, indicating that our sample selection was not biased towards the literature-known orbital properties of SB1 Cepheids. Semi-amplitudes tend to decrease as P_{orb} increases. Thanks to the precision of VELOCE RV measurements and long-term monitoring, we were able to discover many new SB1 systems with very small semi-amplitudes and long orbital periods. A noticeable correlation exists between $a \sin i$ and P_{orb} , and the dispersion along this correlation might stem, at least partially, from fluctuations in the combined masses of the Cepheid and its companion.

The eccentricity versus orbital period distribution (upper right panel in Figure 12) is particularly interesting. We find that the maximum eccentricity increases with orbital period. Despite a large range of eccentricities at most P_{orb} values, an absence of very high $e < 0.6$ is clearly noticeable at $P_{\text{orb}} \lesssim 3 \text{ yr}$. The two Cepheids with the shortest P_{orb} have

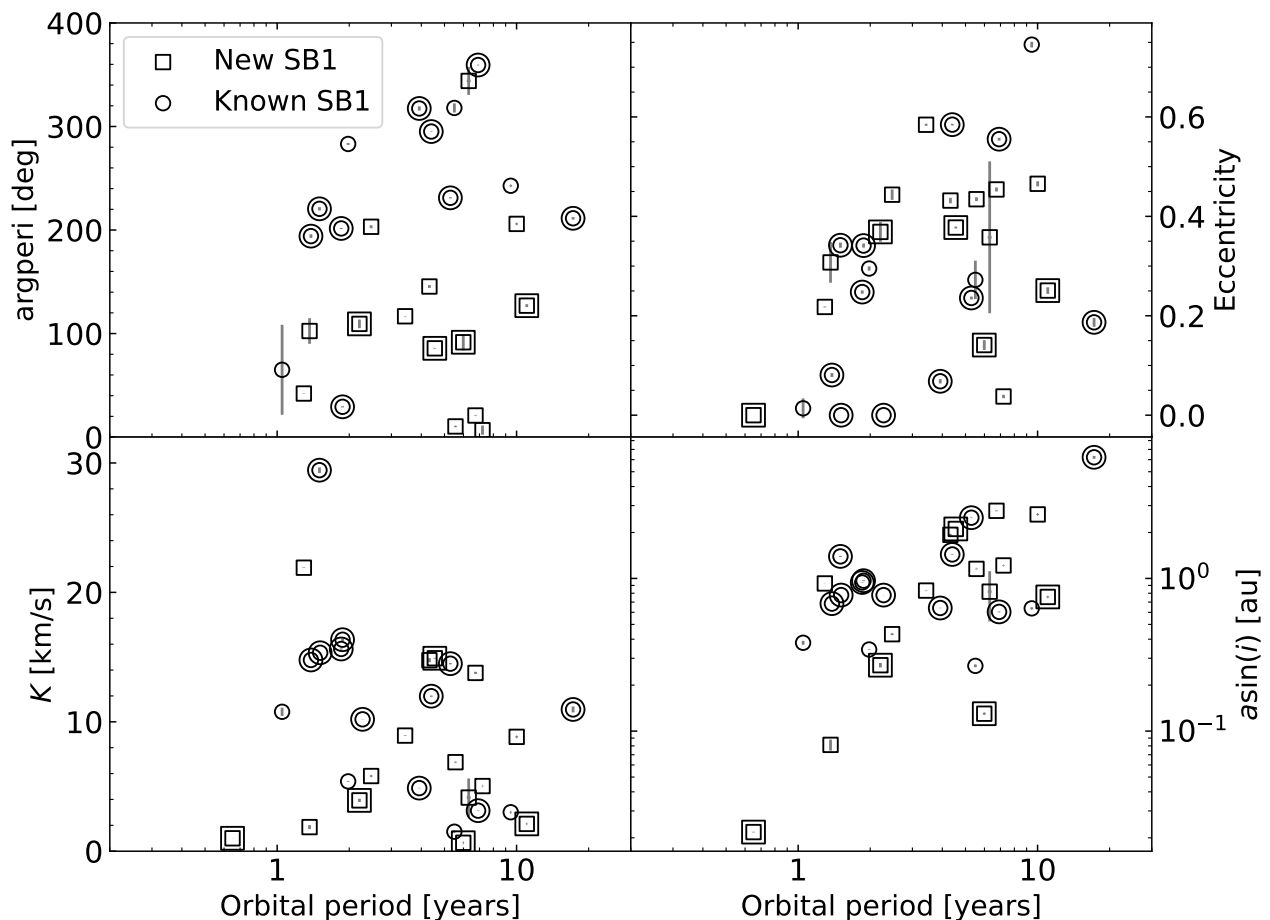


Fig. 12: The distribution of different orbital elements (Upper left: argument of periastron ω ; upper right: eccentricity e ; lower left: semi-amplitude K of the orbital RV variations; lower right: projected semi-major axis $a \sin i$) versus orbital period P_{orb} for Cepheids with orbits determined here. SB1s with newly reported orbits in this study are plotted using open squares, while VЕLOCE orbital estimates of SB1s with literature-known orbits are plotted in open circles. Symbols with double boundaries highlight ‘V+L’ orbits determined using VЕLOCE and zero-point corrected literature RVs. R Cru, SY Nor and YZ Car are absent in the top left panel due to insignificant eccentricity.

very low or no noticeable eccentricity. We also notice an absence of circular orbits at $P_{\text{orb}} \gtrsim 3$ yr, which appears to become an exclusion region at longer P_{orb} . Since such distant companions have most likely evolved in isolation, this could point to a primordial feature of intermediate-mass (B-star) binaries. However, NBODY simulations show that cluster dynamics increase e for long orbital periods over time (Dinnbier et al., in prep.). Additional long-period orbits are required to investigate this effect.

Most of these trends qualitatively agree with the empirical results by Evans et al. (2015), as well as with predictions from the Cepheid binary population synthesis study by Neilson et al. (2015) and Karczmarek et al. (2022), as well as with the dynamical NBODY6 simulations by Dinnbier et al. (2024). However, we do find several Cepheids at high $5 < P_{\text{orb}} < 10$ yr and relatively low eccentricities ($e < 0.2$) where Cepheid binaries have been predicted to have a low probability of occurring (Neilson et al. 2015). Ad-

ditionally, R Cru is very close to the minimum P_{orb} consistent with the synthetic populations by Neilson et al. (2015) and Karczmarek et al. (2022).

Incompletely sampled orbits described in Section 4.2 and illustrated in Figure 6 provide partial information on K and P_{orb} . Comparing A_{p2p} with K (in Figure 12) as a function of P_{orb} , we notice the inverse trends. Shorter orbital periods tend to have larger K , whereas we find larger A_{p2p} over longer baselines. This suggests that most short- P_{orb} orbits with $K \gtrsim 0.5 \text{ km s}^{-1}$ of Cepheids observed by VЕLOCE have been determined. Very low A_{p2p} values are likely to continue growing over longer baselines.

5.2. Cepheids exhibiting proper motion anomaly

Kervella et al. (2022) used *Gaia* to detect astrometric binaries using the proper motion anomaly (PMA). This method compares the proper motion vector determined by the ESA

Hipparcos mission (Perryman et al. 1997) and various *Gaia* data releases (Gaia Collaboration et al. 2016b,a; Michalik et al. 2015; Gaia Collaboration et al. 2018; Lindegren et al. 2018; Gaia Collaboration et al. 2021; Lindegren et al. 2021). PMA quantifies the significance of a long-term rotation of the proper motion vector due to orbital motion. Stars with PMA signals exceeding 3σ were thus labeled as binaries by Kervella et al. (2022). Proper motion probes the on-sky projection of orbital motion, orthogonal to the line-of-sight variations measured using RVs. Therefore, the PMA and RV methods function as complementary tools for binary detection (cf. Kervella et al. (2019b) for details on the sensitivity function of PMA). Consequently, it’s typical for some stars identified as SB1 to lack discernible deviations in their proper motions which would categorize them as PMA-True candidates. This could either be if the Cepheids are located at large distances or possess orbital periods too short for detection. On one hand, companions with orbital periods shorter than ~ 3 years are unlikely to be identified via PMA due to the time window smearing inherent in *Gaia* DR3. On the other hand, extremely long-period companions, spanning hundreds of years, are similarly challenging to detect, representing a limitation shared by VELOCE as well. Importantly, a PMA-False flag does not raise concerns about the SB1 detection. Among the 76 binary Cepheids in our sample, 19 have been reported to exhibit PMA signals (with binary flag ‘BinH2EG3b’ in Kervella et al. (2022) as 1). Evidence for astrometric orbital signals in form of the PMA has been reported for 10 of 33 SB1 (30%) Cepheids with orbital solutions presented here (including tentative ones) as well as for 8 of 30 (25%) SB1 systems with long-term v_γ trends exhibit PMA (Kervella et al. 2022). This also includes 2 of the newly discovered SB1 Cepheids, GX Car and V0659 Cen. Table D.1 lists the PMA binary flags from Kervella et al. (2022) for all stars in common with our sample.

Two systems with reported PMA, RZ Vel and SV Per, deserve a specific mention. For these two stars, we found no evidence of time-variable v_γ . However, SV Per is known to have a very nearby (0.2”) companion that has been resolved using *HST/WFC3* spatial scans (Riess et al. 2018) and which is most likely unresolved by *Gaia*. Time-variable contrast differences due to the Cepheid’s pulsation would affect the measurement of the photocenter for SV Per, which may lead to a spurious PMA signal.

Finally, we note that none of the Cepheids considered to be non-SB1s in VELOCE—stars without evidence for time-variable v_γ —have been reported to exhibit a significant PMA. Specifically, this is true for all stars without evidence for time-variable v_γ based on VELOCE data alone as well as our RVTF analysis (Sect. 3.4), including stars for which our results contradict previous claims of time-variable v_γ .

As this comparison shows, RVs from VELOCE and literature data standardized to the VELOCE zero-points provide the most complete evidence for orbital motion for Cepheids on timescales of up to a few decades. Nonetheless, we caution that signals on the order of 1 km s^{-1} and lower can be introduced also by modulated variability (Anderson 2014). CCF shape parameters, such as the bisector inverse span and full width at half maximum can be informative to this end (Anderson 2016) and will be considered in future work.

5.3. *Gaia* DR3 astrometric quality flags of SB1 Cepheids

Gaia DR3 reports several astrometric quality flags and parameters to aid the interpretation of the reported astrometric measurements. The Renormalized Unit Weight Error (RUWE) has received particular attention and is often considered an indicator of stellar multiplicity. RUWE is calculated as the square root of the normalized χ -square of the astrometric fit to the along-scan observations (Lindegren 2018), and the threshold of $\text{RUWE} < 1.4$ is frequently used to indicate well-behaved astrometric solutions (Lindegren et al. 2018, 2021). However, several factors can result in elevated RUWE, which does not identify the origin of the excess residuals and includes all possible sources of error in the fit to the astrometric model. The latter include any signals affecting photocenter stability, notably involving marginally resolved visual binaries and unmodeled astrometric orbital signals.

In Cepheids, the high-amplitude chromatic variability of Cepheids could also contribute to RUWE. For example, *Gaia* may automatically select different gating schemes and window classes depending on the momentaneous brightness of Cepheids that vary by ~ 1 mag in optical bands. Additionally, chromatic variability may lead to noise due to time-variable chromatic diffraction properties. Given these added difficulties, it is likely for RUWE to be elevated for Cepheids compared to non-variable stars. We therefore investigated to what degree excess RUWE and other astrometric quality indicators reported by *Gaia* may serve as an indicator of multiplicity for Cepheids.

Figure 13 shows the comparison of *Gaia* DR3 RUWE against the projected semimajor axis and P_{orb} . The figure shows a significant excess RUWE near $a \sin i$ values close to 1 au as 5 out of 8 stars with the highest RUWE ($\text{RUWE} > 2$) fall into this category (stars located within the dashed red lines in the left panel of Figure 13). Interestingly, a corresponding feature is not so clearly seen near $P_{\text{orb}} = 1$ yr, suggesting that the size of the orbital ellipse on the sky more directly affects the astrometric solution than the periodicity of the signal. The 6300 d binary with the highest RUWE of 7.8 is AX Cir, whose hot main sequence (likely B6V) companion has been resolved interferometrically (Gallenne et al. 2014b). A photometric contamination is the potential origin of the elevated *Gaia* RUWE.

Figure 14 shows RUWE in *Gaia* DR3 vs the amplitude of trends, A_{p2p} , determined using VELOCE data only in Sect. 4.2. Given that the majority of these orbital signals occur on timescales longer than the VELOCE baseline, it is not surprising that $\text{RUWE} < 1.4$ for the vast majority of these stars. The most significant outlier at $\text{RUWE} \sim 8$ is RW Cam, which was shown to feature a significant UV excess indicative of a hot main sequence companion (Stepien 1968). The star with the second highest RUWE of 1.7 is T Mon, host to a B9.8V companion detected directly from UV spectroscopy (Evans & Lyons 1994) but remained undetected interferometrically in *H*-band (Gallenne et al. 2019). These stars collectively indicate that elevated *Gaia* RUWE values in Cepheids may be attributed to unresolved companions rather than orbital motion.

Figure 15 shows the probability density function of RUWE for SB1 and non-SB1 Cepheids in VELOCE. Approximately 25% of VELOCE SB1s have a $\text{RUWE} > 1.4$ (see Table D.1). While there is a slightly higher probability for an SB1 Cepheid to have excess RUWE com-

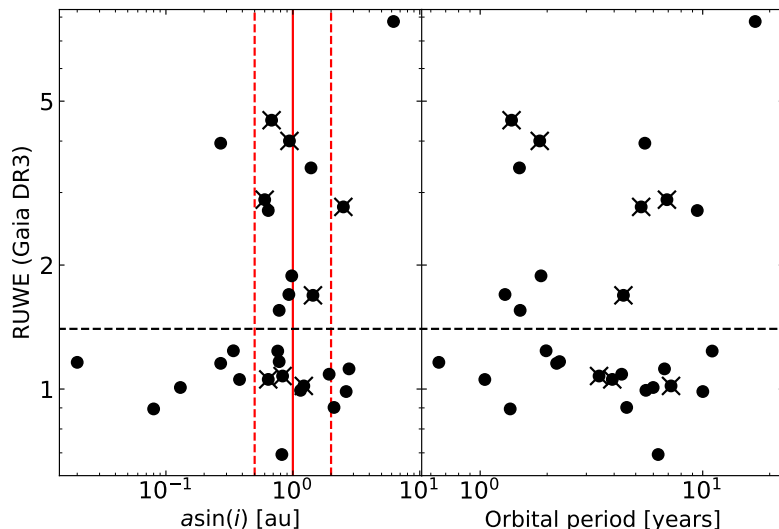


Fig. 13: Distribution of *Gaia* DR3 RUWE with the semi-major axis (left) and orbital period (right) of our sample systems. The stars tagged as binaries from PMA (Kervella et al. 2022) are marked with crosses. The red solid line indicates $a \sin i$ of 1 au, and the dashed red lines indicates the same at 0.5 and 2 au.

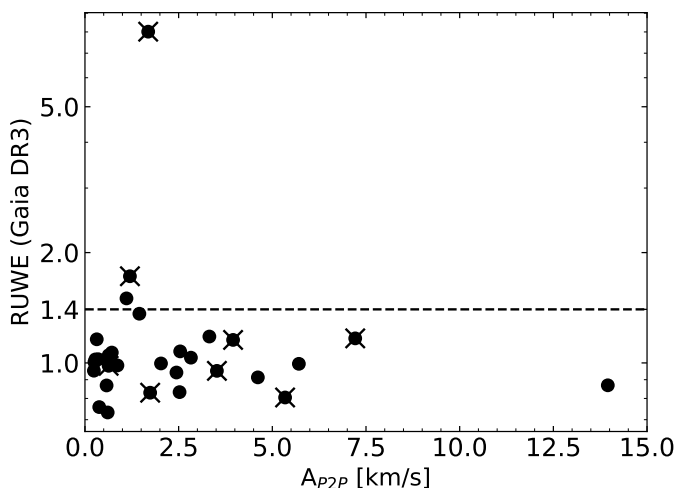


Fig. 14: Distribution of *Gaia* DR3 RUWE with the maximum amplitude of the (linear or non-linear) v_γ variation for SB1 systems with ‘Trend’. The stars tagged as binaries from PMA (Kervella et al. 2022) are marked with crosses.

pared to non-SB1 Cepheids, the difference is not very pronounced. Qualitatively, among the newly identified SB1 systems (RVTF), Figure 15 suggests similar probabilities near $\text{RUWE} \approx 1.7 - 1.8$. However, among these, β Dor’s extreme brightness ($m_V = 3.8$ mag) likely contributes substantially to the high RUWE of 4.5.

Finally, we also investigated the *Gaia* astrometric quality indicators `astrometric_gof_al` and `astrometric_excess_noise` as indicators of multiplicity of Cepheids. However, no significant trends appeared in this comparison aside from a mild increase in `astrometric_excess_noise` near $a \sin i \sim 1$ au.

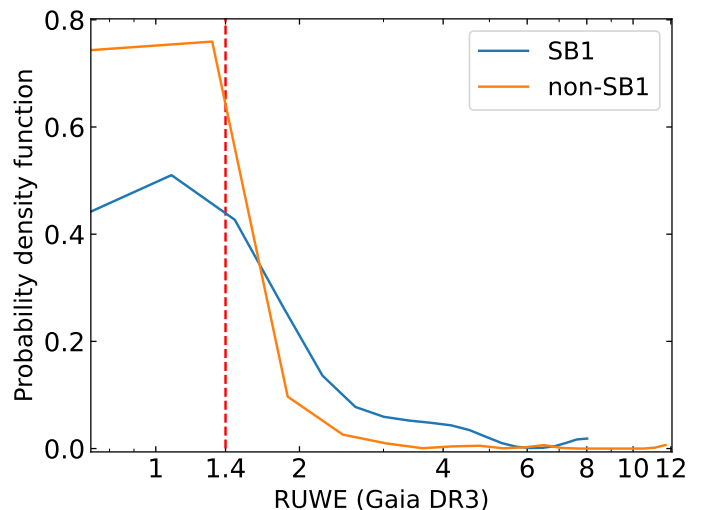


Fig. 15: Probability density function of *Gaia* DR3 RUWE for VELOCE SB1 and non-SB1 systems.

In summary, we find excess RUWE mainly for Cepheid binaries with projected semimajor axis close to 1 au. The parameter `astrometric_excess_noise` is also increased in this range, though the correlation is less clear. In addition to specific orbital configurations, elevated RUWE can arise from photocenter variations in unresolved binaries and in very bright stars, for example. Additionally, the majority of binary Cepheids are not identified by $\text{RUWE} > 1.4$.

5.4. Amplitude ratios as indicators of companion stars

Photometric amplitude ratios can be used to identify Cepheid companion stars in case the photometric contrast is sufficiently low (e.g. Madore 1977; Madore & Fernie 1980;

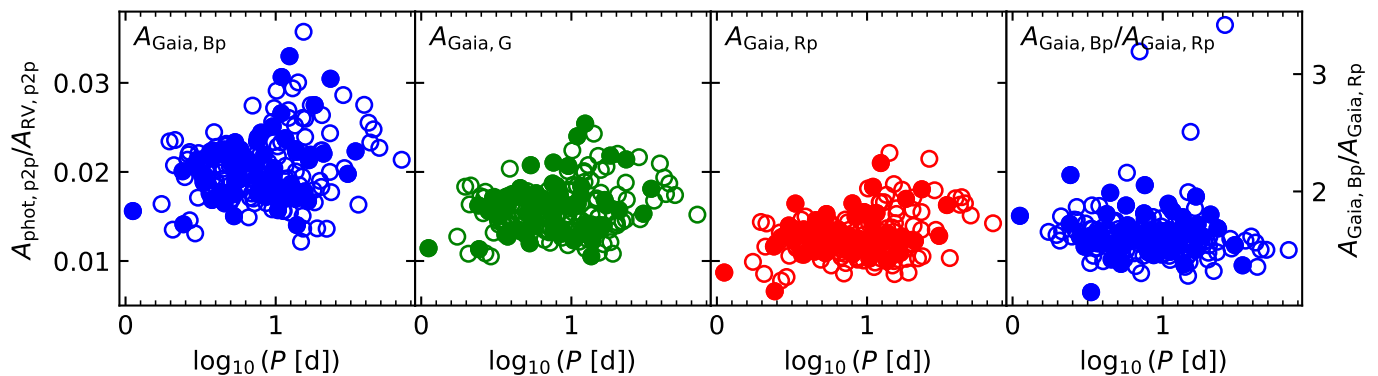


Fig. 16: *First three panels from left to right*: photometric-to-RV amplitude ratios from *Gaia* DR3 and VELOCE against the logarithmic pulsation period, with wavelength of the photometric band increasing from left to right. *Right panel*: ratio of *Gaia* photometric amplitudes in G_{Bp} to G_{Rp} . Filled circles show SB1 Cepheids reported in VELOCE. Other single-mode Cepheids observed by VELOCE are shown as open circles. There is no clear difference between SB1 Cepheids and all others in any of the amplitudes considered, nor a dependence of such a difference on $\log P_{\text{puls}}$.

Evans & Udalski 1994). Since most Cepheid companions are hot early-type stars, shorter-wavelength data is generally more sensitive to companions than longer-wavelength photometry. A noticeable exception are double-lined spectroscopic binaries (SB2) in the Large Magellanic Cloud that consist of a Cepheid and a giant companion (Pilecki et al. 2021).

In the Milky Way, Klagyivik & Szabados (2009) considered low ratios between photometric and RV amplitudes as an indicator for the presence of companion stars. Thanks to *Gaia*'s multi-band photometry, such a comparison is possible here using a large sample of stars. Figure 16 thus shows the ratio between *Gaia* photometric and VELOCE RV amplitudes in three bands (G_{Bp} , G , and G_{Rp}) as a function of the logarithmic pulsation period. The higher ratios at shorter wavelength are readily explained by the larger photometric amplitudes. SB1 Cepheids identified in VELOCE are shown as filled circles, and stars which are not SB1 systems are shown as open circles. As a consequence of the Cepheid period-color relation, the contrast between Cepheid and companion should increase toward longer periods, rendering photometric detection more difficult. Additionally, any signal in the amplitude ratio should be enhanced at shorter wavelengths. However, the comparison between SB1 Cepheids and all others observed in all three bands reveals no indication that bona fide SB1 Cepheids have reduced amplitudes compared to other Cepheids (Figure 16). The only potential signature is a slightly reduced range of amplitude ratios for SB1 Cepheids, which, however, clusters in the center of the distribution. The comparison between photometric amplitudes in G_{Bp} vs G_{Rp} (not shown) yields the same impression. Hence, we find that *Gaia*'s photometric amplitudes are not good indicators of Cepheid companions.

6. Discussion and Summary

We have presented the largest homogeneous investigation of 76 SB1 Cepheids to date based on the unprecedented RV data set provided by the VELOCE project (Paper I). An additional 14 SB1 candidates have been identified in Paper I, but are not discussed here due to their nature as candidate binaries. VELOCE data allow us to extend the search for binary Cepheids to fainter magnitudes, adding 32 new SB1

systems, and 18 first orbital determinations of Cepheids, 11 of which are fainter than $m_V > 8$ mag (cf. Figure 9). Thanks to these improvements, we sharpened the uncertainty on the SB1 fraction of Cepheids by a factor of ~ 2.3 .

We present 30 definitive and 3 tentative orbital solutions, which range from the discovery of the shortest P_{orb} in the Milky Way for R Cru (238 d) to ~ 17 yr (AX Cir), and also include a correction to the orbital solution of δ Cep. For 18 Cepheids, we estimate orbital solutions for the first time. VELOCE observations are particularly sensitive to $P_{\text{orb}} \lesssim 5$ yr, and the available temporal baselines differ from star to star. The ensemble of orbital solutions suggests two peculiar features in the $e - \log(P)$ diagram, which are a possible exclusion zone of low-eccentricity systems ($0 \leq e < 0.2$) at long orbital periods ($P_{\text{orb}} \gtrsim 10$ yr) as well as a dearth of stars with orbital period in the range of 2.5 – 3.5 yr. Further observations and a more detailed analysis of detection limits will be needed to confirm these features.

Based on our search for SB1 Cepheids and a detailed investigation of evidence for orbital signals using literature, we find a SB1 fraction of $29.6 \pm 3.4\%$. This is a lower limit since 14 SB1 candidates reported in Paper I were not considered in this fraction. Furthermore, we estimate the fraction of SB1 Cepheids with $P_{\text{orb}} < 10$ yr of $15.2 \pm 2.4\%$, half of which have P_{orb} of less than 2.5 years. Our binary fraction estimates agree with previous reports, albeit with 2 – 3 \times lower uncertainty. Of course, SB1 Cepheids are detectable mainly for orbital periods of < 100 yr, and other methods must be considered to estimate the total binary fraction of Cepheids. Considerable effort is currently underway to comprehensively determine the binary fraction of Cepheids, employing a diverse array of techniques such as astrometry, spectroscopy, interferometry, and observations across various wavelengths. For example, Evans et al. (2022) estimated a total binary fraction of $57 \pm 12\%$ based on SB1 Cepheids, and Cepheids with evidence for companions from X-ray and UV observations. It is worth noting that future *Gaia* data releases, particularly DR4 and DR5, will contribute significantly with an abundance of astrometric orbits, enriching our understanding of these systems even further.

Several of the SB1 Cepheids studied here are part of triple systems, including AW Per (Evans et al. 2000), FF Aql (Udalski & Evans 1993), S Sge (Evans et al. 1993),

V1334 Cyg (Abt & Levy 1970; Evans 1994), V0659 Cen (Evans et al. 2013, 2022), and W Sgr (Evans et al. 2009). Here, we further identify FO Car, RV Sco, RY Sco, and UX Per as triple systems with an inner SB1 and outer visual companion. Comparing the binary fraction and incidence of triples among Cepheids with dynamical NBODY simulations that assume an initial binary fraction of 100% (Dinnbier et al. 2024) suggests that a significant fraction of Cepheid progenitors (B-type stars) must be formed as triples or even higher-order systems.

Last, but not least, we find that the *Gaia* DR3 parallax quality indicator RUWE is elevated for Cepheid binaries whose projected semimajor axis, $a \sin i$, is close to 1 au. However, upon assessing RUWE for both SB1 and non-SB1 from VELOCE, we ascertain that *Gaia* RUWE is not a reliable indicator for identifying Cepheid spectroscopic binaries and can be noticeably affected by photometric systematics, such as marginally resolved binaries or high apparent brightness. Additionally, RUWE tends to be slightly higher for Cepheids than for non-variable stars.

An examination of PMA in relation to various orbital properties of our stars does not reveal any correlation between the orbital orientation and PMA detection. Furthermore, all VELOCE Cepheids with previously reported PMA detections are also identified to be SB1 systems.

Precision radial velocities provide the most sensitive diagnostic of multiplicity of Cepheids to date. Future *Gaia* data releases will allow to determine systemic masses of Cepheids using the combined astrometric and spectroscopic orbital signals. In *Gaia* DR3, only one Cepheid was reported with a non-single-star astrometric solution. Suspiciously, the orbital period of RX Cam was given as 33 months, matching exactly the observational baseline of *Gaia* DR3. However, RX Cam was unfortunately not observed as part of the VELOCE project. The upcoming fourth *Gaia* data release in combination with VELOCE data will be a treasure trove for determining accurate Cepheid masses and to establish a well-sampled mass-luminosity relation required to elucidate the physics of Cepheids, notably with respect to mixing processes, such as convection and rotation, required to explain the mass discrepancy problem (e.g. Prada Moroni et al. 2012; Anderson 2014).

Acknowledgments

RIA, SS, and GV acknowledge support from the European Research Council (ERC) under the European Union's Horizon 2020 research and innovation programme (Grant Agreement No. 947660). RIA, and SS further acknowledge support through a Swiss National Science Foundation Eccellenza Professorial Fellowship (award PCEFP2_194638). SS would further like to extend their acknowledgement to the Research Foundation-Flanders (grant number: 1239522N). This work has made use of data from the European Space Agency (ESA) mission *Gaia* (<https://www.cosmos.esa.int/gaia>), processed by the *Gaia* Data Processing and Analysis Consortium (DPAC, <https://www.cosmos.esa.int/web/gaia/dpac/consortium>). Funding for the DPAC has been provided by national institutions, in particular the institutions participating in the *Gaia* Multilateral Agreement. The lead authors would like to acknowledge the very useful compilation of information on binary Cepheids provided by Laszlo Szabados at Konkoly Observatory (Szabados (2003), <https://cep.konkoly.hu/intro.html>).

References

- Abt, H. A. & Levy, S. G. 1970, *PASP*, 82, 334
 Anderson, R. I. 2013, PhD thesis, Université de Genève
 Anderson, R. I. 2014, *A&A*, 566, L10
 Anderson, R. I. 2016, *MNRAS*, 463, 1707
 Anderson, R. I. 2019, *A&A*, 623, A146
 Anderson, R. I. 2020, Proc. conf. Stars and their Variability Observed from Space, eds. C. Neiner, W. W. Weiss, D. Baade, R. E. Griffin, C. C. Lovekin, & A. J. Moffat, Univ. of Vienna, pp. 61-66 [[arXiv:2001.03028](https://arxiv.org/abs/2001.03028)]
 Anderson, R. I., Casertano, S., Riess, A. G., et al. 2016a, *ApJS*, 226, 18
 Anderson, R. I., Eyer, L., & Mowlavi, N. 2013, *MNRAS*, 434, 2238
 Anderson, R. I., Mérand, A., Kervella, P., et al. 2016b, *MNRAS*, 455, 4231
 Anderson, R. I. & Riess, A. G. 2018, *ApJ*, 861, 36
 Anderson, R. I., Sahlmann, J., Holl, B., et al. 2015, *ApJ*, 804, 144
 Anderson, R. I., Saio, H., Ekström, S., Georgy, C., & Meynet, G. 2016c, *A&A*, 591, A8
 Anderson, R. I., Viviani, G., Shreeya Shetye, S., et al. 2024, *arXiv e-prints*, [arXiv:2404.12280](https://arxiv.org/abs/2404.12280)
 Arellano-Ferro, A. & Madore, B. F. 1985, *The Observatory*, 105, 207
 Babel, J., Burki, G., Mayor, M., Chmielewski, Y., & Waelkens, C. 1989, *A&A*, 216, 125
 Barnes, III, T. G., Jeffery, E. J., Montemayor, T. J., & Skillen, I. 2005, *ApJS*, 156, 227
 Barnes, III, T. G., Moffett, T. J., & Slovak, M. H. 1987, *ApJS*, 65, 307
 Belokurov, V., Penoyre, Z., Oh, S., et al. 2020, *MNRAS*, 496, 1922
 Benedict, G. F., Barnes, T. G., Evans, N. R., et al. 2022, *AJ*, 163, 282
 Bersier, D. 2002, *ApJS*, 140, 465
 Bersier, D., Burki, G., Mayor, M., & Duquenois, A. 1994, *A&AS*, 108, 25
 Binnenfeld, A., Shahaf, S., Anderson, R. I., & Zucker, S. 2022, *A&A*, 659, A189
 Borgniet, S., Kervella, P., Nardetto, N., et al. 2019, *A&A*, 631, A37
 Breitfelder, J., Mérand, A., Kervella, P., et al. 2016, *A&A*, 587, A117
 Burki, G., Mayor, M., & Benz, W. 1982, *A&A*, 109, 258
 Caputo, F., Bono, G., Fiorentino, G., Marconi, M., & Musella, I. 2005, *ApJ*, 629, 1021
 Coulson, I. M. & Caldwell, J. A. R. 1985, *South African Astronomical Observatory Circular*, 9, 5
 Csörnyei, G., Szabados, L., Molnár, L., et al. 2022, *MNRAS*, 511, 2125
 Dinnbier, F., Anderson, R. I., & Kroupa, P. 2024, under review in *A&A*
 Ekström, S., Georgy, C., Eggenberger, P., et al. 2012, *A&A*, 537, A146
 Evans, N. R., Bond, H. E., Schaefer, G. H., et al. 2013, *AJ*, 146, 93
 Evans, N. R. 1988, *ApJS*, 66, 343
 Evans, N. R. 1991, *ApJ*, 372, 597
 Evans, N. R. 1992, *ApJ*, 384, 220
 Evans, N. R. 1994, *ApJ*, 436, 273
 Evans, N. R. 1995, *ApJ*, 445, 393
 Evans, N. R. 2000, *AJ*, 119, 3050
 Evans, N. R., Arellano Ferro, A., & Udalska, J. 1992, *AJ*, 103, 1638
 Evans, N. R., Berdnikov, L., Lauer, J., et al. 2015, *AJ*, 150, 13
 Evans, N. R., Engle, S., Pillitteri, I., et al. 2022, *ApJ*, 938, 153
 Evans, N. R., Günther, H. M., Bond, H. E., et al. 2020, *ApJ*, 905, 81
 Evans, N. R. & Lyons, R. W. 1994, *AJ*, 107, 2164
 Evans, N. R., Massa, D., & Proffitt, C. 2009, *AJ*, 137, 3700
 Evans, N. R., Szabados, L., & Udalska, J. 1990, *PASP*, 102, 981
 Evans, N. R. & Udalski, A. 1994, *AJ*, 108, 653
 Evans, N. R., Vinko, J., & Wahlgren, G. M. 2000, *AJ*, 120, 407
 Evans, N. R., Welch, D. L., Slovak, M. H., Barnes, Thomas G., I., & Moffett, T. J. 1993, *AJ*, 106, 1599
 Ford, E. B. 2005, *AJ*, 129, 1706
 Ford, E. B. 2006, *ApJ*, 642, 505
 Foreman-Mackey, D., Hogg, D. W., Lang, D., & Goodman, J. 2013, *PASP*, 125, 306
 Fulton, B. J., Petigura, E. A., Blunt, S., & Sinukoff, E. 2018, *Publications of the Astronomical Society of the Pacific*, 130, 044504
 Gaia Collaboration, Arenou, F., Babusiaux, C., et al. 2022, *arXiv e-prints*, [arXiv:2206.05595](https://arxiv.org/abs/2206.05595)
 Gaia Collaboration, Brown, A. G. A., Vallenari, A., et al. 2018, *A&A*, 616, A1
 Gaia Collaboration, Brown, A. G. A., Vallenari, A., et al. 2021, *A&A*, 649, A1
 Gaia Collaboration, Brown, A. G. A., & Vallenari, A. e. a. 2016a, *A&A*, 595, A2

- Gaia Collaboration, Prusti, T., de Bruijne, J. H. J., & et al. 2016b, *A&A*, 595, A1
- Gallenne, A., Kervella, P., Borgniet, S., et al. 2019, *A&A*, 622, A164
- Gallenne, A., Kervella, P., Evans, N. R., et al. 2018, *ApJ*, 867, 121
- Gallenne, A., Kervella, P., Mérand, A., et al. 2014a, in *Precision Astero-seismology*, ed. J. A. Guzik, W. J. Chaplin, G. Handler, & A. Pigulski, Vol. 301, 411–412
- Gallenne, A., Mérand, A., Kervella, P., et al. 2014b, *A&A*, 561, L3
- Gallenne, A., Mérand, A., Kervella, P., et al. 2015, *A&A*, 579, A68
- Gallenne, A., Mérand, A., Kervella, P., et al. 2016, *MNRAS*, 461, 1451
- Gallenne, A., Monnier, J. D., Mérand, A., et al. 2013, *A&A*, 552, A21
- Genovali, K., Lemasle, B., Bono, G., et al. 2014, *A&A*, 566, A37
- Gieren, W. 1982, *ApJS*, 49, 1
- Gieren, W. P. 1985, *ApJ*, 295, 507
- Gorynya, N. A., Irsamambetova, T. R., Rastorguev, A. S., & Samus, N. N. 1992, *Soviet Astronomy Letters*, 18, 316
- Gorynya, N. A., Rastorguev, A. S., & Samus, N. N. 1996a, *Astronomy Letters*, 22, 33
- Gorynya, N. A., Samus', N. N., Rastorguev, A. S., & Sachkov, M. E. 1996b, *Astronomy Letters*, 22, 175
- Griffin, R. F. 2016, *The Observatory*, 136, 209
- Groenewegen, M. A. T. 2008, *A&A*, 488, 25
- Hertzsprung, E. 1913, *Astronomische Nachrichten*, 196, 201
- Hilditch, R. W. 2001, *An Introduction to Close Binary Stars* (Cambridge Univ. Press)
- Hintz, E. G., Harding, T. B., & Hintz, M. L. 2021, *AJ*, 162, 149
- Imbert, M. 1984, *A&AS*, 58, 529
- Karczmarek, P., Smolec, R., Hajdu, G., et al. 2022, *ApJ*, 930, 65
- Kervella, P., Arenou, F., Mignard, F., & Thévenin, F. 2019a, *A&A*, 623, A72
- Kervella, P., Arenou, F., & Thévenin, F. 2022, *A&A*, 657, A7
- Kervella, P., Gallenne, A., Remage Evans, N., et al. 2019b, *A&A*, 623, A116
- Khan, S., Anderson, R. I., Miglio, A., Mosser, B., & Elsworth, Y. P. 2023, *A&A*, 680, A105
- Kiss, L. L. 1998, *MNRAS*, 297, 825
- Kiss, L. L. & Bedding, T. R. 2005, *MNRAS*, 358, 883
- Klagyivik, P. & Szabados, L. 2009, *A&A*, 504, 959
- Kovtyukh, V., Lemasle, B., Bono, G., et al. 2022, *MNRAS*, 510, 1894
- Kovtyukh, V., Szabados, L., Chekhonadskikh, F., Lemasle, B., & Belik, S. 2015, *MNRAS*, 448, 3567
- Leavitt, H. S. & Pickering, E. C. 1912, *Harvard College Observatory Circular*, 173, 1
- Lindgren, L. 2018, *gAIA-C3-TN-LU-LL-124*
- Lindgren, L., Hernández, J., Bombrun, A., et al. 2018, *A&A*, 616, A2
- Lindgren, L., Klioner, S. A., Hernández, J., et al. 2021, *A&A*, 649, A2
- Lloyd Evans, T. 1968, *MNRAS*, 141, 109
- Lloyd Evans, T. 1980, *South African Astronomical Observatory Circular*, 1, 257
- Lloyd Evans, T. 1982, *MNRAS*, 199, 925
- Luck, R. E. & Lambert, D. L. 2011, *AJ*, 142, 136
- Madore, B. F. 1977, *MNRAS*, 178, 505
- Madore, B. F. & Fernie, J. D. 1980, *PASP*, 92, 315
- Michalik, D., Lindgren, L., & Hobbs, D. 2015, *A&A*, 574, A115
- Mochejska, B. J., Macri, L. M., Sasselov, D. D., & Stanek, K. Z. 2000, *AJ*, 120, 810
- Molnár, L., Derekas, A., Szabó, R., et al. 2017, *MNRAS*, 466, 4009
- Moore, J. H. 1929, *PASP*, 41, 56
- Nardetto, N., Hocdé, V., Kervella, P., et al. 2024, *A&A*, 684, L9
- Neilson, H. R., Schneider, F. R. N., Izzard, R. G., Evans, N. R., & Langer, N. 2015, *A&A*, 574, A2
- Perryman, M. A. C., Lindgren, L., Kovalevsky, J., et al. 1997, *A&A*, 323, L49
- Petterson, O. K. L., Cottrell, P. L., & Albrow, M. D. 2004, *MNRAS*, 350, 95
- Pilecki, B., Pietrzyński, G., Anderson, R. I., et al. 2021, *ApJ*, 910, 118
- Poggio, E., Drimmel, R., Cantat-Gaudin, T., et al. 2021, *A&A*, 651, A104
- Pont, F., Mayor, M., & Burki, G. 1994, *A&A*, 285, 415
- Prada Moroni, P. G., Gennaro, M., Bono, G., et al. 2012, *ApJ*, 749, 108
- Proust, D., Ochsenbein, F., & Pettersen, B. R. 1981, *A&AS*, 44, 179
- Queloz, D., Mayor, M., Udry, S., et al. 2001, *The Messenger*, 105, 1
- Raskin, G., van Winckel, H., Hensberge, H., et al. 2011, *A&A*, 526, A69
- Riess, A. G., Casertano, S., Yuan, W., et al. 2018, *ApJ*, 861, 126
- Russo, G., Sollazzo, C., & Coppola, M. 1981, *A&A*, 102, 20
- Shetye, S. 2022, *Video Memorie della Societa Astronomica Italiana*, 2, 20
- Stassun, K. G. & Torres, G. 2021, *ApJ*, 907, L33
- Stepien, K. 1968, *Acta Astron.*, 18, 537
- Storm, J., Carney, B. W., Gieren, W. P., et al. 2004, *A&A*, 415, 531
- Szabados, L. 1989, *Communications of the Konkoly Observatory Hungary*, 94, 1
- Szabados, L. 1992, *The Observatory*, 112, 57
- Szabados, L. 1996, *A&A*, 311, 189
- Szabados, L. 2003, *Information Bulletin on Variable Stars*, 5394
- Szabados, L., Anderson, R. I., Derekas, A., et al. 2013a, *MNRAS*, 434, 870
- Szabados, L., Cseh, B., Kovács, J., et al. 2014, *MNRAS*, 442, 3155
- Szabados, L., Derekas, A., Kiss, L. L., et al. 2013b, *MNRAS*, 430, 2018
- Szabados, L. & Pont, F. 1998, *A&AS*, 133, 51
- Szatmary, K. 1990, *JAAVSO*, 19, 52
- Torres, G. 2023, *MNRAS*, 526, 2510
- Turner, D. G., Bryukhanov, I. S., Balyuk, I. I., et al. 2007, *PASP*, 119, 1247
- Udalski, A. & Evans, N. R. 1993, *AJ*, 106, 348
- Vinko, J. 1991, *Ap&SS*, 183, 17
- Virtanen, P., Gommers, R., Oliphant, T. E., et al. 2020, *Nature Methods*, 17, 261
- Wahlgren, G. M. & Evans, N. R. 1998, *A&A*, 332, L33
- Wilson, T. D., Carter, M. W., Barnes, III, T. G., van Citters, Jr., G. W., & Moffett, T. J. 1989, *ApJS*, 69, 951
- Zhou, A. Y. 2010, *arXiv e-prints*, arXiv:1002.2729

Table 3: Orbital elements of the new spectroscopic binary Cepheids' orbits presented in this work. Table notes are provided at the end of Table 4.

Cepheid	P_{puls} (d)	$T_0-2.4M$	data	P_{orb} (d) $\sigma_{P_{orb}}$	e σ_e	K (km s ⁻¹) σ_K	$a \sin i$ (au) σ_{asini}	f_{mass} $\sigma_{f_{mass}}$	ω (deg) $\sigma_{argperi}$	M_1 M_\odot	rms (km s ⁻¹)
New orbits from current work											
ASAS	3.0147	59 013.59	V	901.18	0.444	5.810	0.4313	1.3×10^{-2}	203.14	5.0	0.13
J064540+0330.4		2.67	B.1	2.81	0.011	0.059	0.0052	4.7×10^{-4}	1.39		
ASAS	3.7889	57 854.64	V	1578.27	0.432	14.760	1.9314	3.9×10^{-1}	145.44	4.9	0.26
J084951-4627.2		6.60	B.2	3.41	0.005	0.158	0.0218	1.3×10^{-2}	1.37		
ASAS	3.7665	58 067.71	V	2458.57	0.454	13.777	2.7740	4.7×10^{-1}	20.85	4.2	0.23
J100814-5856.6		1.79	B.3	1.22	0.004	0.083	0.0179	9.1×10^{-3}	0.29		
ASAS	2.5724	58 980.80	V	2302.73	0.358	4.145	0.8192	1.4×10^{-2}	344.02	4.9	0.22
J174603-3528.1		97.27	B.4	41.74	0.153	1.476	0.2966	1.5×10^{-2}	13.49		
FN Vel	5.3242	56 407.87	V	471.79	0.218	21.908	0.9273	4.8×10^{-1}	42.07	6.4	0.16
		0.36	B.7	0.06	0.001	0.025	0.0011	1.7×10^{-3}	0.21		
FO Car	10.3569	58 244.27	V	1667.57	0.378	14.932	2.1194	4.6×10^{-1}	85.26	6.1	0.16
		2.99	B.8	2.82	0.002	0.030	0.0059	3.1×10^{-3}	0.59		
		58 244.89	V+L	1662.25	0.378	14.911	2.1096	4.5×10^{-1}	85.72		0.58
		1.81	C.5	1.57	0.002	0.025	0.0044	2.6×10^{-3}	0.27		
GX Car	7.1969	56 836.78	V	2630.34	0.038	5.034	1.2163	3.5×10^{-2}	6.69	5.6	0.12
		32.46	B.9	5.82	0.003	0.017	0.0049	3.6×10^{-4}	4.44		
IT Car	7.5330	59 460.47	V	1249.33	0.584	8.934	0.8327	4.9×10^{-2}	116.70	6.0	0.09
		0.66	B.10	0.79	0.002	0.025	0.0028	4.9×10^{-4}	0.20		
MU Cep	3.7678	56 071.16	V	2028.14	0.434	6.880	1.1552	5.0×10^{-2}	10.29	5.8	0.19
		3.02	B.11	2.70	0.004	0.035	0.0066	8.3×10^{-4}	0.68		
MY Pup	5.6941	57 936.81	V	2082.44	0.103	0.671	0.1277	6.4×10^{-5}	80.71	5.0	0.12
		431.76	B.12	54.54	0.052	0.023	0.0056	6.9×10^{-6}	84.82		
		57 974.90	V+L	2186.14	0.141	0.654	0.1300	6.1×10^{-5}	91.59		0.31
		39.93	C.6	10.44	0.010	0.008	0.0018	2.4×10^{-6}	7.95		
NT Pup	15.5603	56 679.13	V	3653.65	0.466	8.838	2.6268	1.8×10^{-1}	205.92	9.7	0.41
		6.43	3	17.42	0.005	0.052	0.0214	3.7×10^{-3}	0.64		
R Cru	5.8257	57 292.65	V	237.42	0.017	1.029	0.0224	2.7×10^{-5}	205.14	5.5	0.16
		26.80	B.13	0.14	0.013	0.012	0.0003	9.5×10^{-7}	34.00		
		57 158.38	V+L	237.62		0.999	0.0218	2.5×10^{-5}			0.25
		0.17	C.7	0.03		0.003	0.0001	2.5×10^{-7}			
V0407 Cas	4.5661	57 445.28	V	498.36	0.307	1.864	0.0812	2.9×10^{-4}	102.46	5.3	0.09
		11.76	B.19	0.83	0.041	0.153	0.0068	7.2×10^{-5}	12.37		
VY Per	5.5319	57 861.60	V	806.18	0.382	3.835	0.2626	3.7×10^{-3}	108.71	5.0	0.08
		10.45	B.21	0.78	0.015	0.083	0.0060	2.5×10^{-4}	2.32		
		57 858.11	V+L	805.08	0.369	3.928	0.2702	4.1×10^{-3}	109.34		0.45
		15.58	C.17	0.63	0.020	0.127	0.0091	4.1×10^{-4}	4.17		
VZ Pup	23.1743	58 234.08	V	3674.13	0.151	2.036	0.6798	3.1×10^{-3}	128.74	8.3	0.38
		241.00	B.22	222.86	0.036	0.054	0.0452	3.2×10^{-4}	9.43		
		58 184.47	V+L	4026.33	0.251	2.112	0.7566	3.6×10^{-3}	126.95		0.58
		21.25	C.18	17.82	0.007	0.013	0.0060	7.1×10^{-5}	1.35		
New 'Tentative' orbits from current work											
BP Cir	2.3981	55 730.42	V+L	4339.48	0.779	2.185	0.5463	1.2×10^{-3}	228.69		0.35
		11.60	C.2	8.49	0.006	0.055	0.0153	9.7×10^{-5}	0.81		
R Mus	7.5103	58 352.07	V+L	4446.72	0.551	1.694	0.5779	1.3×10^{-3}	220.23		1.75
		19.28	C.8	19.04	0.005	0.009	0.0045	2.6×10^{-5}	1.15		
V0659 Cen	5.6240	52 812.11	V+L	9276.06	0.323	8.260	6.6651	4.6×10^{-1}	182.52		0.86
		81.52	C.15	130.38	0.052	1.519	1.2358	2.5×10^{-1}	0.90		

Table 4: Orbital elements of VELOCE SB1 Cepheids with literature-known orbits.

Cepheid	P_{puls} (d)	$T_{0-2.4M}$	data	P_{orb} (d)	e	K (km s ⁻¹)	$a \sin i$ (au)	fmass	ω (deg)	M_1	rms
				$\sigma_{P_{orb}}$	σ_e	σ_K	σ_{asini}	σ_{fmass}	$\sigma_{argperi}$	M_\odot	(km s ⁻¹)
Update to literature-known SB1s orbits											
AX Cir	5.2734	54 483.59	V+L	6284.51	0.187	10.954	6.2167	8.1×10^{-1}	211.34	5.0	1.76
		33.04	C.1	12.41	0.009	0.229	0.1311	5.1×10^{-2}	1.21		
δ Cep	5.3663	58 696.03	V	3450.96	0.745	3.012	0.6367	2.9×10^{-3}	242.75	5.0	0.09
		13.61	2	19.57	0.006	0.018	0.0081	9.9×10^{-5}	0.56		
DL Cas	8.0009	58 113.85	V	684.89	0.344	16.656	0.9846	2.7×10^{-1}	25.92	7.1	0.30
		1.00	B.5	0.21	0.005	0.098	0.0061	5.0×10^{-3}	0.60		
		57 434.67	V+L	684.67	0.341	16.343	0.9668	2.6×10^{-1}	29.25		1.43
		0.99	C.3	0.06	0.004	0.102	0.0062	5.0×10^{-3}	0.61		
FF Aql	4.4710	58 253.28	V	1433.20	0.050	4.788	0.6300	1.6×10^{-2}	304.87	5.8	0.14
		35.41	B.6	5.66	0.011	0.028	0.0045	3.0×10^{-4}	6.55		
		58 302.23	V+L	1431.70	0.068	4.877	0.6403	1.7×10^{-2}	317.41		3.68
		7.86	C.4	0.55	0.004	0.014	0.0019	1.5×10^{-4}	2.02		
S Mus	9.6600	56 663.89	V	505.27	0.087	14.786	0.6842	1.7×10^{-1}	197.92	6.0	0.09
		1.39	B.14	0.09	0.002	0.019	0.0009	6.5×10^{-4}	0.96		
		56 152.57	V+L	505.16	0.081	14.777	0.6839	1.7×10^{-1}	194.11		2.18
		2.43	C.9	0.09	0.004	0.020	0.0009	6.8×10^{-4}	1.75		
S Sge	8.3821	58 141.06	V	675.84	0.236	15.525	0.9371	2.4×10^{-1}	200.47	6.0	0.25
		2.16	B.15	0.27	0.003	0.071	0.0044	3.3×10^{-3}	0.98		
		57 468.20	V+L	676.01	0.248	15.626	0.9407	2.4×10^{-1}	201.53		1.98
		1.19	C.10	0.06	0.003	0.050	0.0031	2.4×10^{-3}	0.54		
SU Cyg	3.8458	56 395.19	V+L	548.26	0.342	29.444	1.3944	1.2	220.48	5.2	3.28
		1.74	C.11	0.10	0.005	0.218	0.0107	2.8×10^{-2}	1.57		
SY Nor	12.6452	57 784.70	V	551.92	0.001	15.329	0.7777	2.1×10^{-1}	255.16	6.8	0.24
		321.35	B.16	0.77	0.003	0.055	0.0030	2.2×10^{-3}	196.34		
		57 945.67	V+L	551.96		15.335	0.7781	2.1×10^{-1}			0.49
		0.16	C.12	0.06		0.013	0.0007	5.3×10^{-4}			
TX Mon	8.7021	59 204.55	V	1602.20	0.583	11.985	1.4338	1.5×10^{-1}	295.49	7.1	0.18
		4.50	B.17	2.47	0.004	0.124	0.0157	5.0×10^{-3}	0.45		
		57 599.41	V+L	1606.98	0.585	11.980	1.4359	1.5×10^{-1}	295.12		0.73
		1.91	C.13	0.91	0.002	0.048	0.0061	1.9×10^{-3}	0.26		
U Vul	7.9907	59 935.90	V	2528.77	0.551	3.154	0.6120	4.8×10^{-3}	1.37	7.1	0.12
		5.28	B.18	8.57	0.005	0.045	0.0094	2.2×10^{-4}	0.69		
		57 404.92	V+L	2521.23	0.555	3.133	0.6039	4.6×10^{-3}	359.36		1.02
		2.47	4	0.94	0.003	0.017	0.0036	8.1×10^{-5}	0.33		
V1334 Cyg	3.3325	57 172.49	V	1947.79	0.229	14.208	2.4763	5.3×10^{-1}	227.11	5.2	0.05
		1.74	B.20	2.08	0.001	0.037	0.0070	4.2×10^{-3}	0.37		
		57 186.80	V+L	1931.17	0.236	14.492	2.4999	5.6×10^{-1}	231.09		0.89
		2.62	C.16	1.12	0.003	0.049	0.0087	5.8×10^{-3}	0.56		
W Sgr	7.5951	58 121.40	V	2006.30	0.272	1.507	0.2675	6.3×10^{-4}	317.92	5.5	0.20
		26.28	B.23	17.78	0.039	0.013	0.0045	2.8×10^{-5}	4.43		
XX Cen	10.9520	58 211.33	V	722.44	0.295	5.396	0.3424	1.0×10^{-2}	283.11	6.4	0.12
		1.66	B.24	0.42	0.004	0.026	0.0017	1.6×10^{-4}	0.92		
YZ Car	18.1696	57 936.96	V	827.20	0.029	10.380	0.7889	9.6×10^{-2}	352.67	7.4	0.24
		38.68	B.25	1.21	0.004	0.062	0.0048	1.7×10^{-3}	16.68		
		57 120.73	V+L	830.02		10.191	0.7776	9.1×10^{-2}			1.87
		0.15	C.14	0.11		0.009	0.0007	2.3×10^{-4}			
Z Lac	10.8859	58 534.56	V	382.77	0.014	10.774	0.3790	5.0×10^{-2}	65.01	8.0	0.10
		54.21	B.26	0.14	0.020	0.322	0.0113	4.4×10^{-3}	43.45		

Notes. The pulsation period and epoch are retrieved after the RV fitting following the method described in Paper 1. In column 4, ‘V’ denotes when the orbits were strictly fitted with VELOCE data alone, while ‘V+L’ denotes when the orbit was fitted using the combination of v_r residuals from VELOCE and literature datasets (See Section 3.2 for more details). The second row in the ‘data’ column contains links to the orbital fit figures presented in the paper. The next columns list the different orbital elements, namely, orbital period (P_{orb}), eccentricity (e), semi-amplitude (K), projected semi-major axis ($a \sin i$), mass function (fmass), argument of periastron (ω). We estimated the individual Cepheid masses (M_1) using period-mass relations based on Geneva stellar evolution models (Ekström et al. 2012), our method was similar to the one described in Anderson et al. (2016a). The last column presents the ‘rms’ (root mean square) of the fit between the Fourier+Keplerian model and the RV data for ‘V’ orbits and between the keplerian model and epoch residuals for ‘V+L’ orbits.

Table 5: List of SB1 from our sample where we found some evidence of orbital motion, and a polynomial was fitted as the orbit could not be sampled/covered adequately.

Cepheid	deg	A_{p2p} (km s^{-1})	ΔT_{p2p} (d)	Trend
SB1s discovered in the current work				
AQ Pup	3	3.32	2500	up
ASAS J064553+1003.8	3	1.11	2347	down
ASAS J103158-5814.7	4	13.95	3658	down
ASAS J155847-5341.8	1	0.58	3587	down
ASAS J174108-2328.5	1	0.38	2533	up
DR Vel	2	0.25	1657	down
OX Cam	1	0.87	2549	down
RY Sco	1	0.61	2646	up
RY Vel	6	2.54	2126	up
SX Vel	1	0.28	2140	up
V0391 Nor	2	2.52	3511	down
V0492 Cyg	2	2.03	1895	up
V0827 Cas	1	0.31	2568	up
V1162 Aql	2	0.24	656	up
V1803 Aql	1	2.44	3635	down
V2475 Cyg	2	5.71	3404	down
Literature-known SB1s				
AD Pup	4	1.45	818	down
AH Vel	1	1.74	2126	up
AQ Car	1	0.72	2817	down
AW Per	1	3.95	2567	down
FR Car	1	0.35	2116	up
KN Cen	3	2.83	2857	down
LR TrA	3	3.52	3664	up
RV Sco	2	5.34	3429	up
RW Cam	1	1.69	2680	up
RX Aur	1	0.63	1224	up
T Mon	1	1.20	3841	up
UX Per	2	7.21	3657	down
UZ Sct	4	4.61	1426	up
XZ Car	1	0.63	3658	up

Notes. Column 2 represents the degree of polynomial used in our analysis, Column 3 lists the peak-to-peak amplitude of the (linear or non-linear) v_y variation and Column 4 lists the timeline (in days) over which this amplitude was computed. The last column indicates the direction of the trend, up for increasing velocity, down for decreasing.

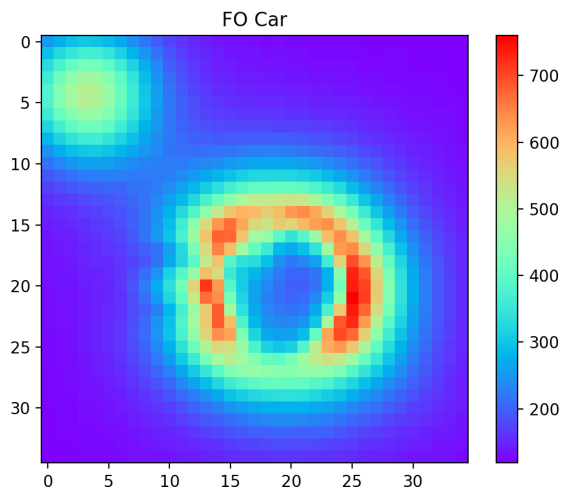


Fig. A.1: *Coralie* guiding camera image of FO Car. The center of the Cepheid is dark because of the fiber placement during the integration. The object at the top left is an outer (visual) companion, which renders the SB1 Cepheid FO Car a triple system.

Appendix A: Guiding camera Image

When available, the *Coralie* and *Hermes* guiding camera images were utilized to examine for triple systems. In Figure A.1, we present a guiding camera image of FO Car obtained from *Coralie*.

Appendix B: Orbital fitting

From Figure B.1 to B.26, we present all the orbital fits obtained using VELOCE data alone. The orbital fittings were derived using the method described in Section 3.2.

Appendix C: V_γ Orbits

In Figure C.1 to Figure C.18 we present the orbital fittings obtained using the combination of RV data from VELOCE and literature datasets. These orbital fits were derived using the MCMC method described in Section 3.2.

Appendix D: Gaia astrometry

In Table D.1, we present all the *Gaia* RUWE and PMA flags used in this study for all our sample stars.

Appendix E: RV Template fits after zero-point offset correction for sample stars with no signs of SB1

Figures E.1 and E.1 showcase the long-term trends in v_γ for sample stars where we find no signs of binarity through the RVTF analysis of Section 3.4.

Appendix F: SU Cyg RVTF

In Table F.1, we present the zero-point corrected v_γ residuals (ϵ_{v_γ}) of SU Cyg. The details of how these were obtained are provided in Section 4.5.

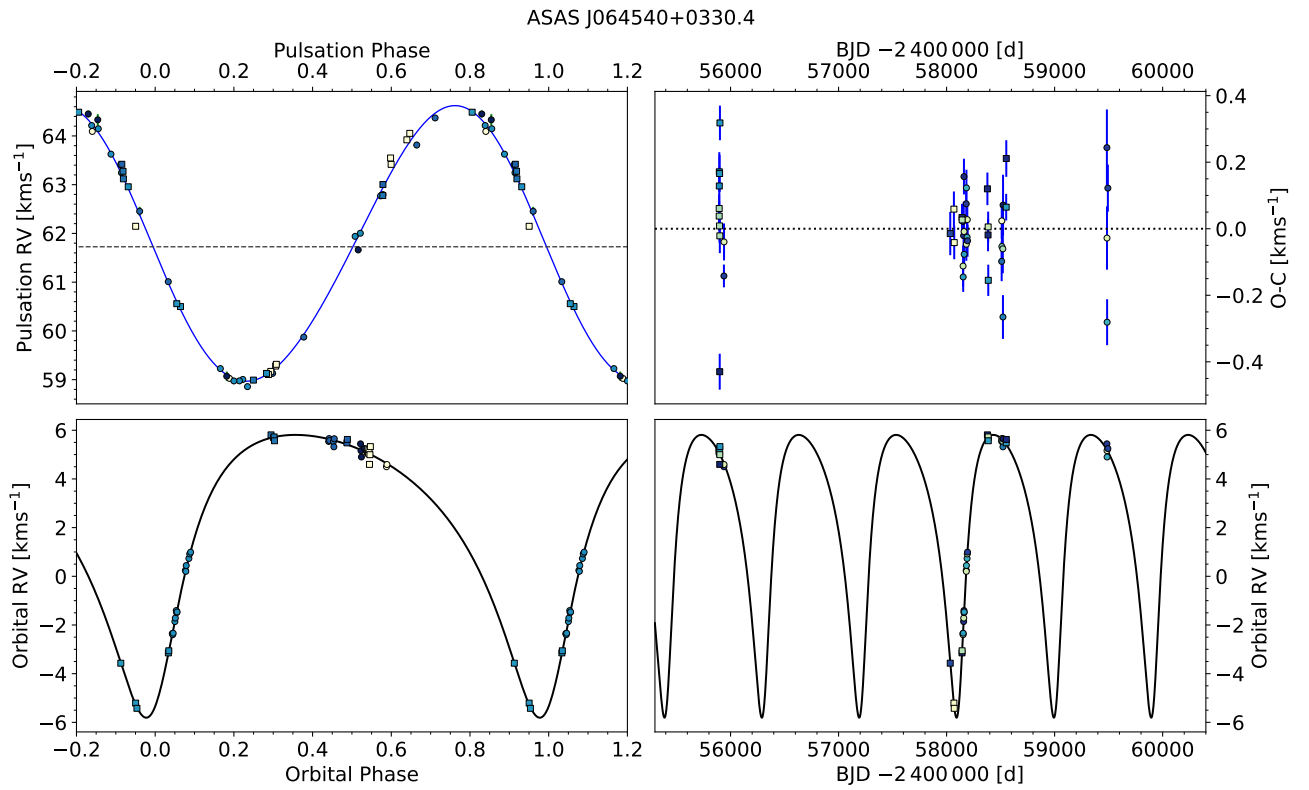


Fig. B.1: Pulsational and orbital fit of ASAS J064540+0330.4. Figure description is same as Figure 2.

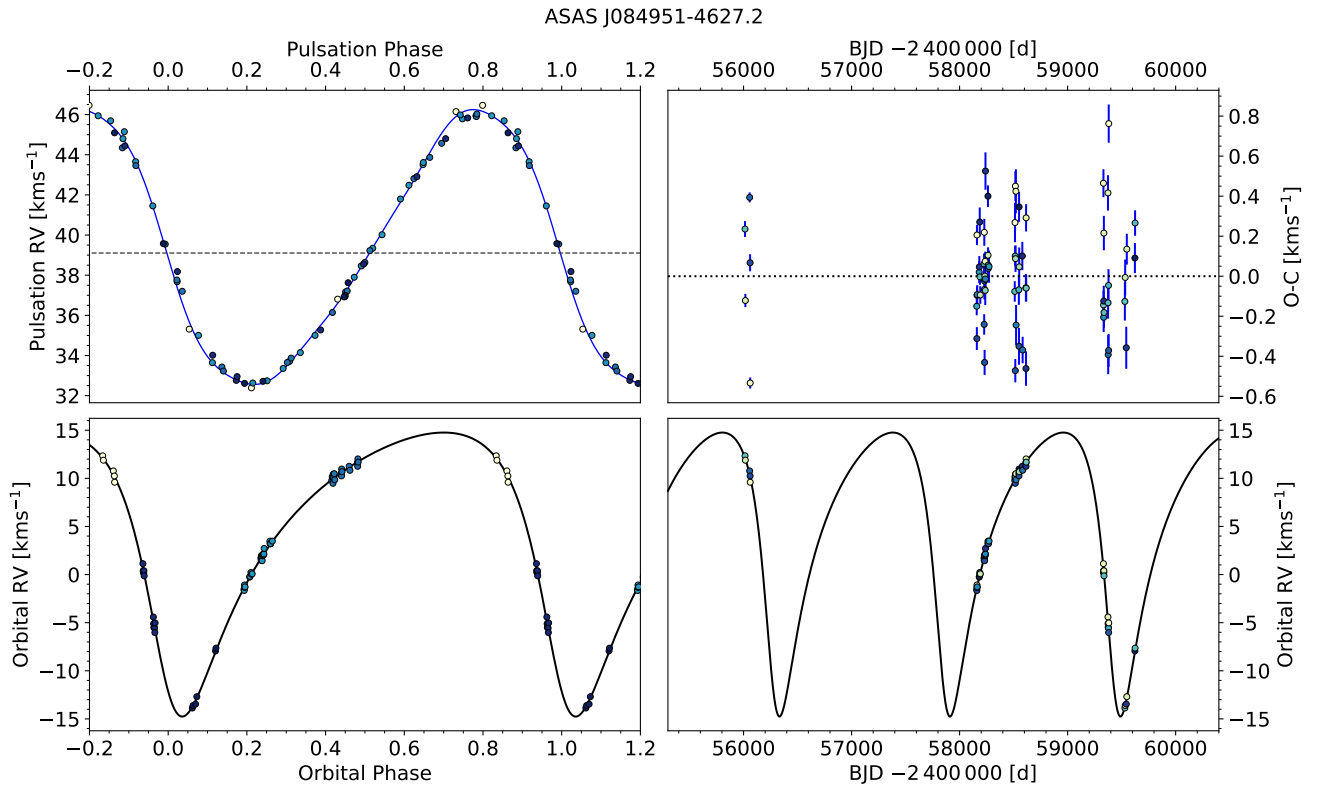


Fig. B.2: Pulsational and orbital fit of ASAS J084951-4627.2. Figure description is same as Figure 2. The pulsational RV curve amplitude modulation is apparent in the top left panel.

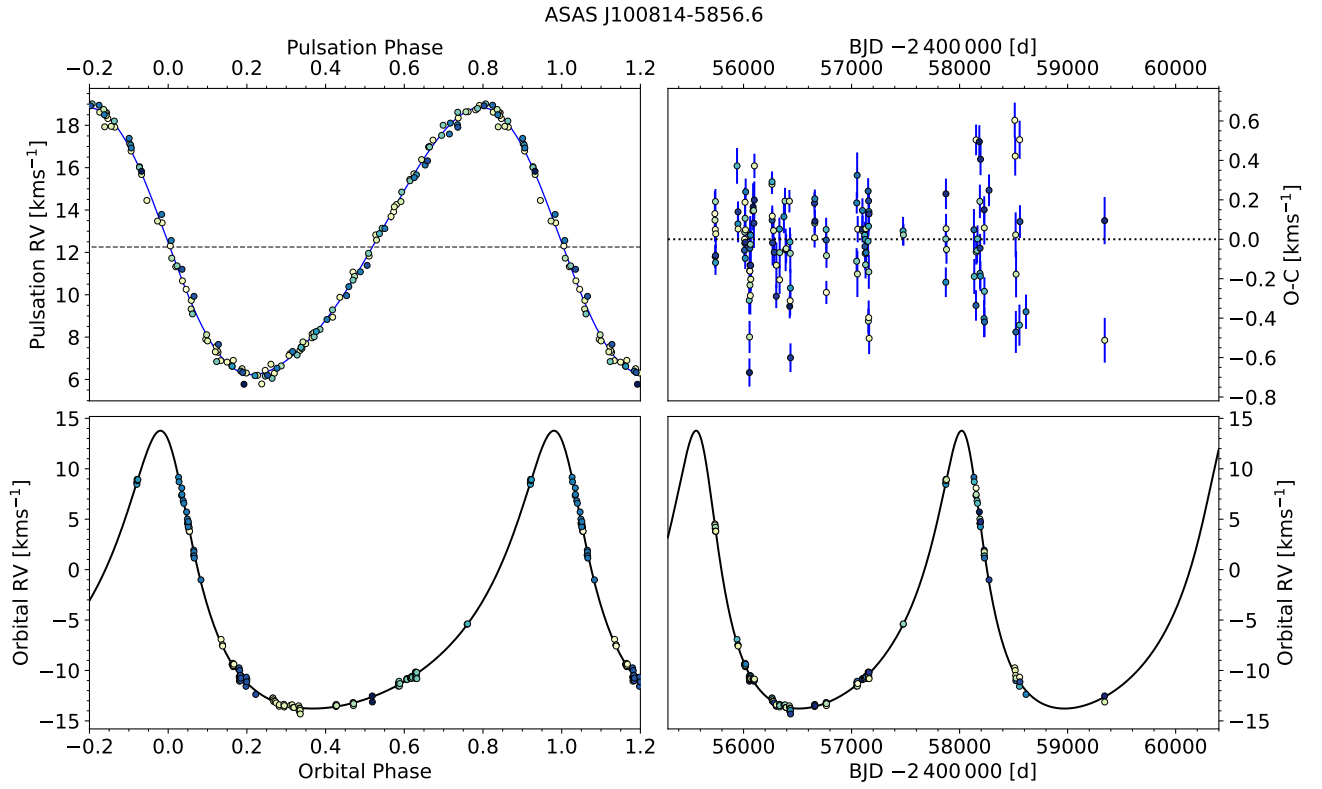


Fig. B.3: Pulsational and orbital fit of ASAS J100814-5856.6. Figure description is same as Figure 2.

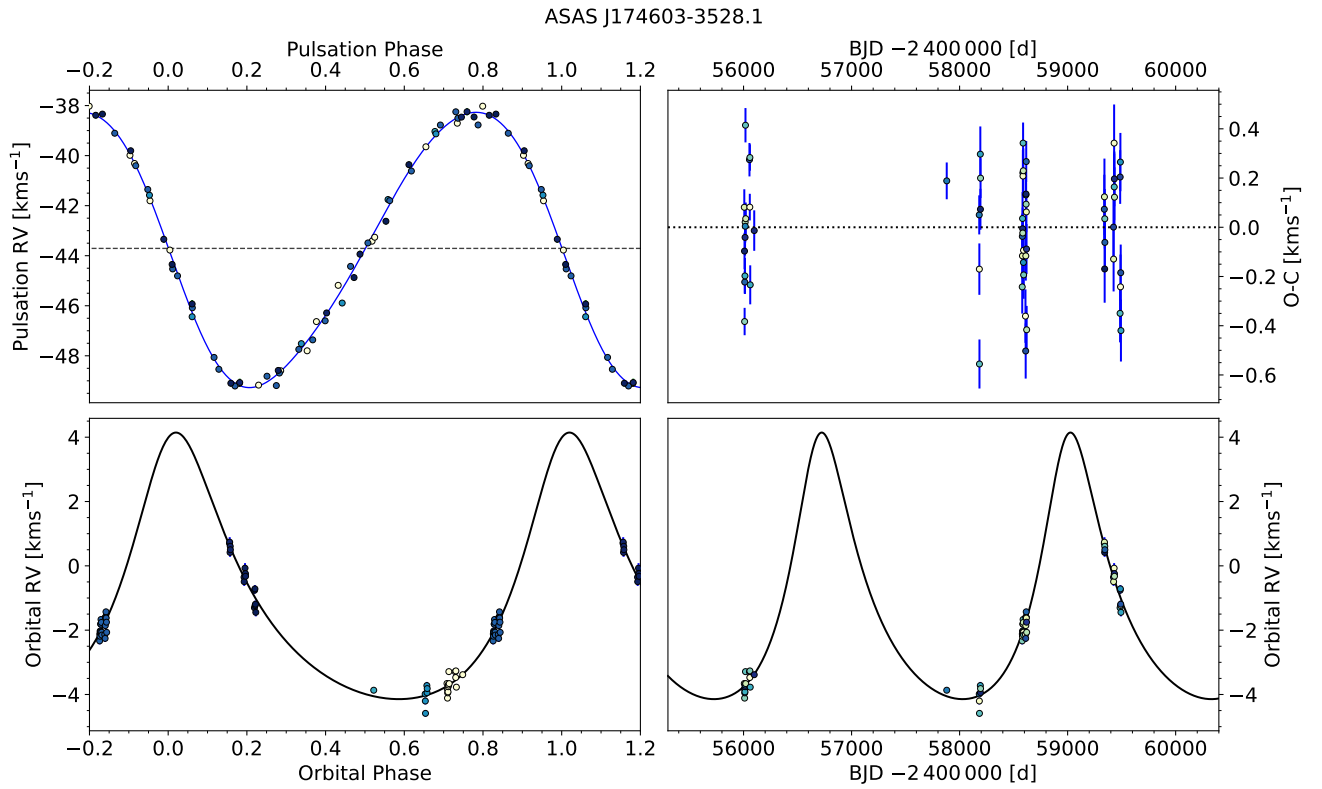


Fig. B.4: Pulsational and orbital fit of ASAS J174603-3528.1. Figure description is same as Figure 2.

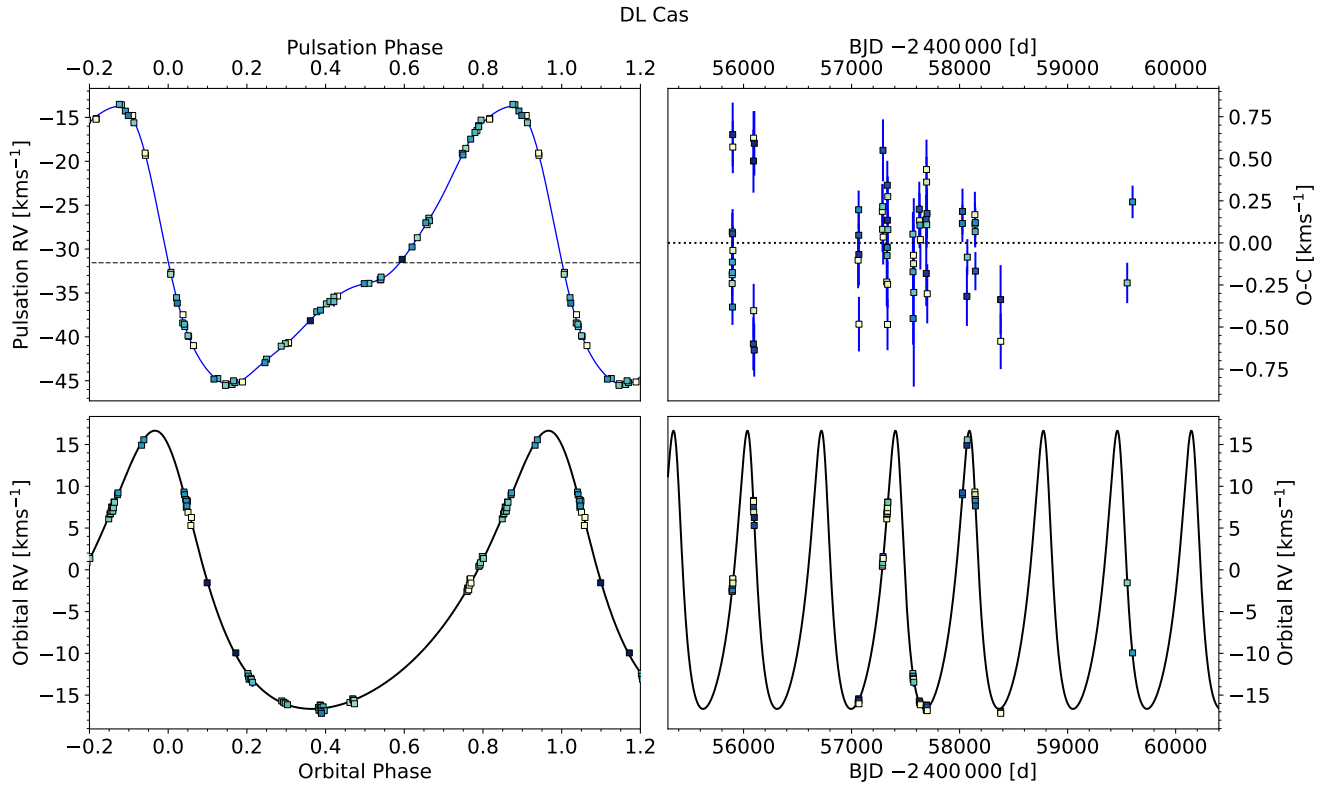


Fig. B.5: Pulsational and orbital fit of DL Cas. Figure description is same as Figure 2.

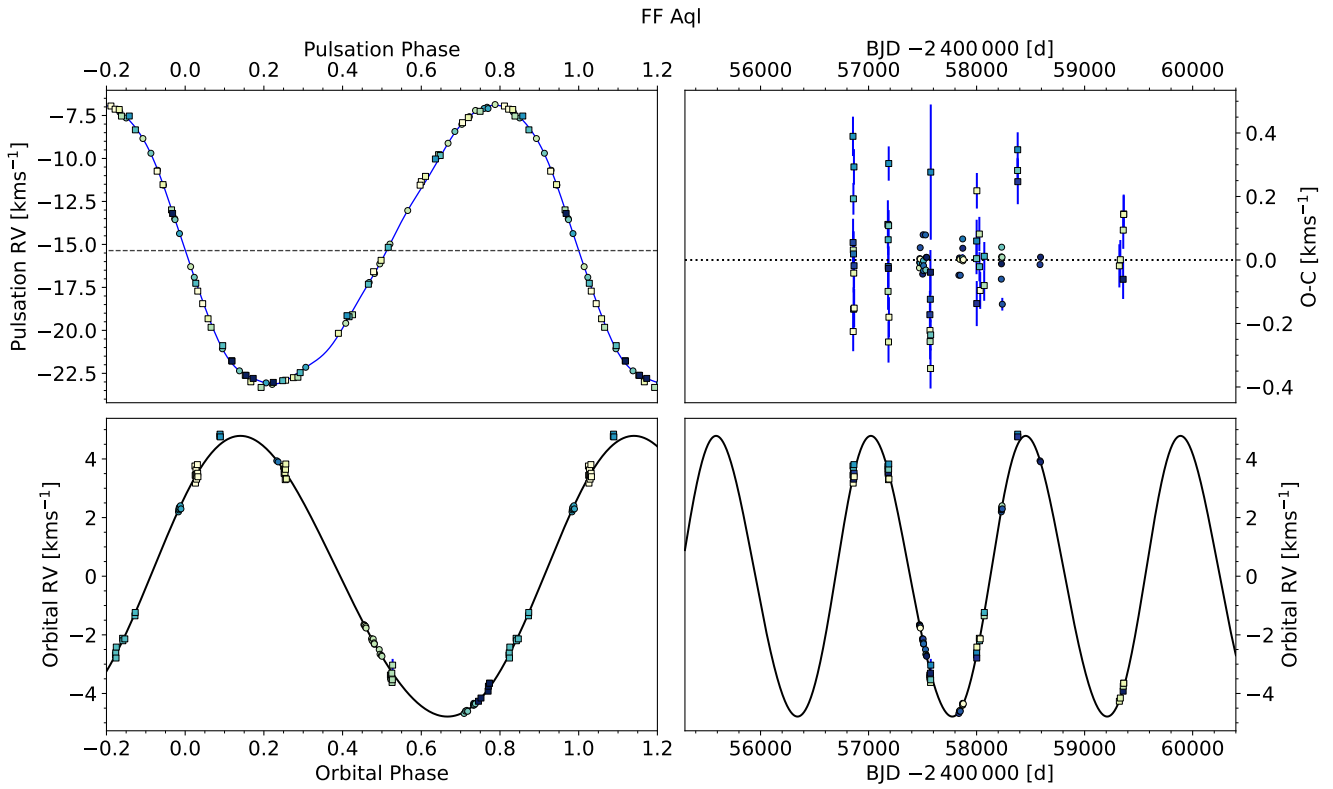


Fig. B.6: Pulsational and orbital fit of FF Aql. Figure description is same as Figure 2.

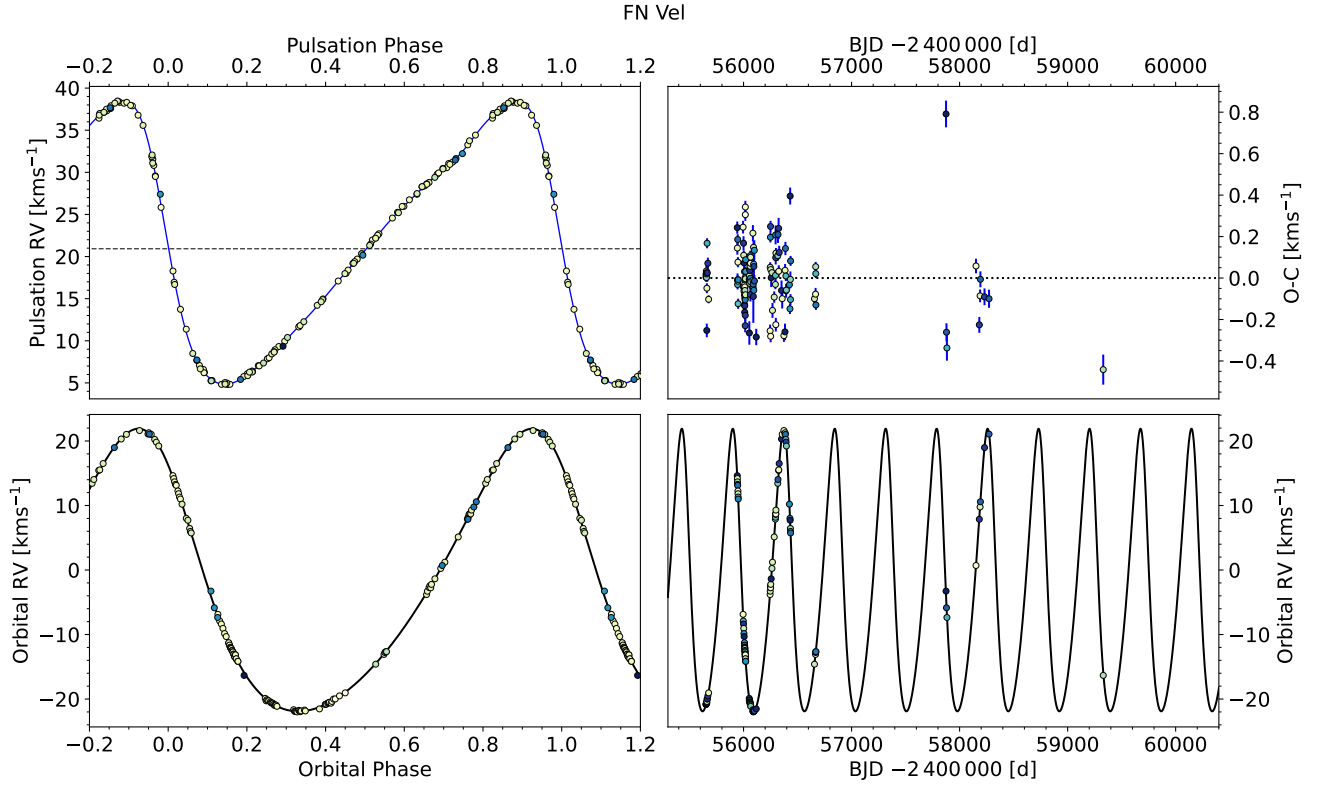


Fig. B.7: Pulsational and orbital fit of FN Vel. Figure description is same as Figure 2.

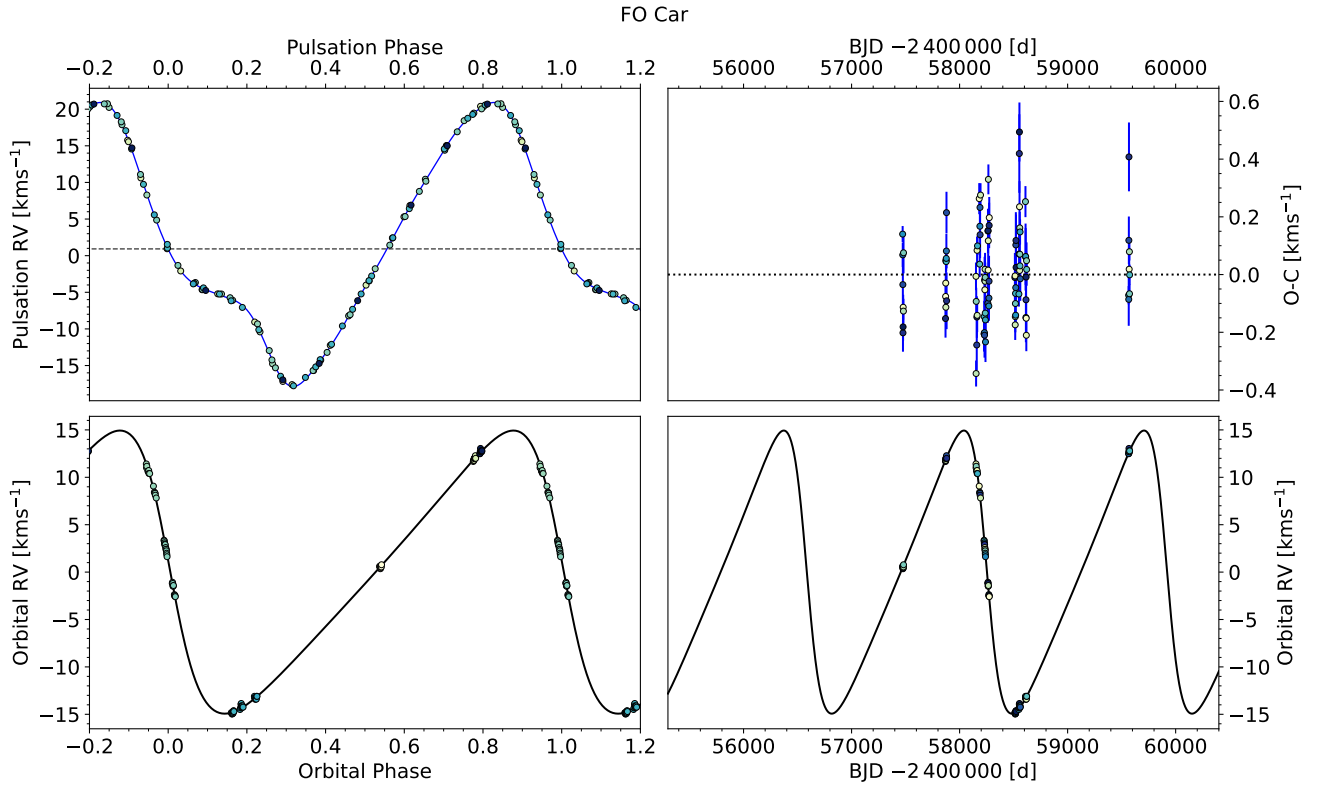


Fig. B.8: Pulsational and orbital fit of FO Car. Figure description is same as Figure 2.

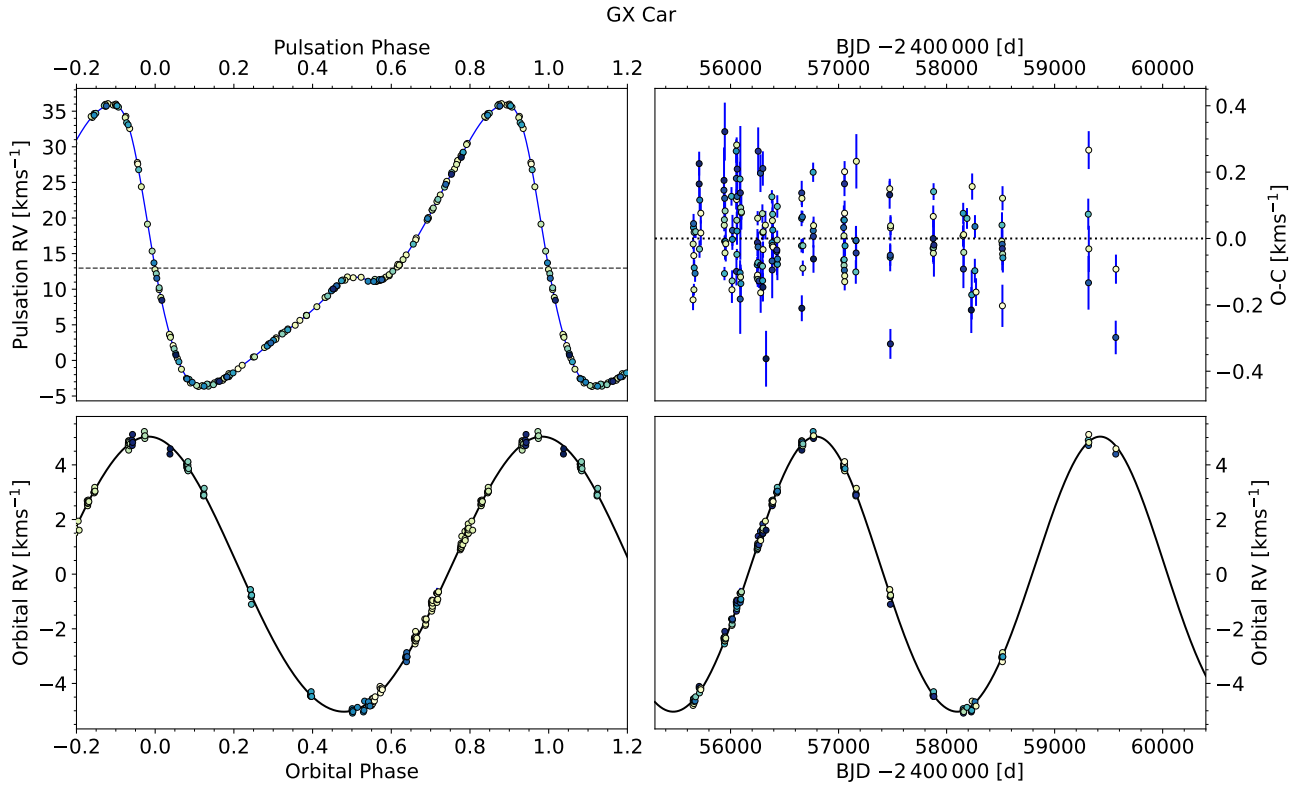


Fig. B.9: Pulsational and orbital fit of GX Car. Figure description is same as Figure 2.

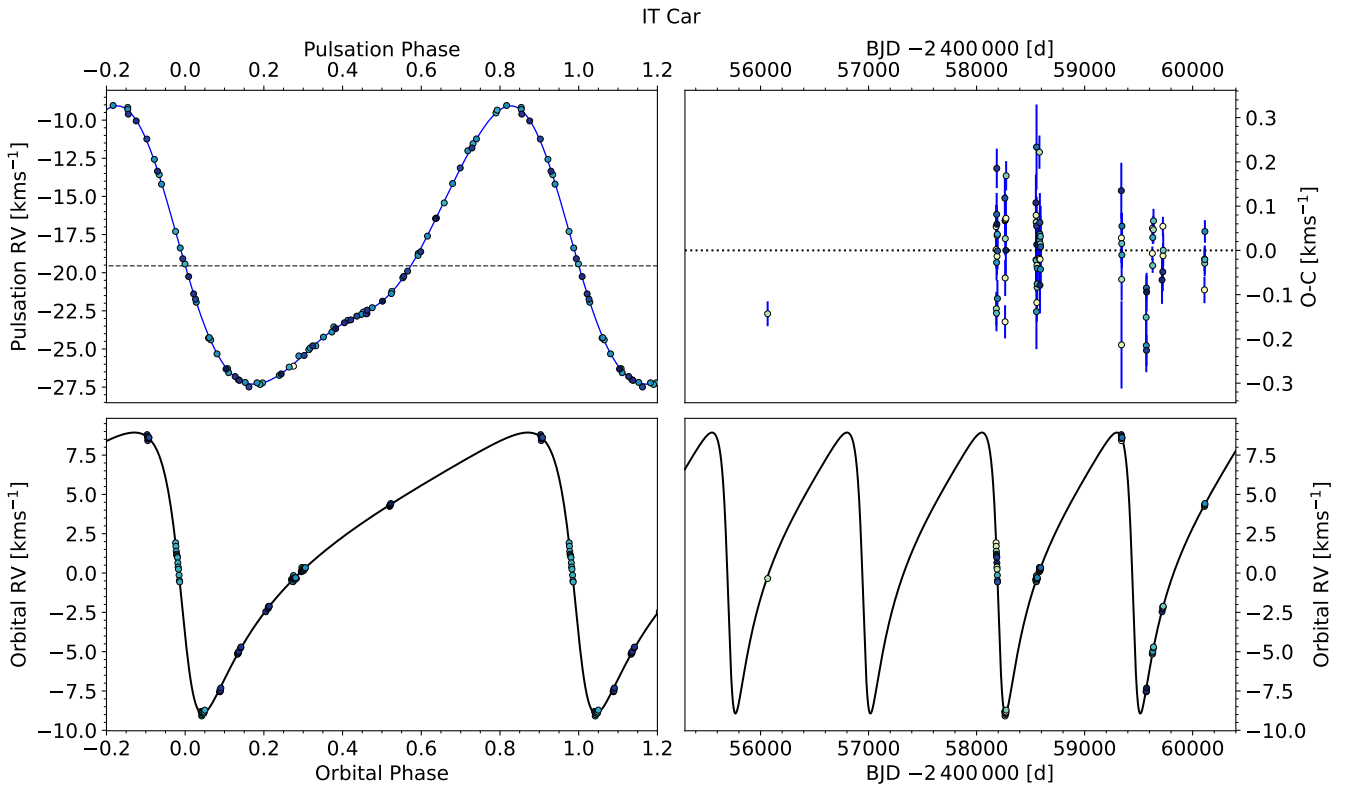


Fig. B.10: Pulsational and orbital fit of IT Car. Figure description is same as Figure 2.

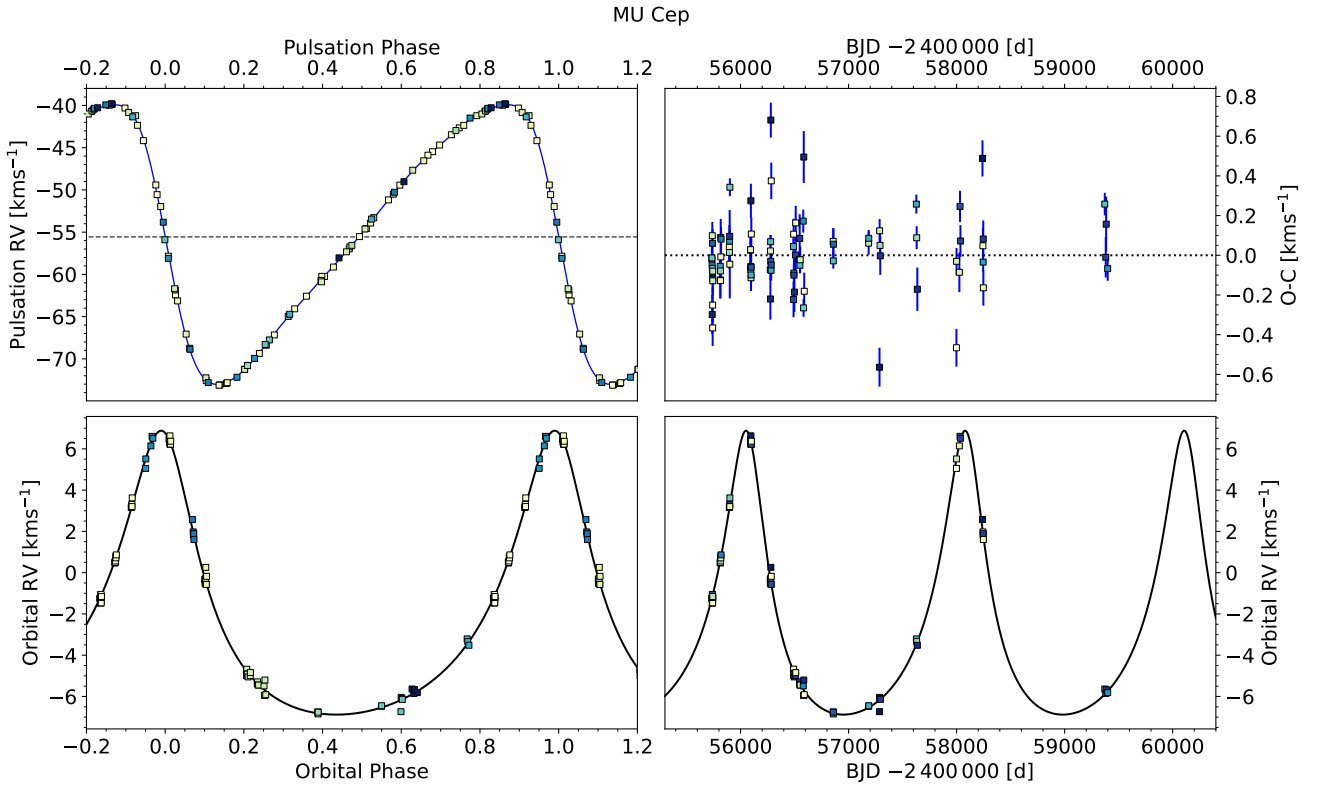


Fig. B.11: Pulsational and orbital fit of MU Cep. Figure description is same as Figure 2.

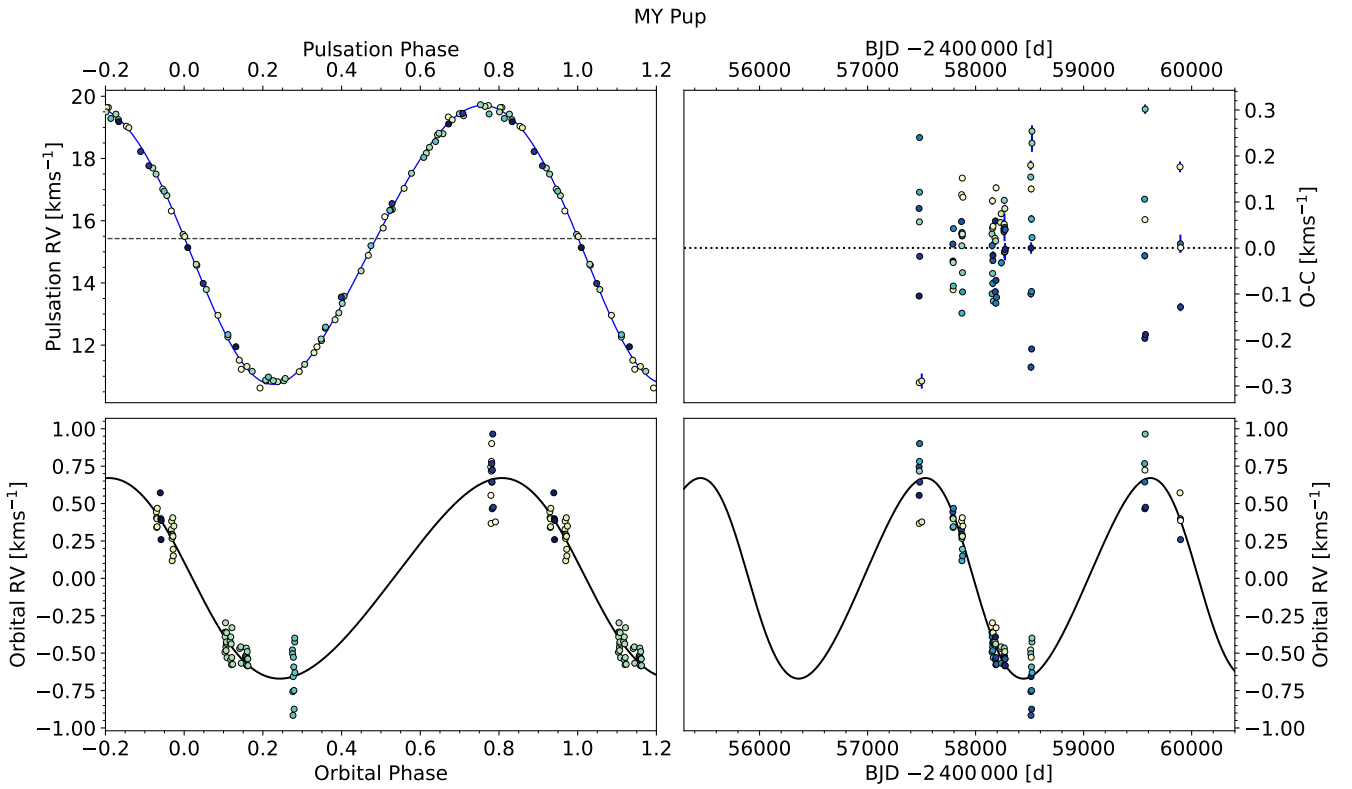


Fig. B.12: Pulsational and orbital fit of MY Pup. Figure description is same as Figure 2.

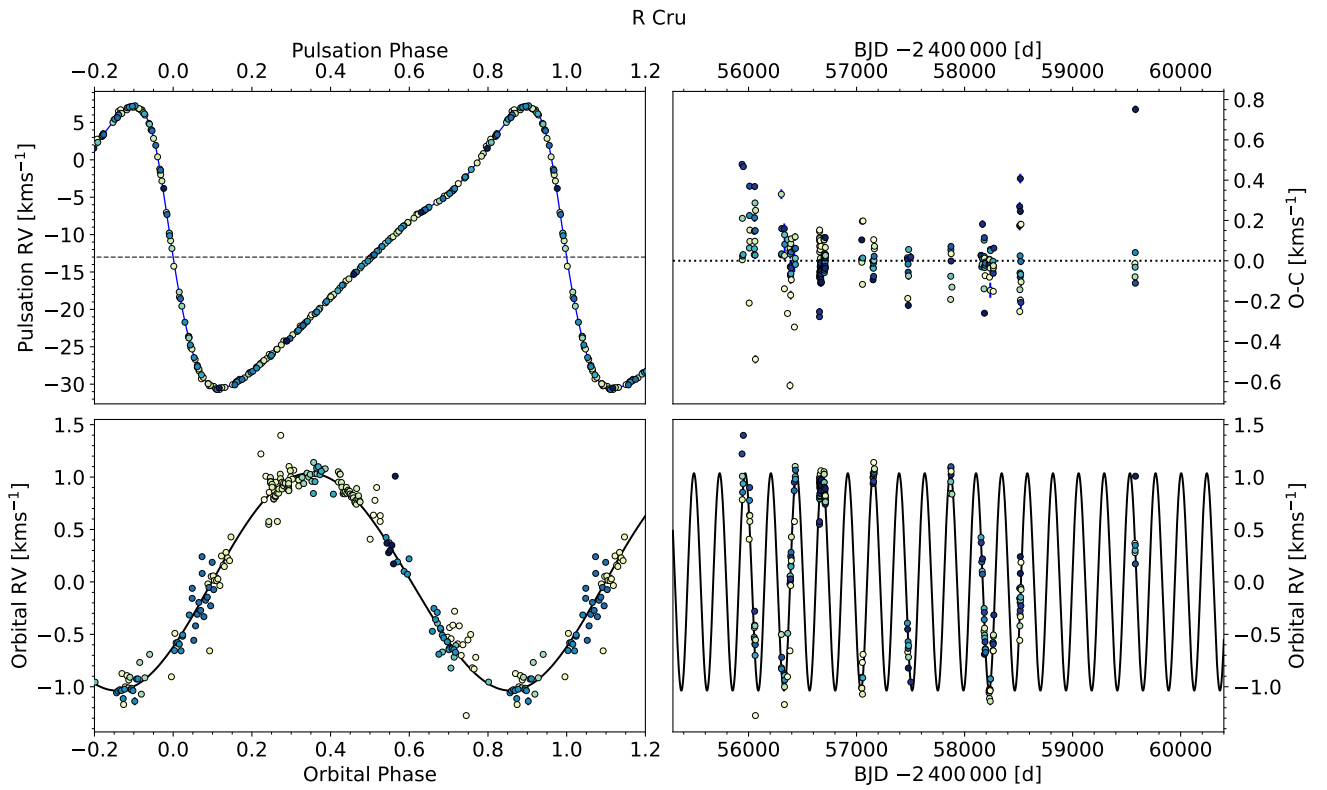


Fig. B.13: Pulsational and orbital fit of R Cru. Figure description is same as Figure 2.

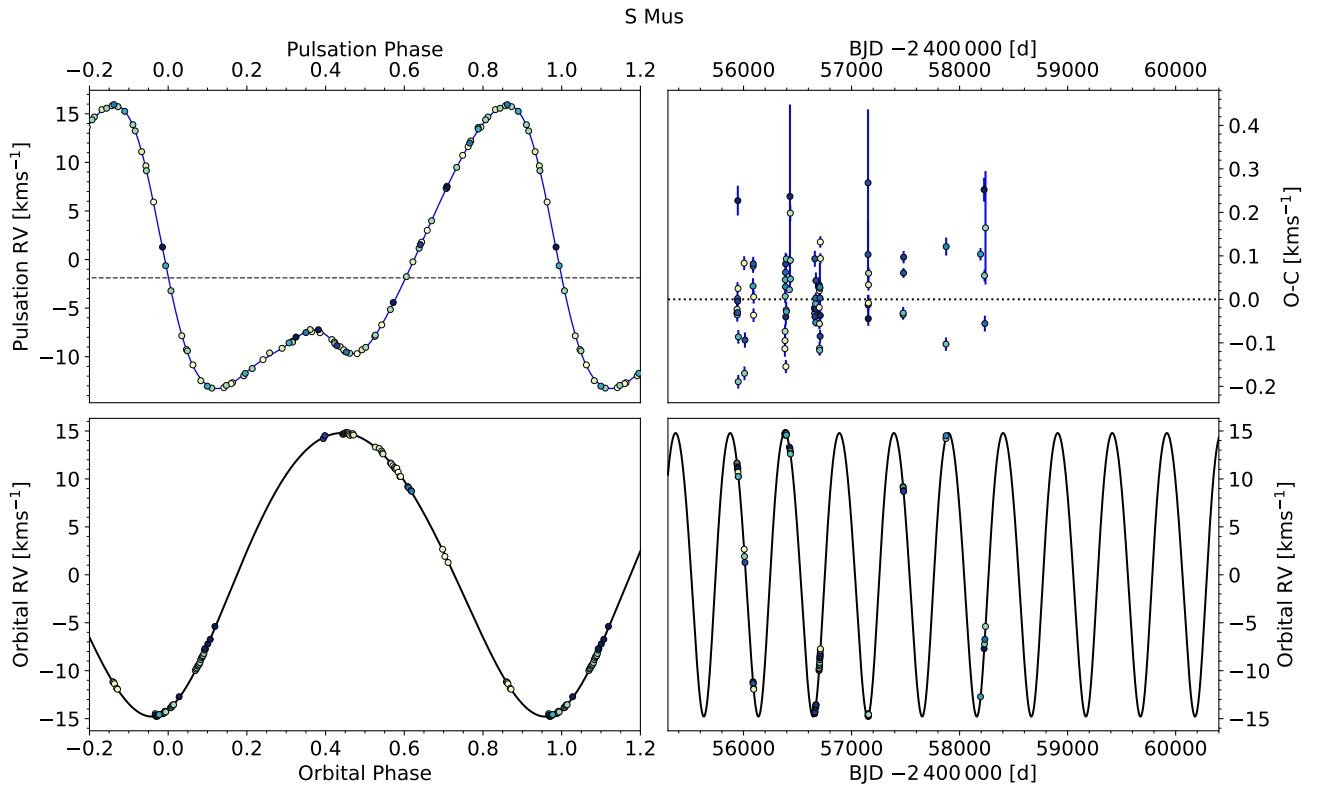


Fig. B.14: Pulsational and orbital fit of S Mus. Figure description is same as Figure 2.

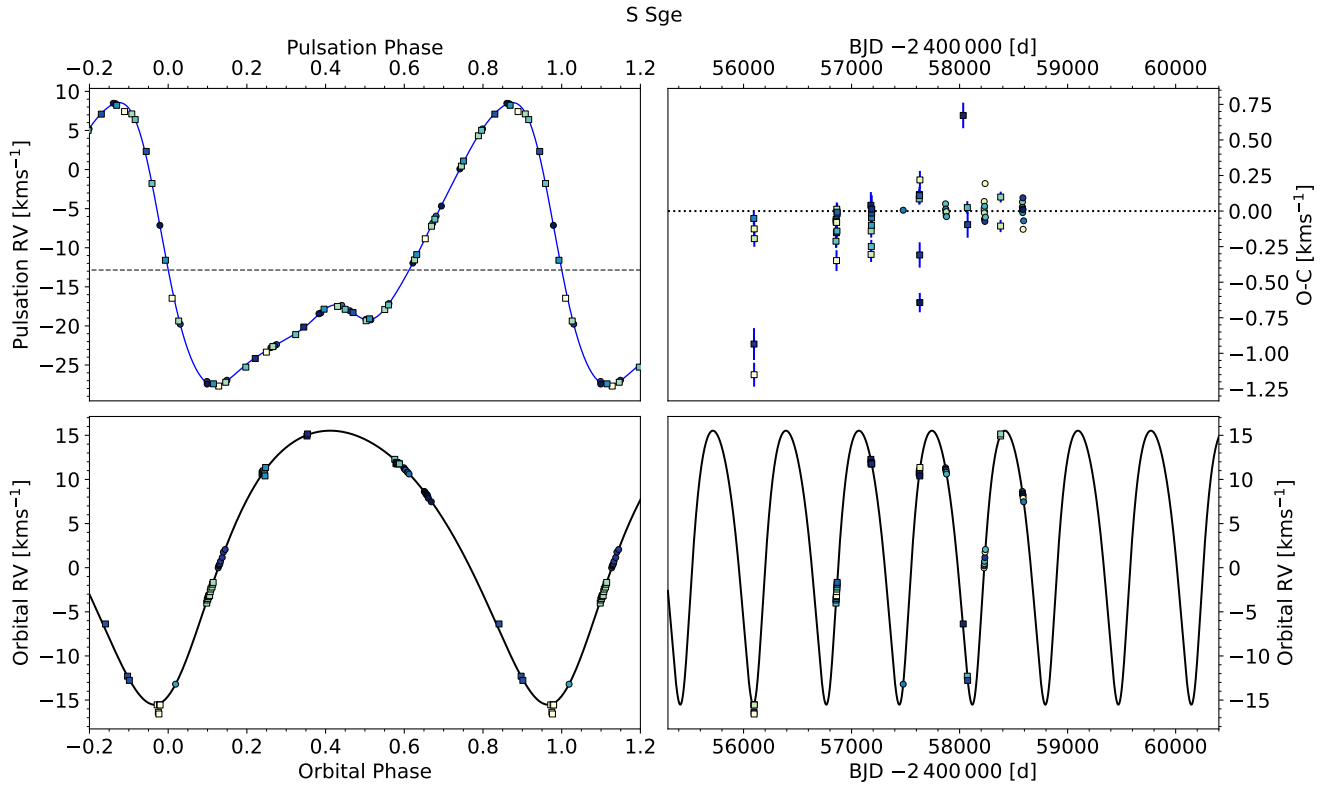


Fig. B.15: Pulsational and orbital fit of S Sge. Figure description is same as Figure 2.

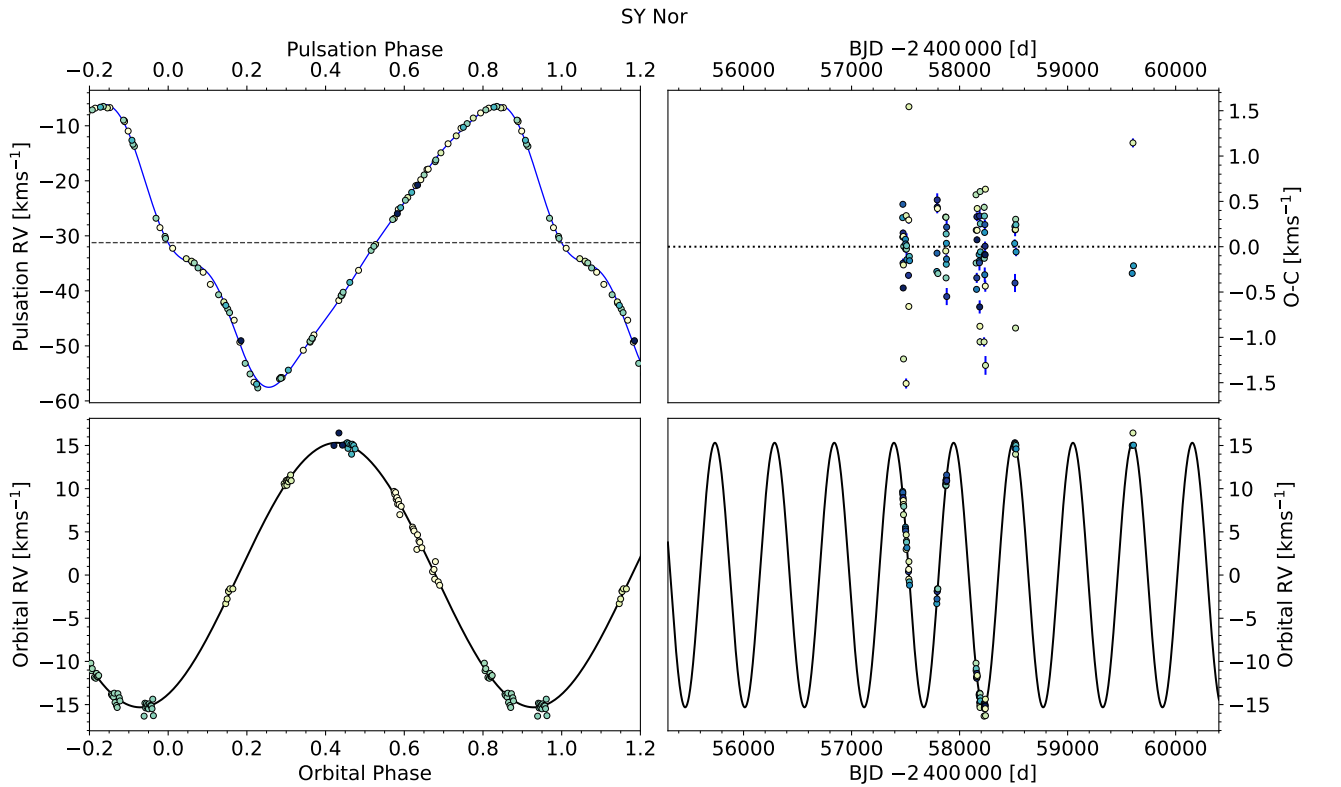


Fig. B.16: Pulsational and orbital fit of SY Nor. Figure description is same as Figure 2.

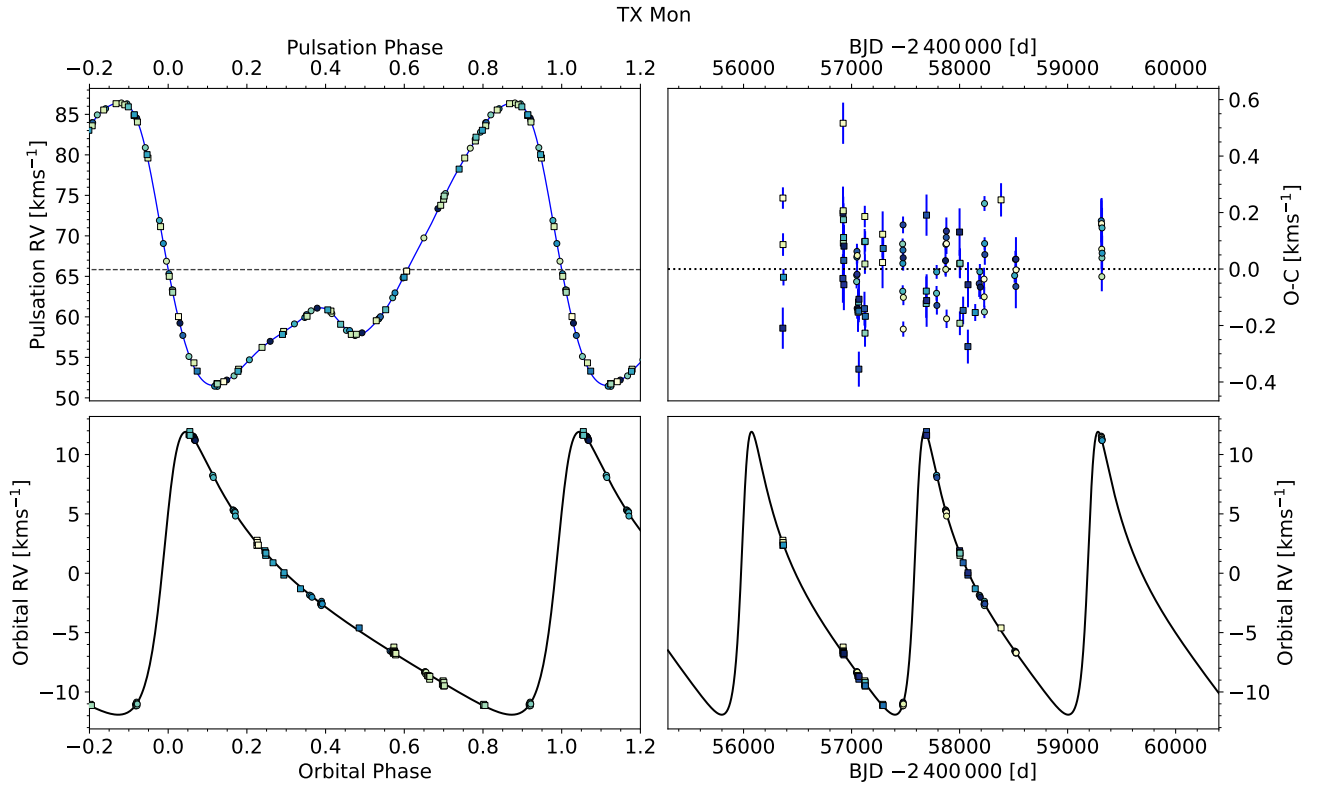


Fig. B.17: Pulsational and orbital fit of TX Mon. Figure description is same as Figure 2.

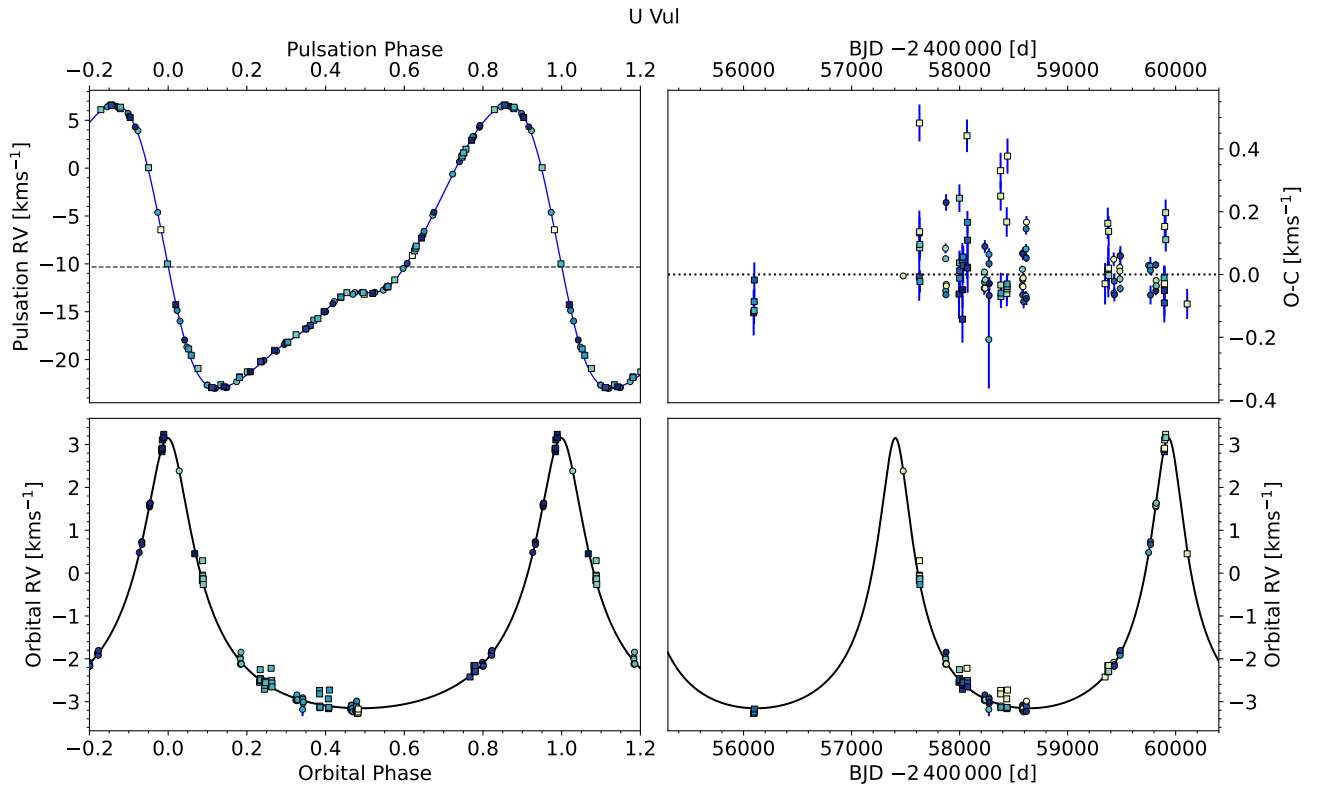


Fig. B.18: Pulsational and orbital fit of U Vul. Figure description is same as Figure 2.

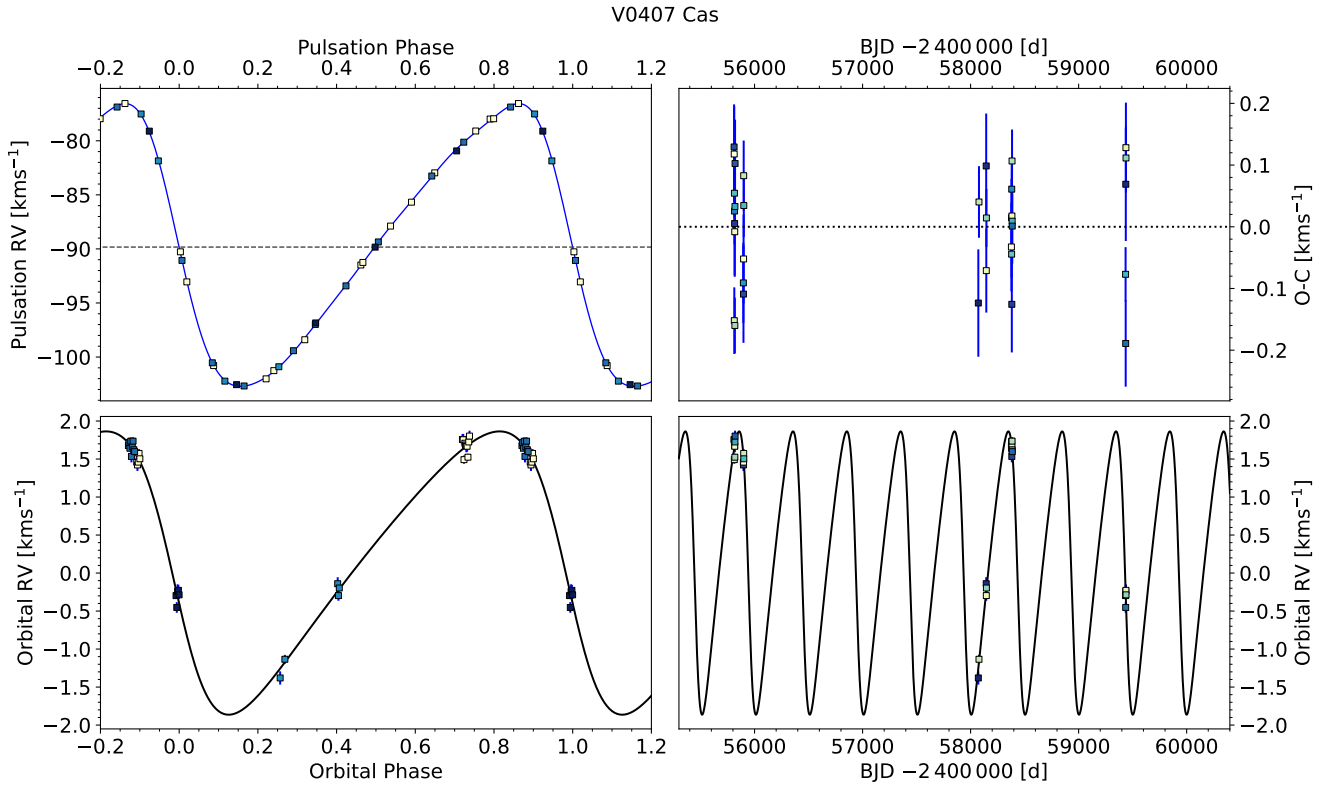


Fig. B.19: Pulsational and orbital fit of V0407 Cas. Figure description is same as Figure 2.

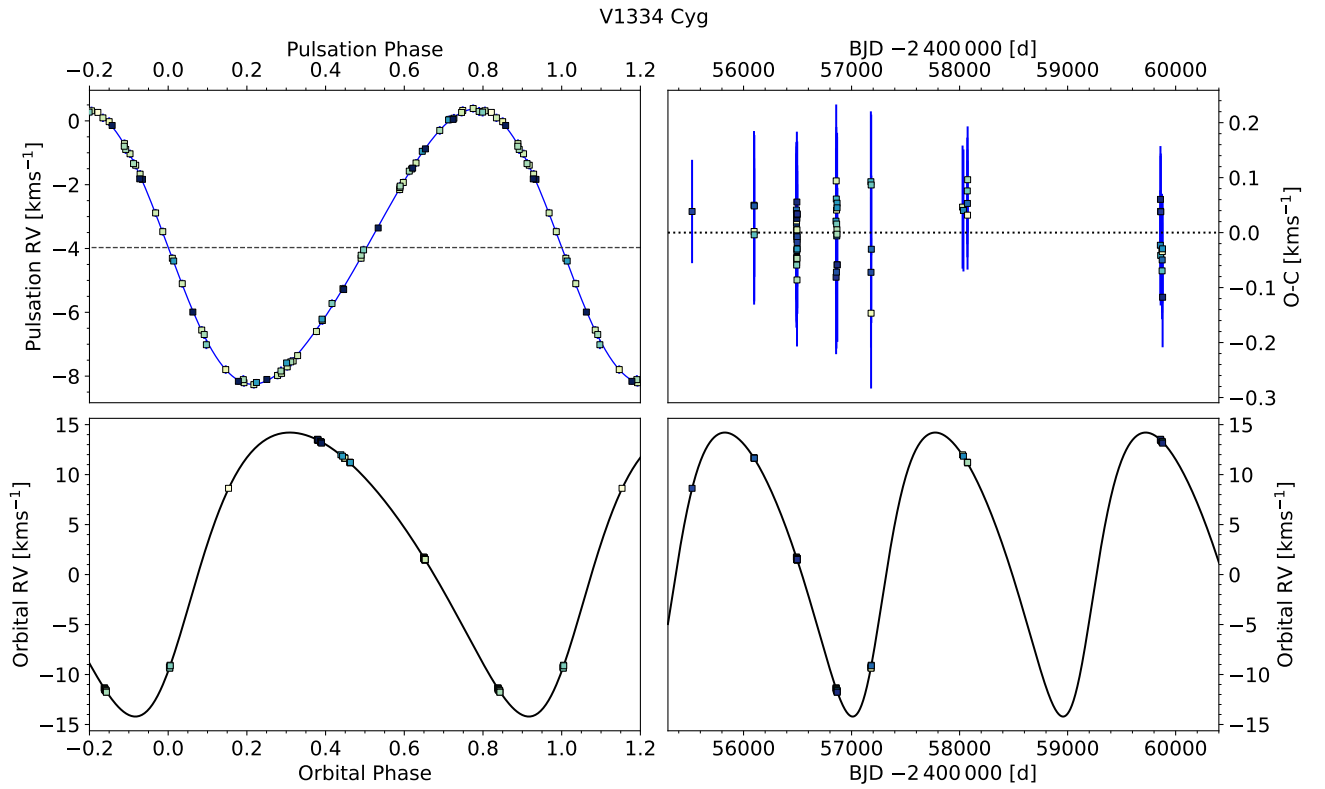


Fig. B.20: Pulsational and orbital fit of V1334 Cyg. Figure description is same as Figure 2.

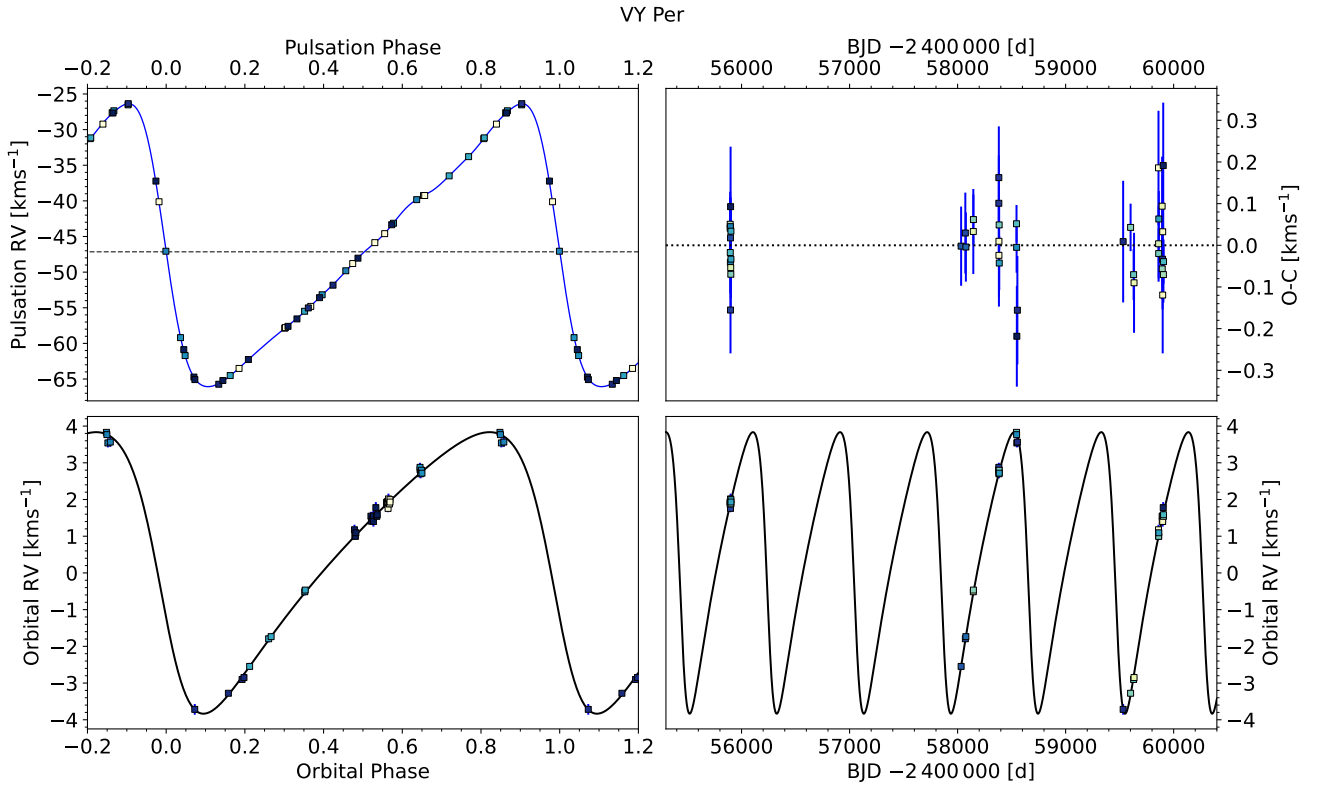


Fig. B.21: Pulsational and orbital fit of VY Per. Figure description is same as Figure 2.

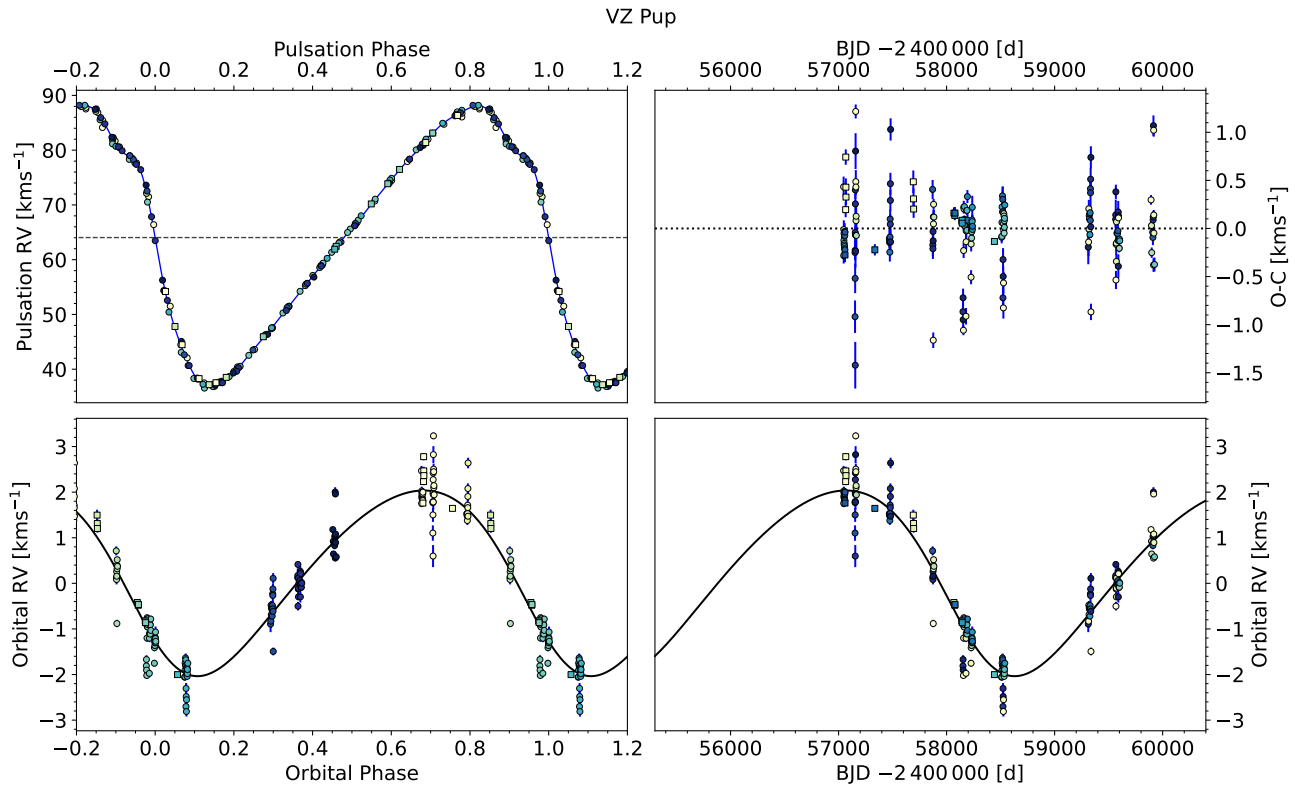


Fig. B.22: Pulsational and orbital fit of VZ Pup. Figure description is same as Figure 2.

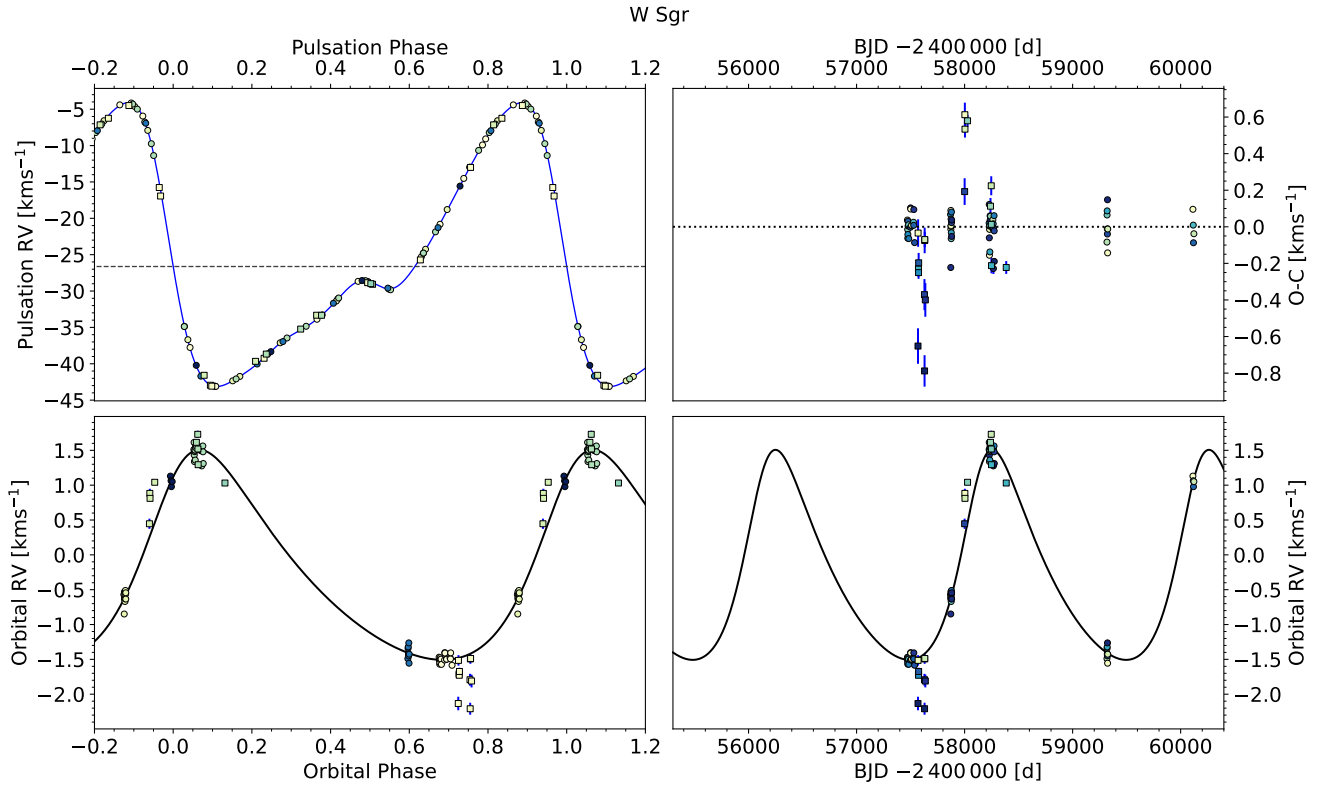


Fig. B.23: Pulsational and orbital fit of W Sgr. Figure description is same as Figure 2. The bottom right panel suggests that the orbit of W Sgr could be more eccentric than the best fit model obtained here.

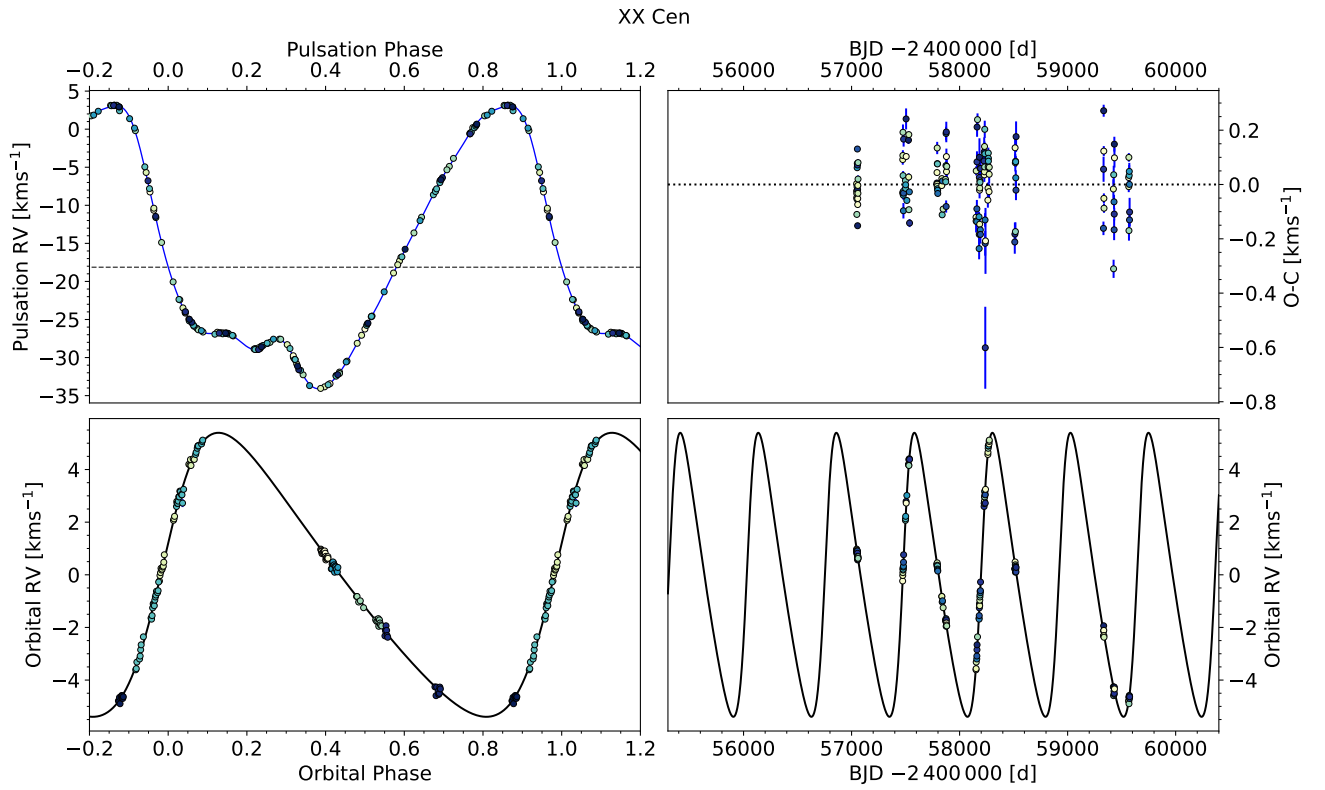


Fig. B.24: Pulsational and orbital fit of XX Cen. Figure description is same as Figure 2.

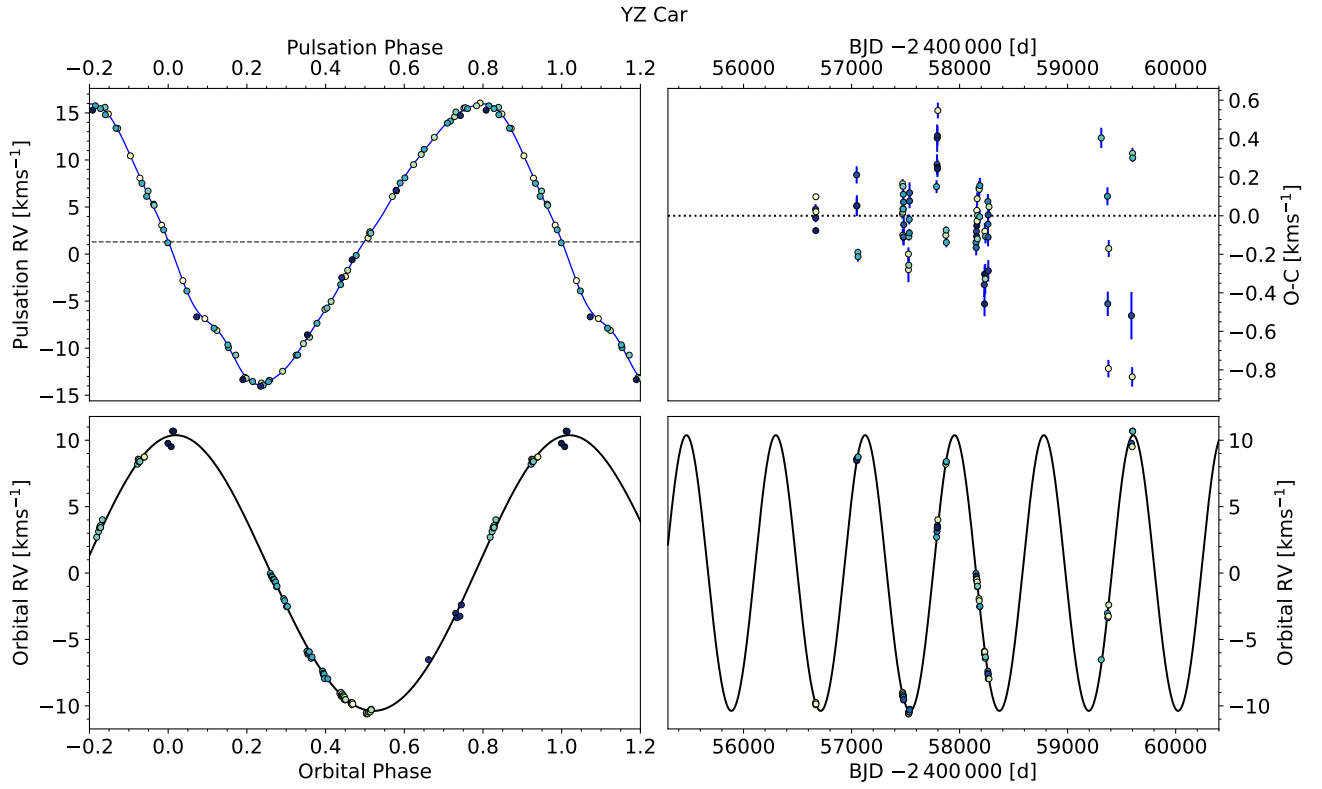


Fig. B.25: Pulsational and orbital fit of YZ Car. Figure description is same as Figure 2.

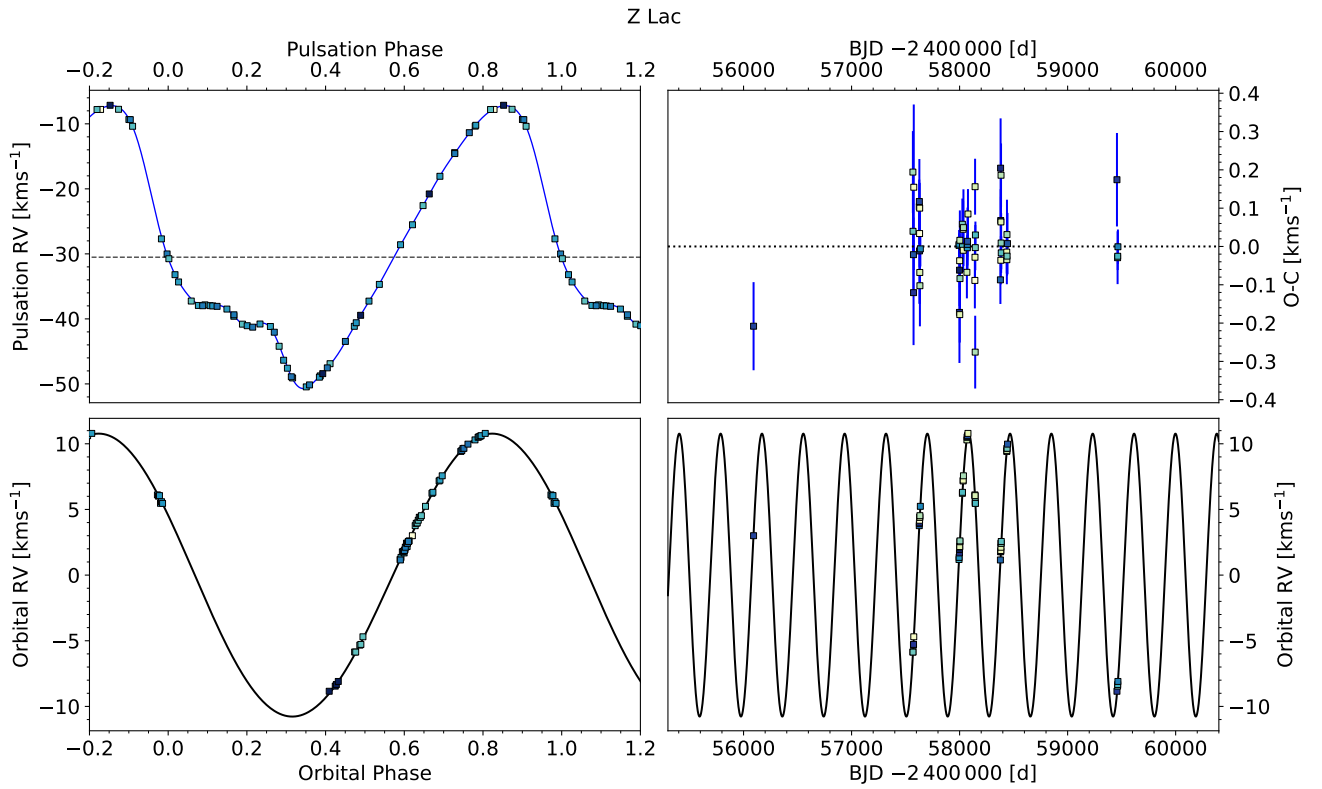


Fig. B.26: Pulsational and orbital fit of Z Lac. Figure description is same as Figure 2.

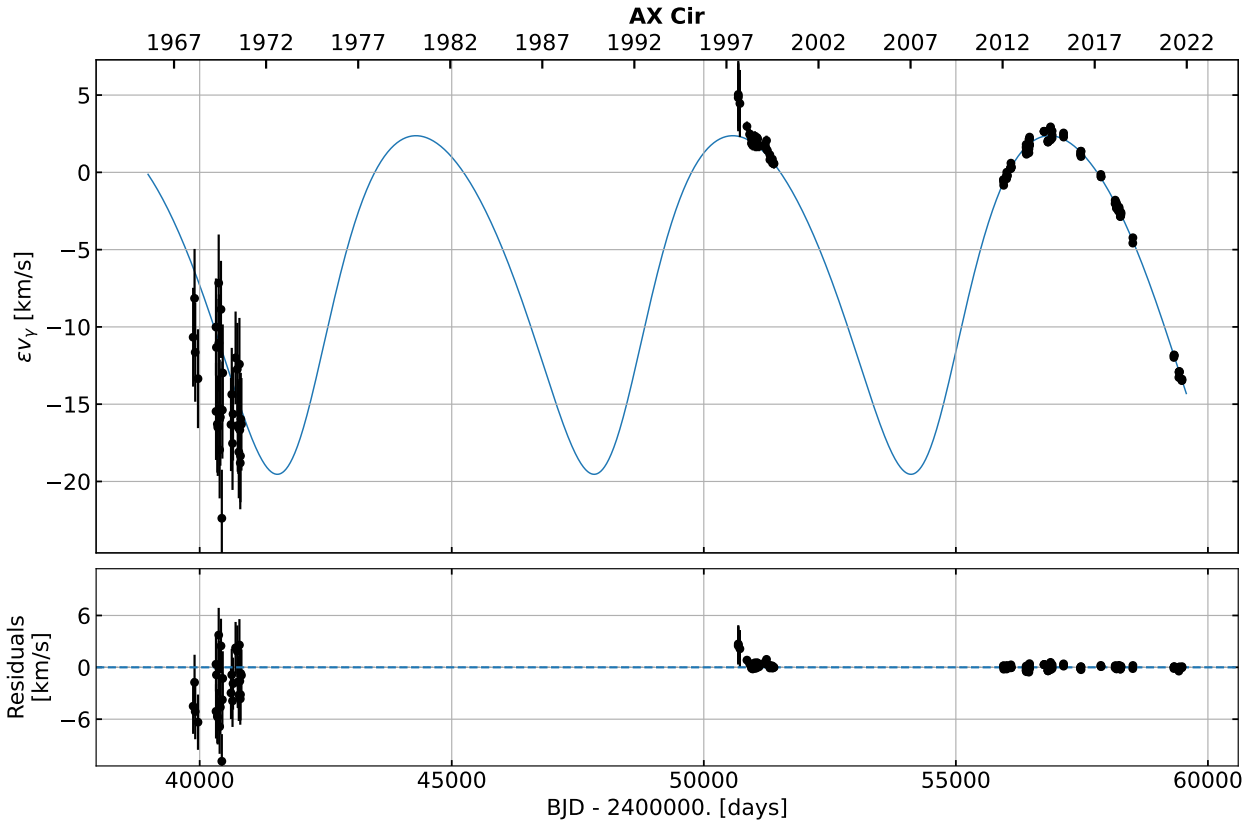


Fig. C.1: V_γ residuals Orbit fitting for AX Cir.

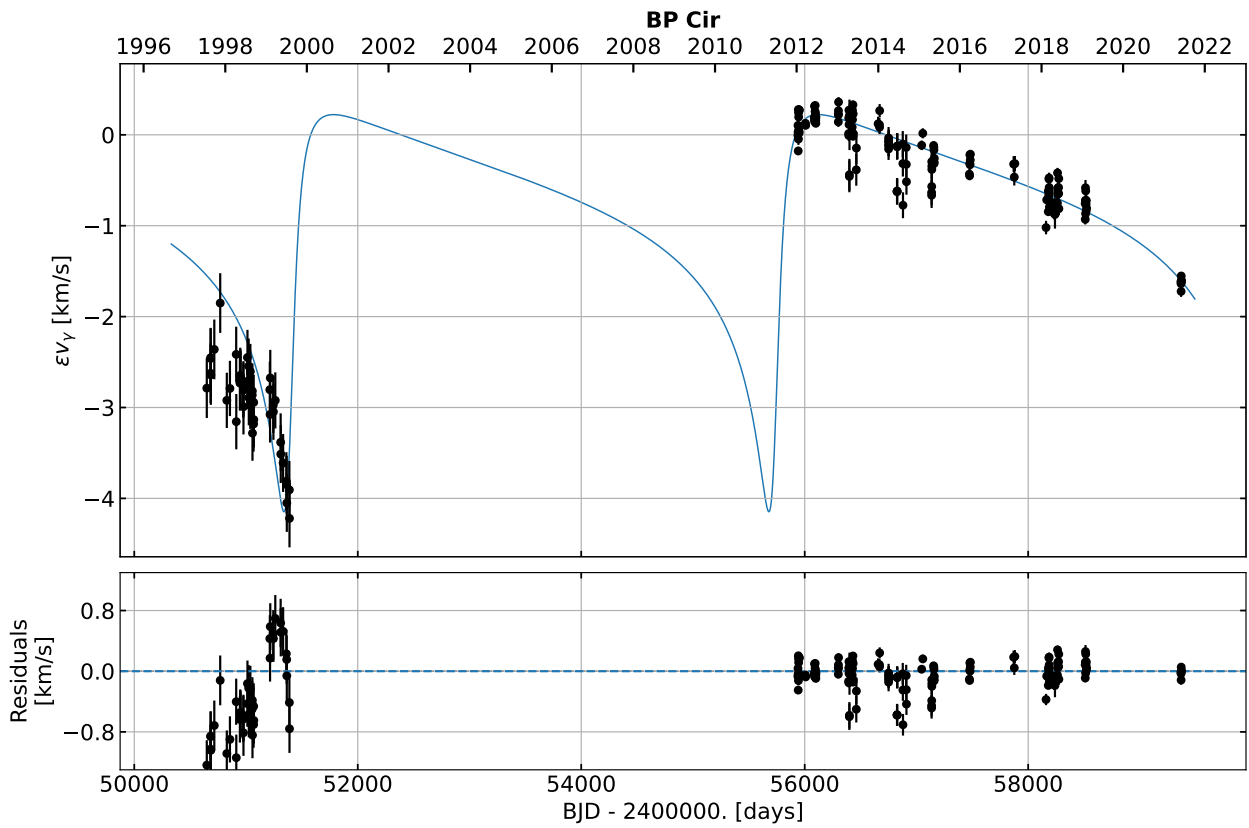


Fig. C.2: V_γ residuals Orbit fitting for BP Cir.

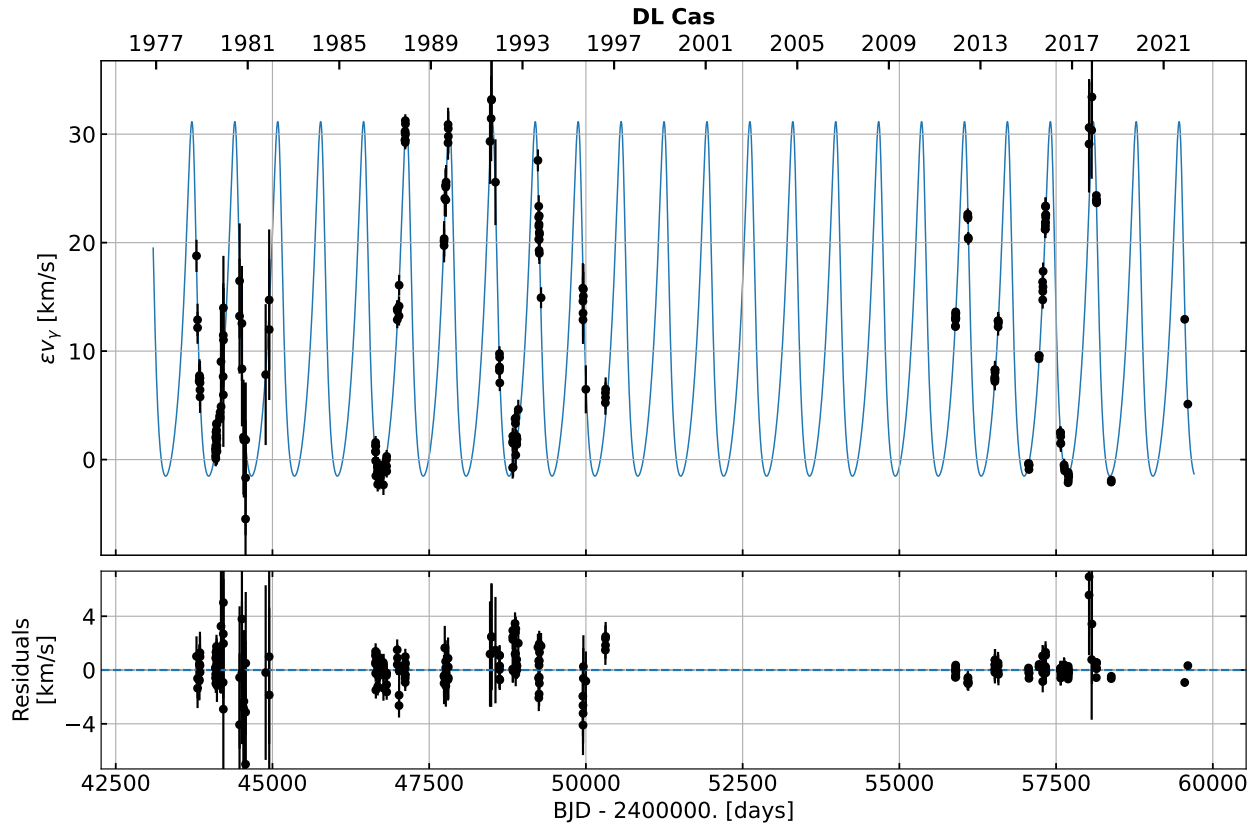


Fig. C.3: V_γ residuals Orbit fitting for DL Cas.

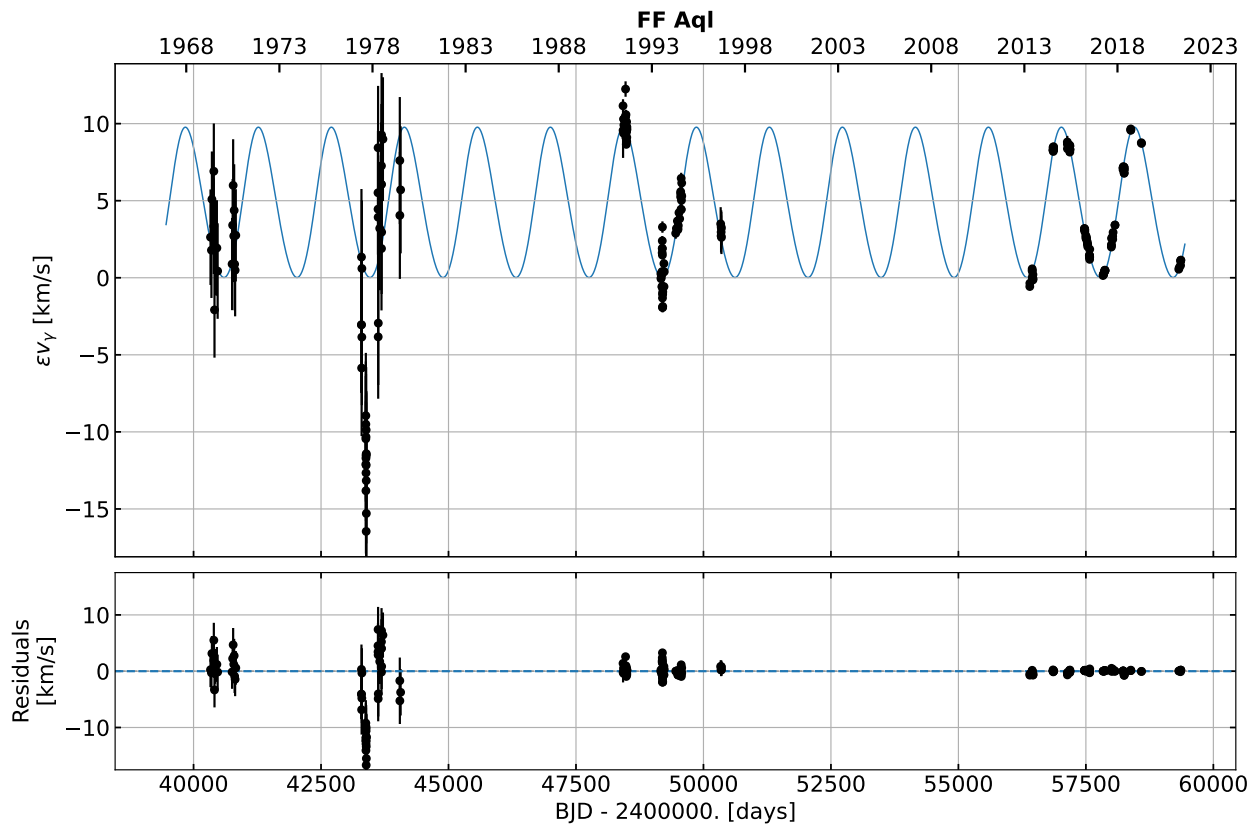


Fig. C.4: V_γ residuals Orbit fitting for FF Aql.

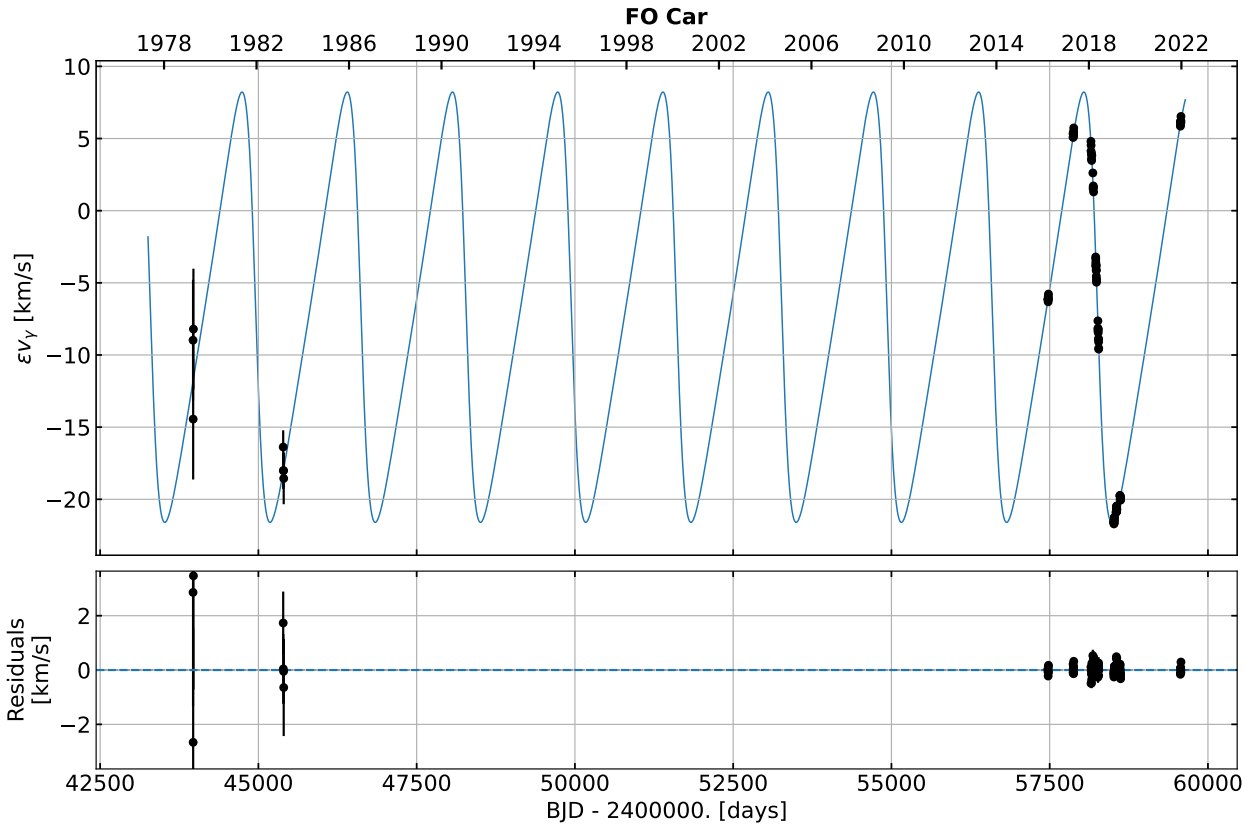


Fig. C.5: V_γ residuals Orbit fitting for FO Car.

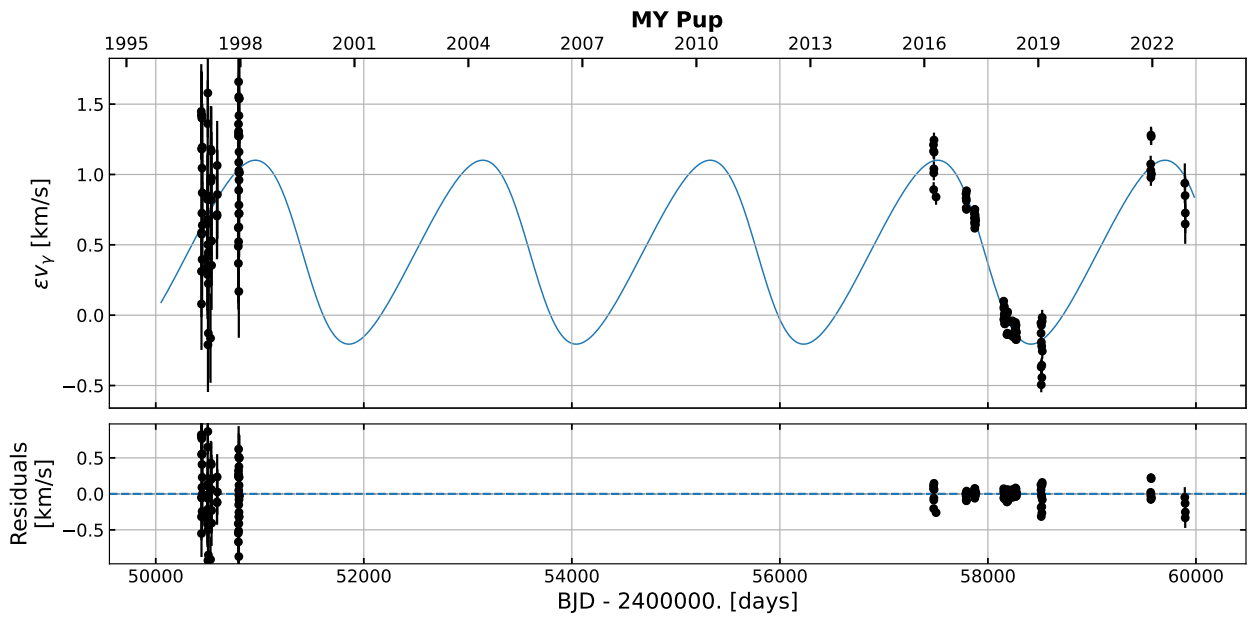


Fig. C.6: V_γ residuals Orbit fitting for MY Pup.

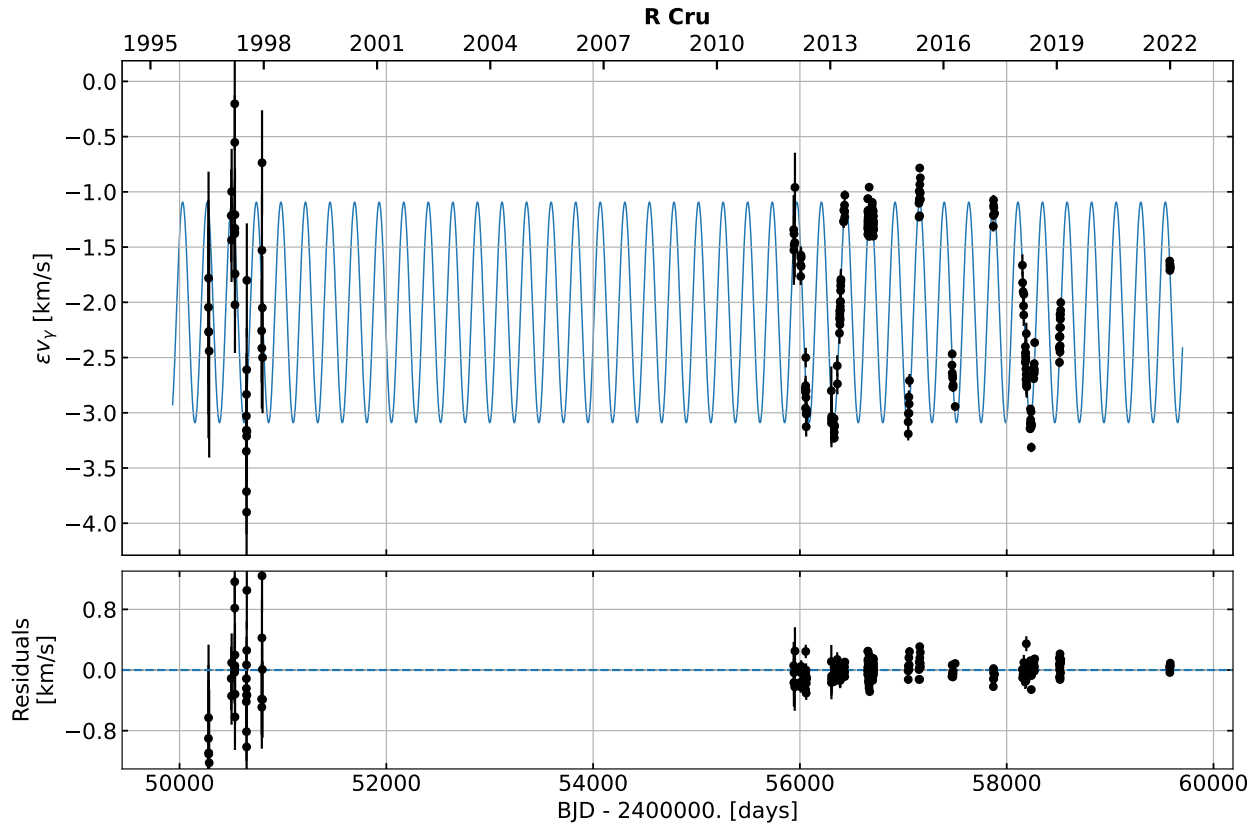


Fig. C.7: V_γ residuals Orbit fitting for R Cru.

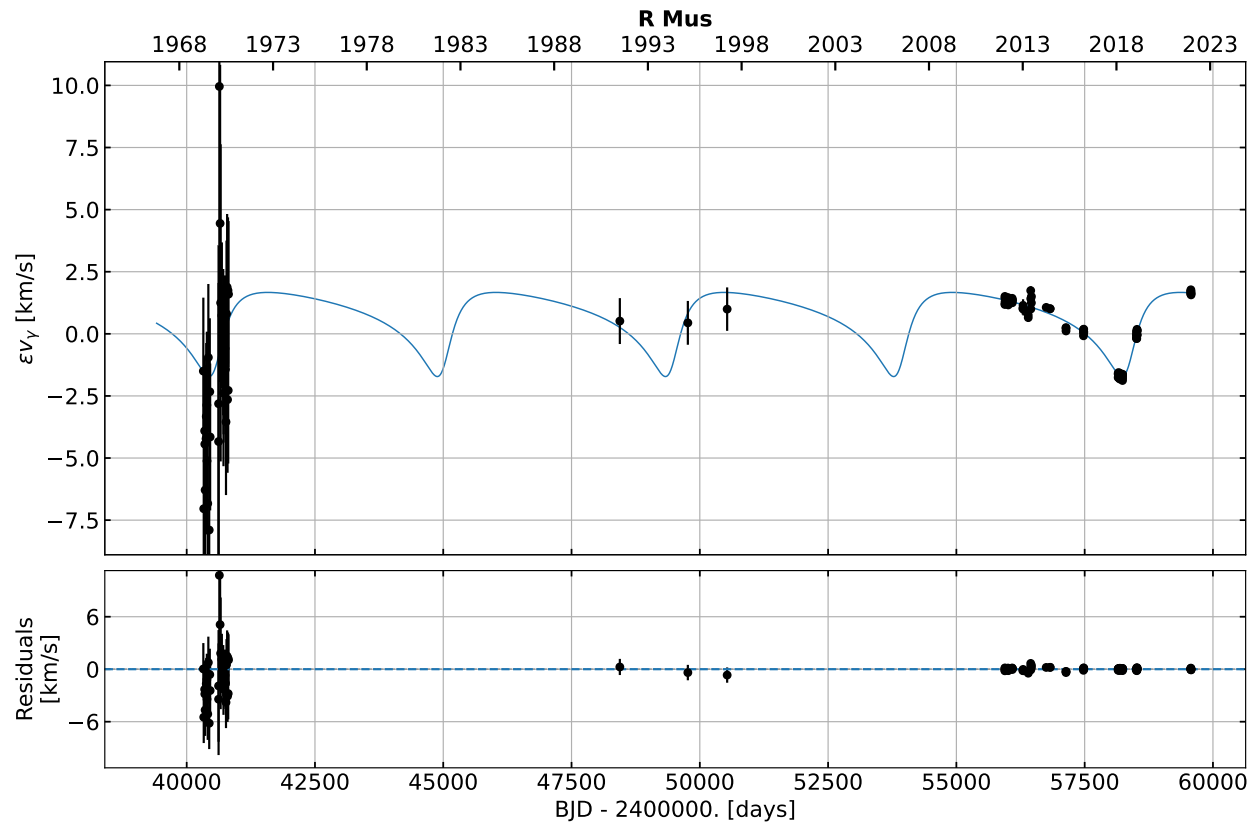


Fig. C.8: V_γ residuals Orbit fitting for R Mus.

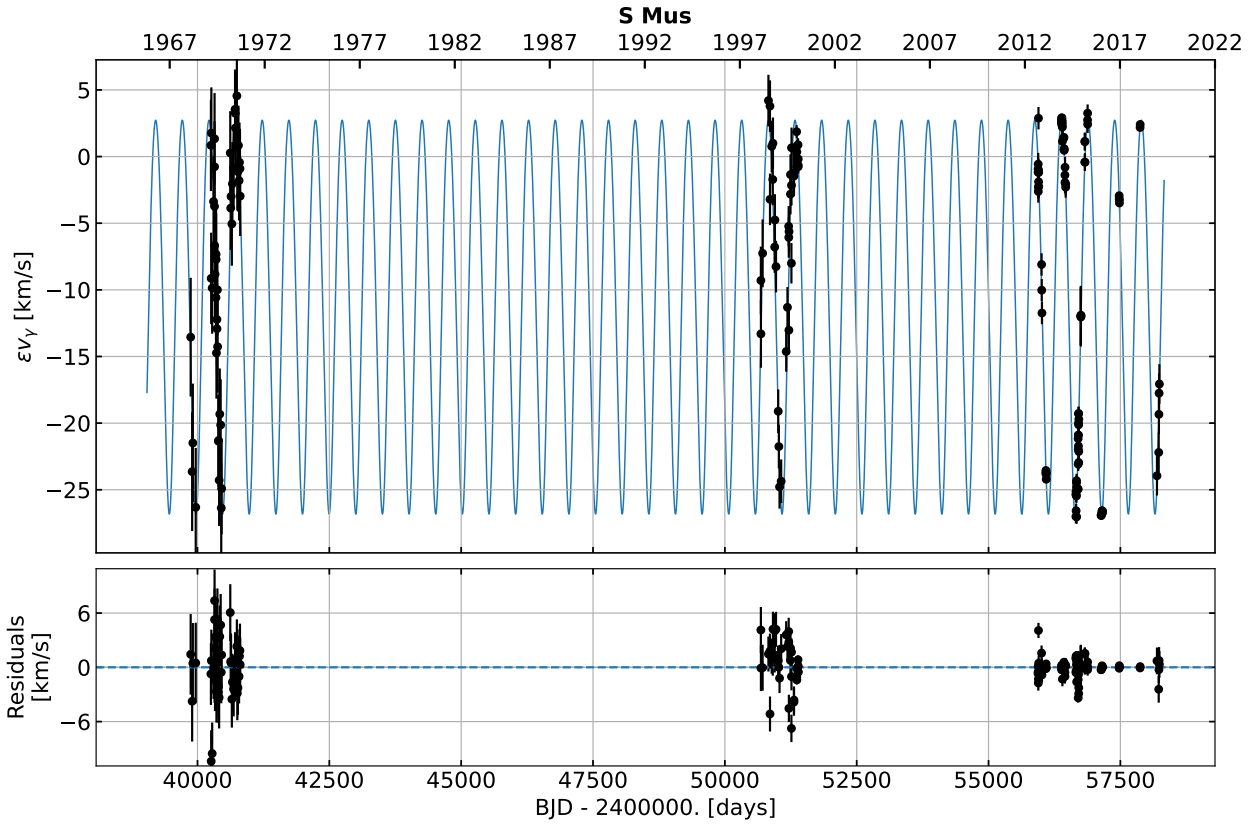


Fig. C.9: V_γ residuals Orbit fitting for S Mus.

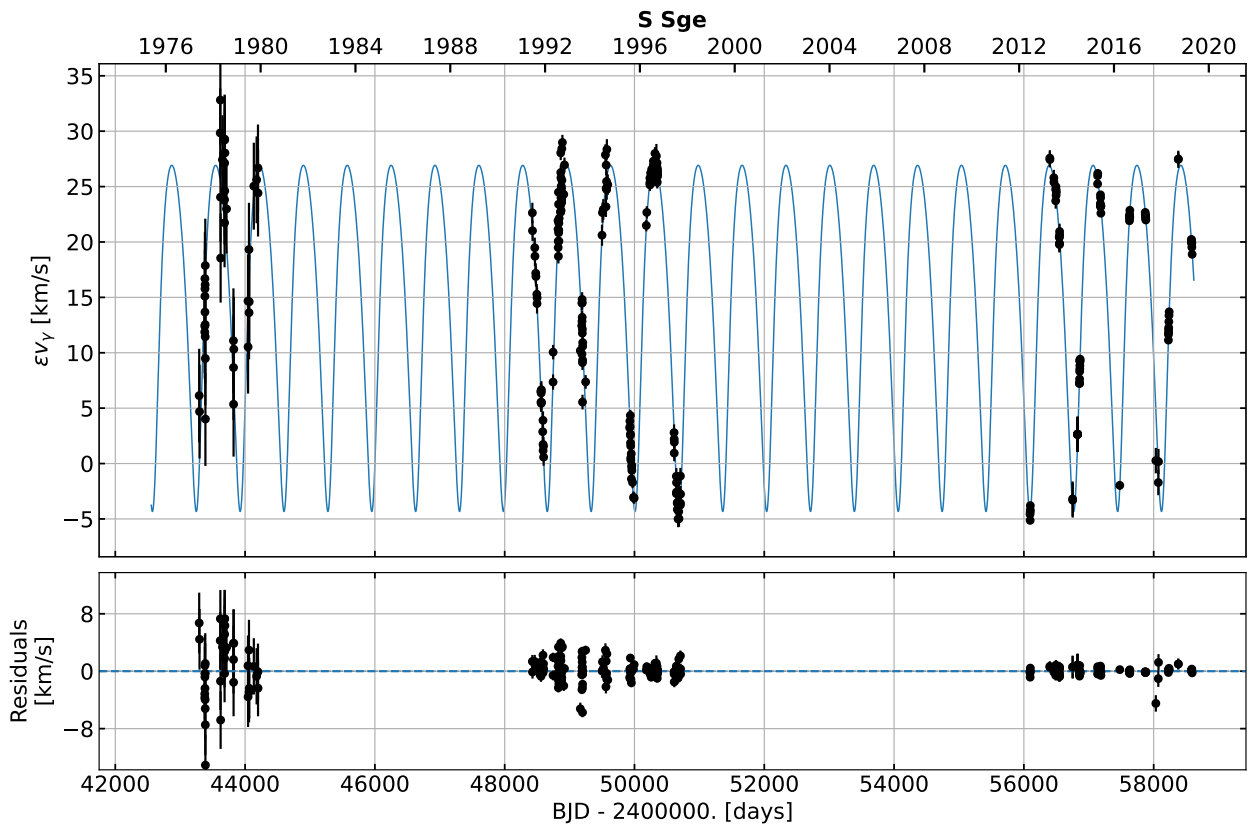


Fig. C.10: V_γ residuals Orbit fitting for S Sge.

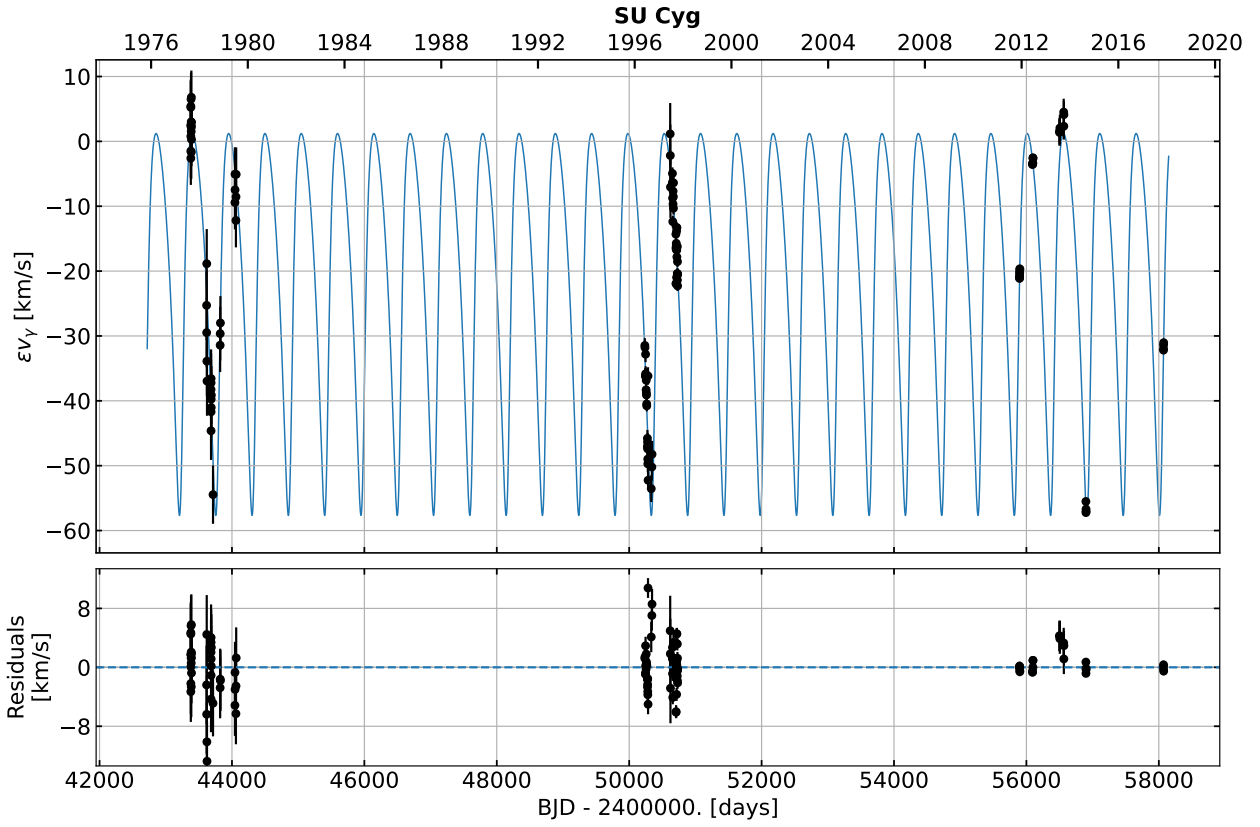


Fig. C.11: V_γ residuals Orbit fitting for SU Cyg.

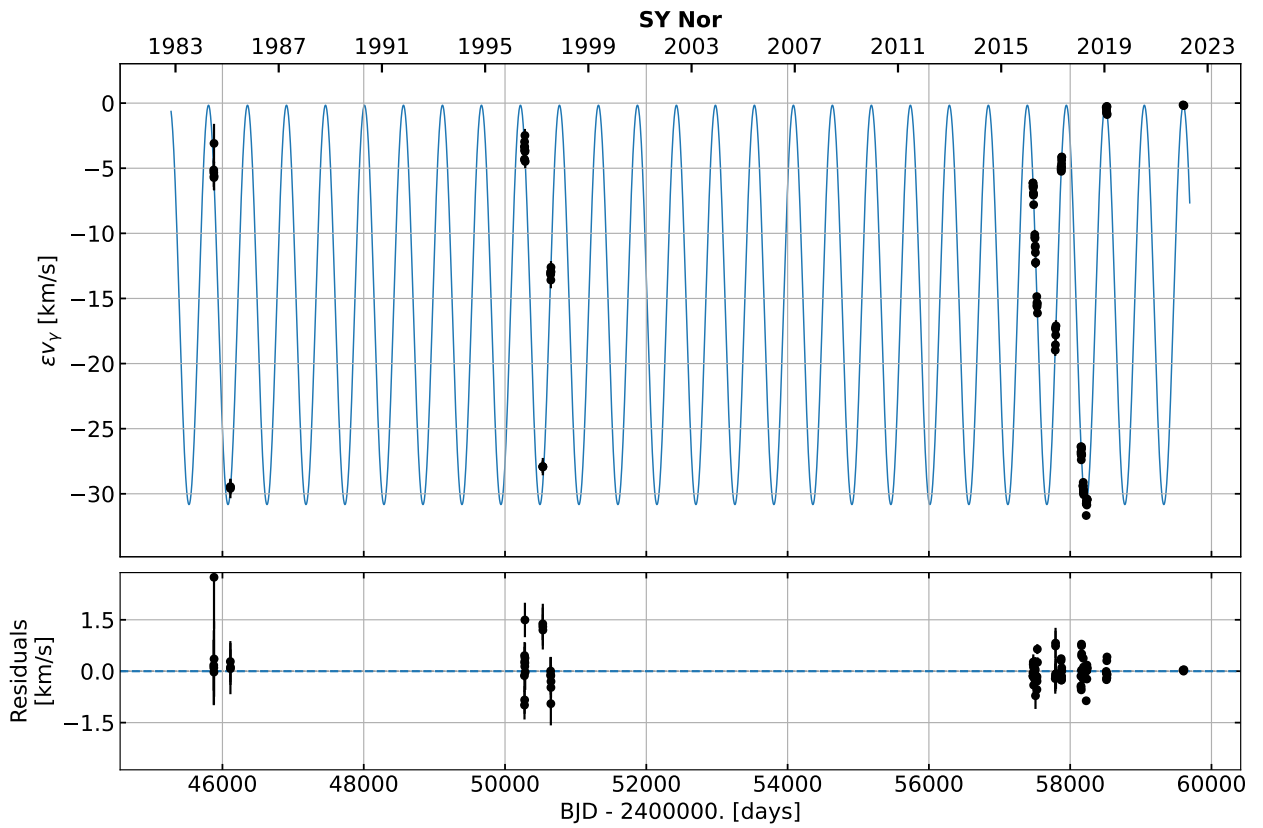


Fig. C.12: V_γ residuals Orbit fitting for SY Nor.

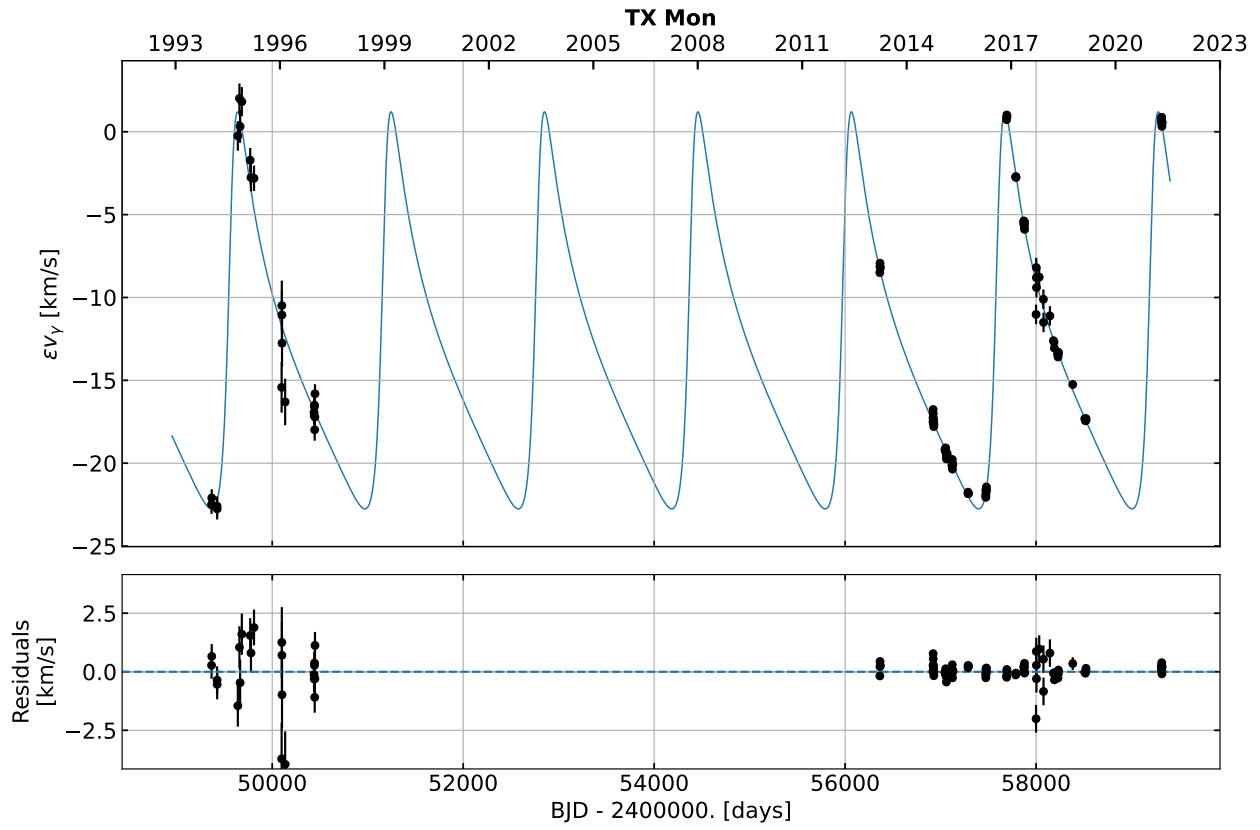


Fig. C.13: V_γ residuals Orbit fitting for TX Mon.

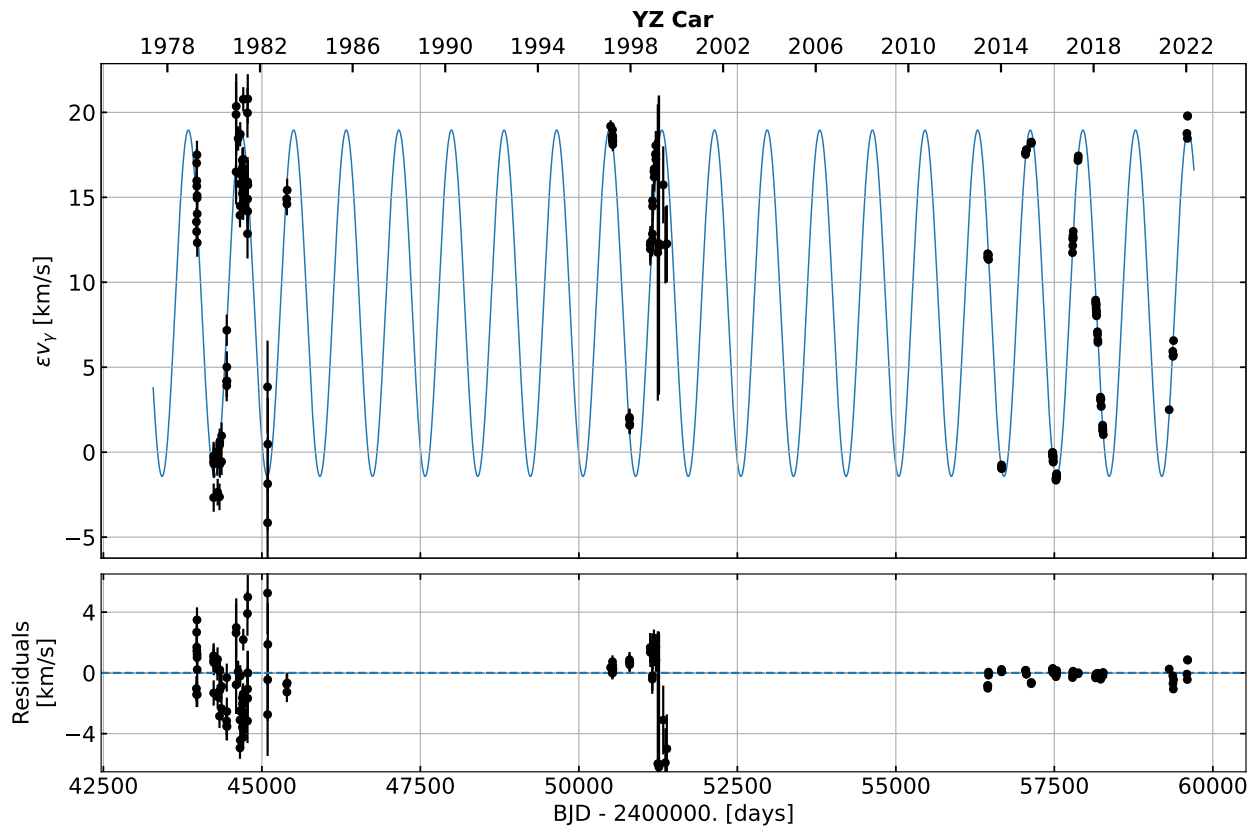


Fig. C.14: V_γ residuals Orbit fitting for YZ Car.

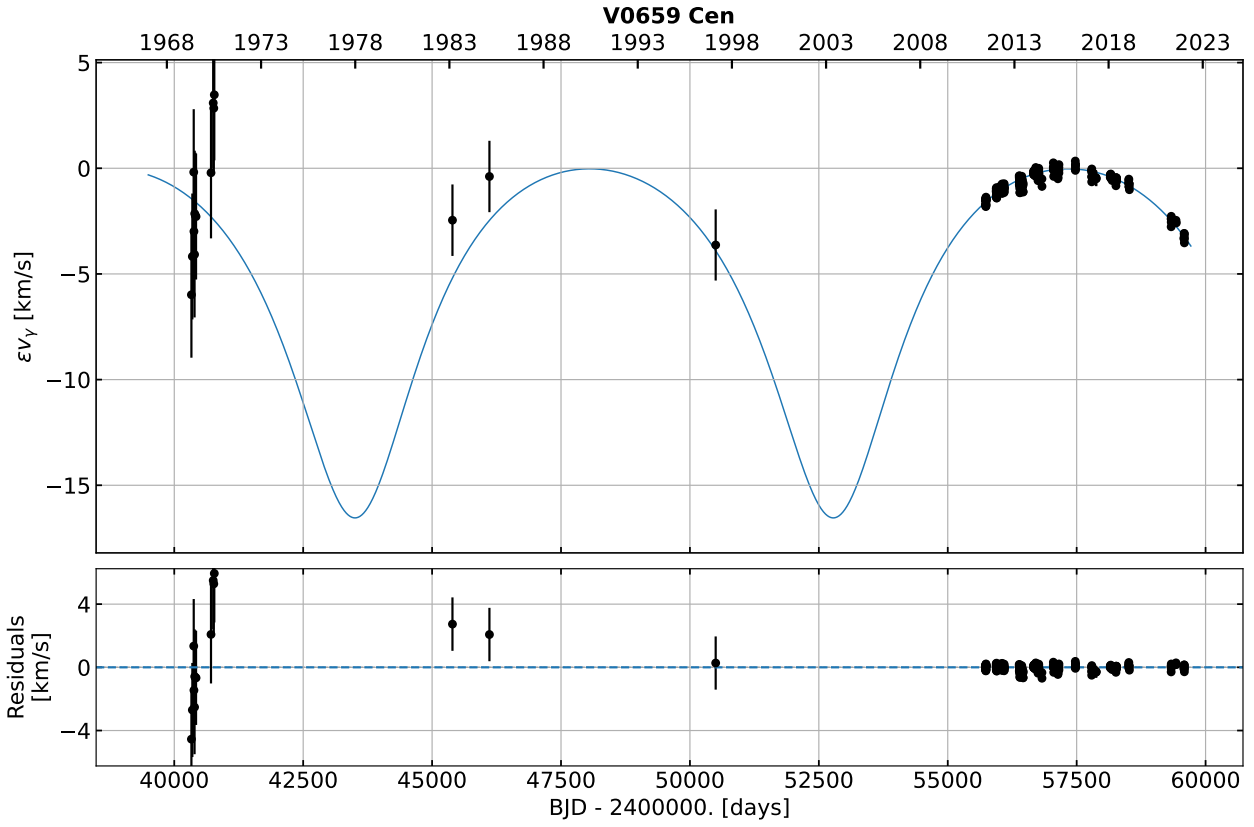


Fig. C.15: V_γ residuals Orbit fitting for V0659 Cen.

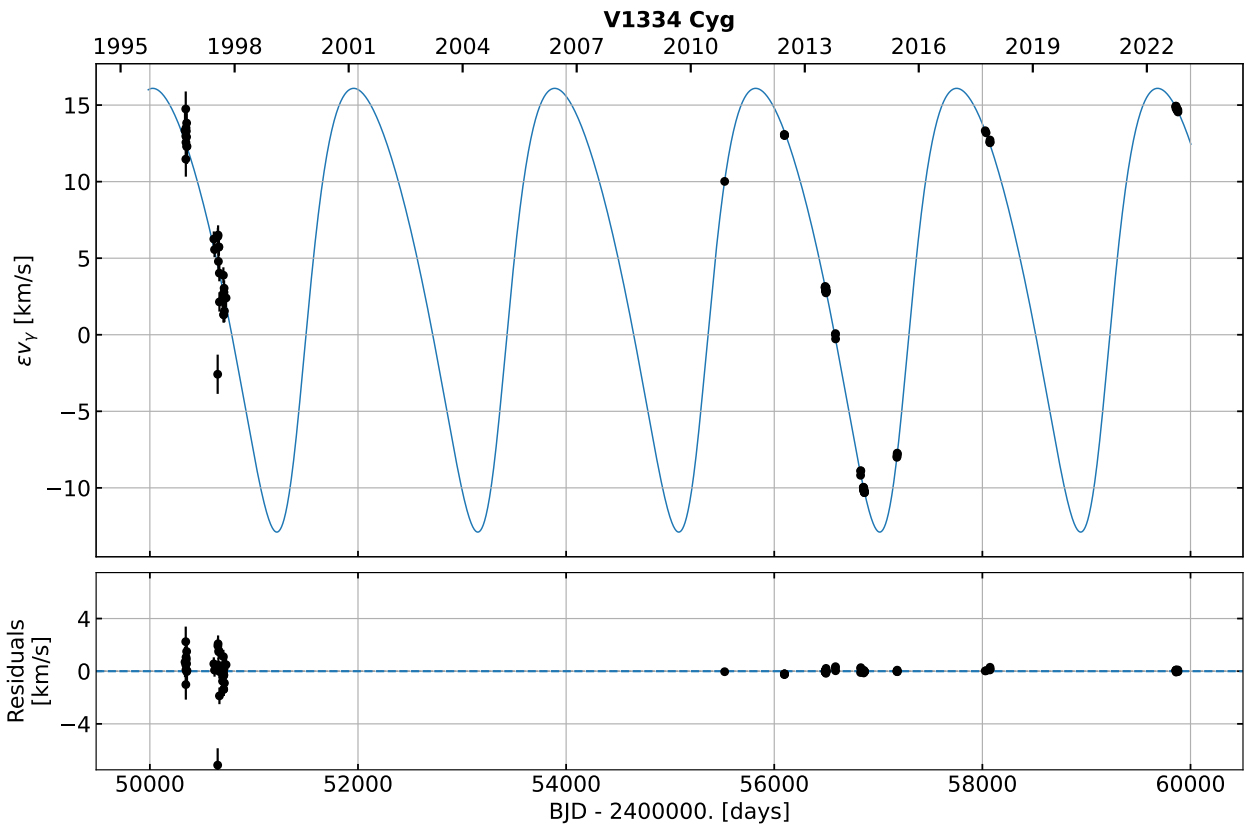


Fig. C.16: V_γ residuals Orbit fitting for V1334 Cyg.

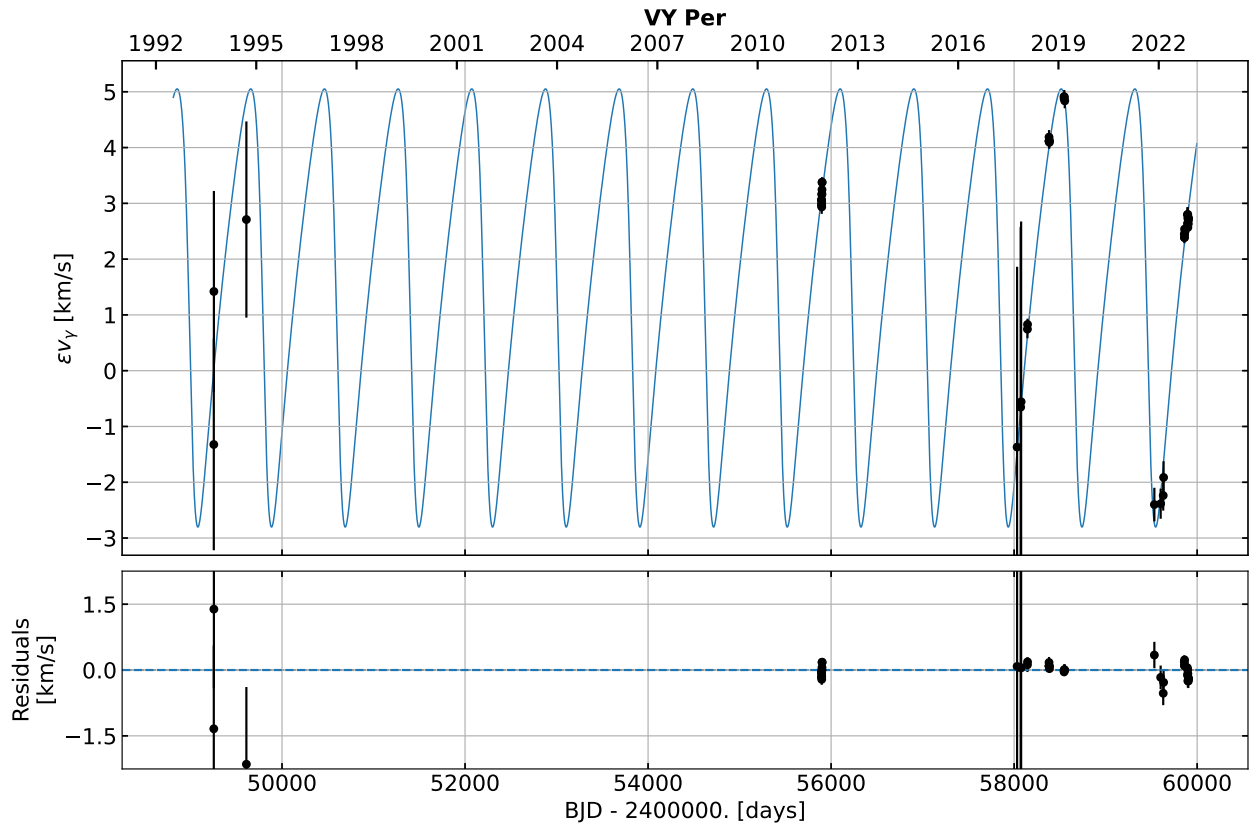


Fig. C.17: V_γ residuals Orbit fitting for VY Per.

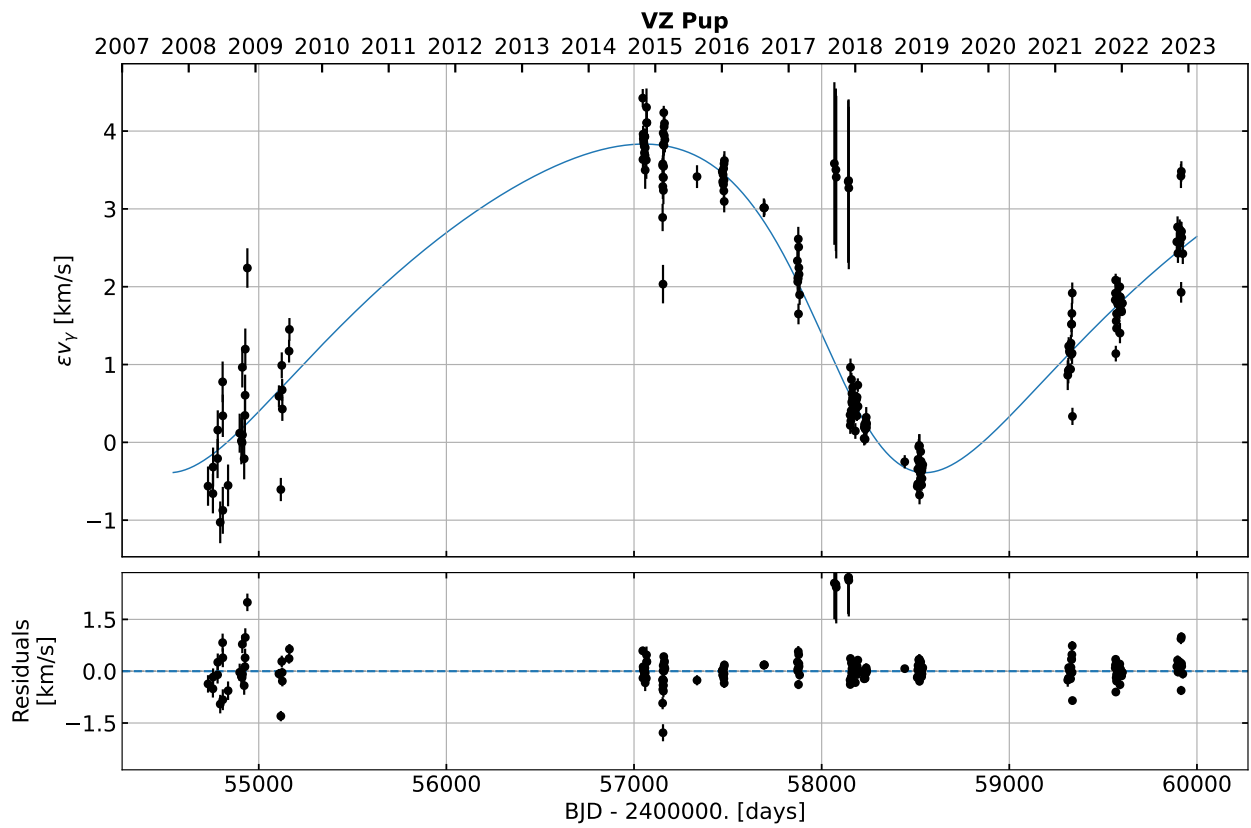
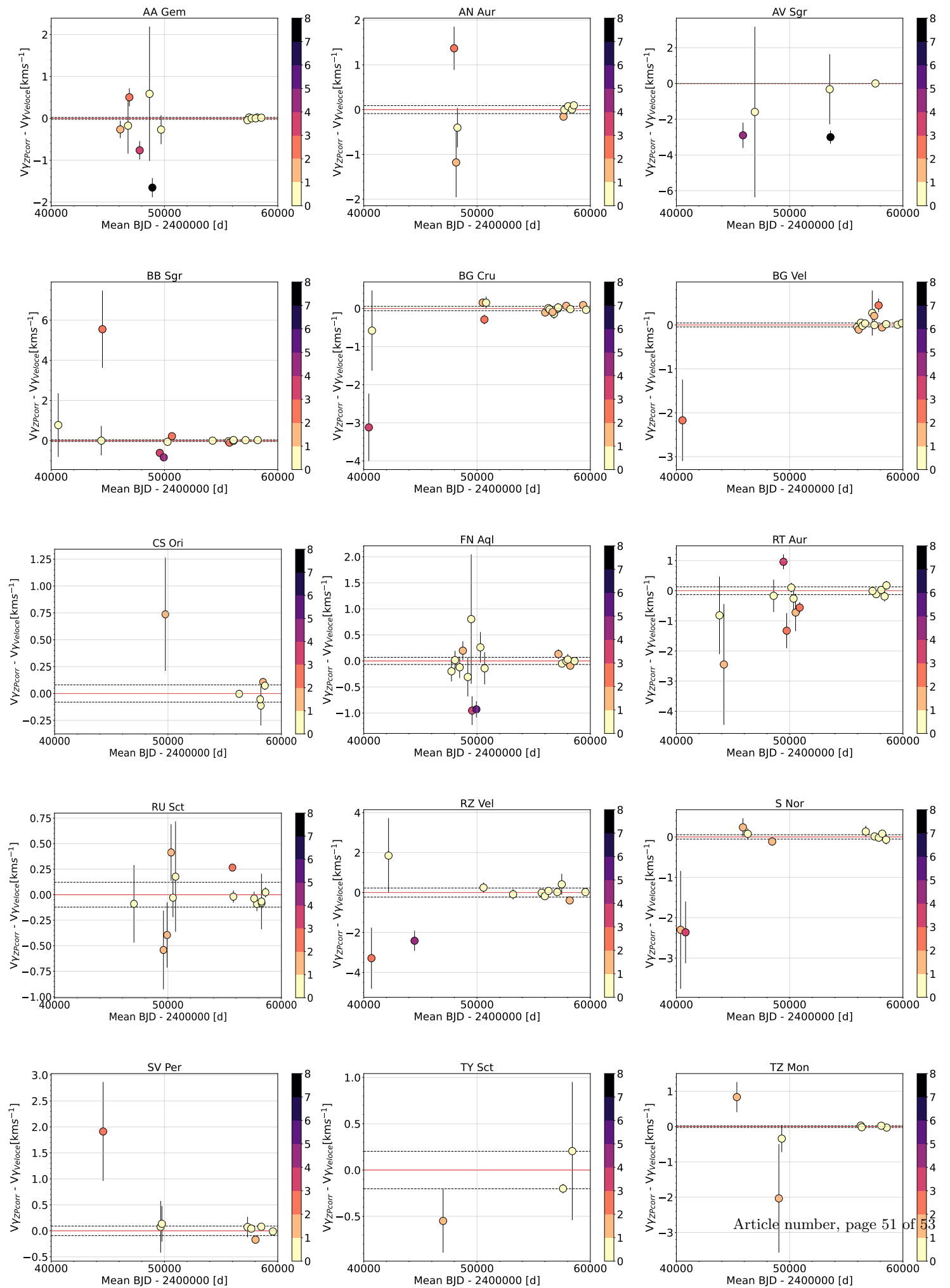


Fig. C.18: V_γ residuals Orbit fitting for VZ Pup.

Table D.1: *Gaia* astrometry and PMA tags for the confirmed SB1 Cepheids within VELOCE. Here, binary flag of ‘1’ means that the star was flagged as binary through PMA, and binary flag of ‘0’ means the PMA did not detect them as binaries.

Star	RUWE	Bin flag from PMA	Star	RUWE	Bin flag from PMA	Star	RUWE	Bin flag from PMA
SB1 with Orbits			SB1 with Trends			SB1 with RVTF-Yes		
ASAS J064540+0330.4			AD Pup	1.3621	0	β Dor	4.5348	0
ASAS J084951-4627.2	1.0863		AH Vel	0.8293	1	η Aql	2.5610	0
ASAS J100814-5856.6	1.1193		AQ Pup	1.1803	0	CD Cyg	1.0070	0
ASAS J174603-3528.1	0.6934		AQ Car	1.0672	0	RS Ori	1.1190	0
AX Cir	7.8052		ASAS J064553+1003.8	1.4999		SS CMa	1.1134	0
BP Cir	1.0495		ASAS J103158-5814.7	0.8688		SZ Aql	0.9400	0
δ Cep	2.7131		ASAS J155847-5341.8	0.8680		SZ Cyg	0.9560	0
DL Cas	1.8830	0	ASAS J174108-2328.5	0.7577		V0340 Ara	0.9316	0
FF Aql	1.0554	1	AW Per	1.1555	1	V0402 Cyg	0.9200	0
FN Vel	1.6964	0	DR Vel	1.0050		V0916 Aql	0.9160	
FO Car	0.9023		FR Car	1.0235	0	VY Sgr	0.8057	
GX Car	1.0176	1	KN Cen	1.0336	0	X Cyg	1.2774	1
IT Car	1.0755	1	LR TrA	0.9513	1			
MU Cep	0.9928		OX Cam	0.9844				
MY Pup	1.0087	0	RY Vel	1.0752	0			
NT Pup	0.9861		RX Aur	0.9821	1			
R Cru	1.1609		RV Sco	0.8048	1			
R Mus	1.0742	1	RW Cam	8.0130	1			
S Mus	4.4948	1	RY Sco	0.7326	0			
S Sge	4.0033	1	SX Vel	1.0222	0			
SU Cyg	3.4429	0	T Mon	1.7239	1			
SY Nor	1.5525	0	UX Per	1.1668	1			
TX Mon	1.6886	1	UZ Sct	0.9132				
U Vul	2.8825	1	V0391 Nor	0.8320				
V0407 Cas	0.8948		V0492 Cyg	0.9966				
V0659 Cen	2.9896	1	V0827 Cas	1.1600				
V1334 Cyg	2.7684	1	V1162 Aql	0.9524	0			
VY Per	1.1544		V1803 Aql	0.9415				
VZ Pup	1.2366	0	V2475 Cyg	0.9943				
W Sgr	3.9524	0	XZ Car	1.0491	0			
XX Cen	1.2385	0						
YZ Car	1.1658	0						
Z Lac	1.0548	0						



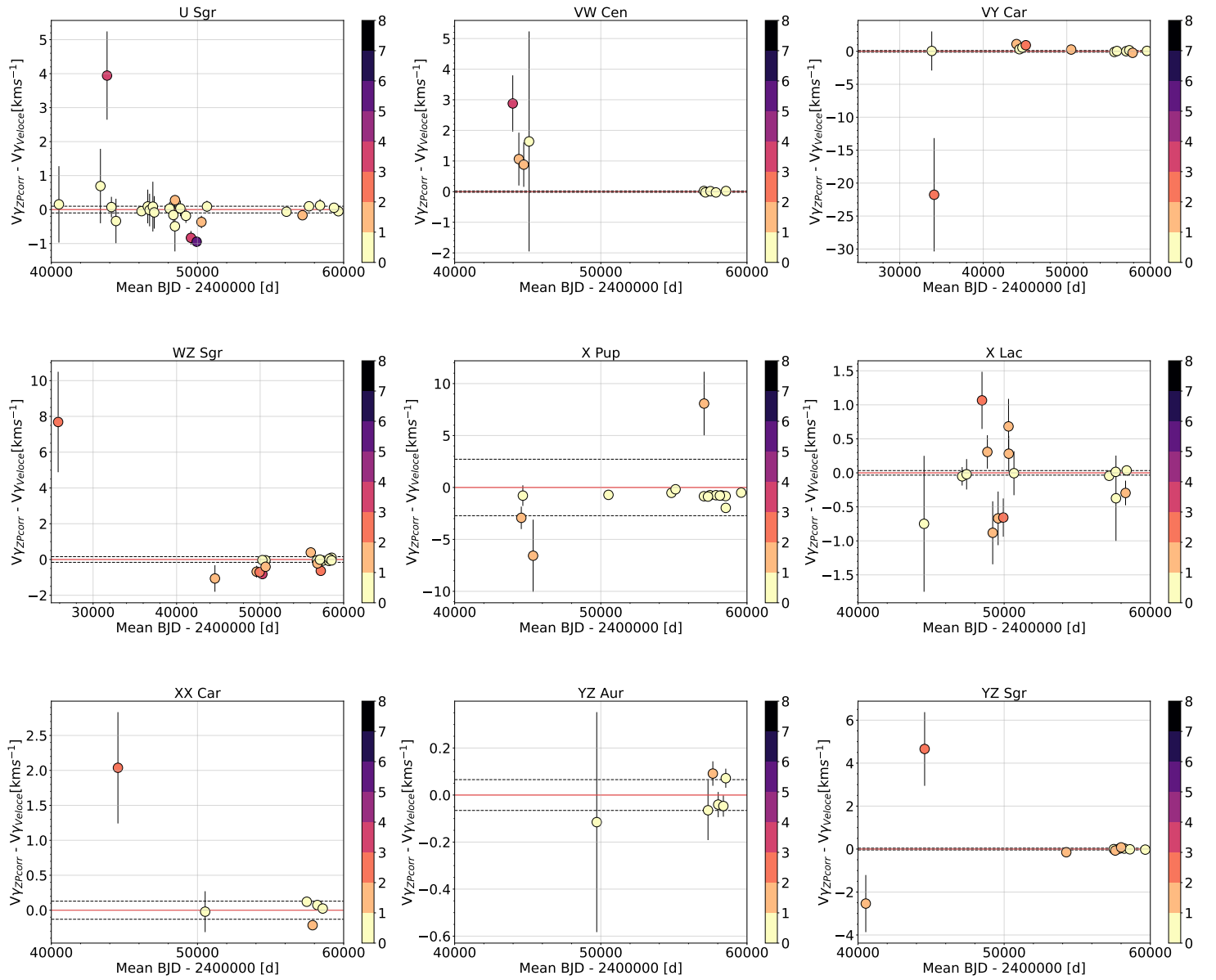


Fig. E.1: Same as Figure 8 for stars within VELOCE with no signs of SB1 from their v_γ RVTF analysis.

Table F.1: RV data used for the ‘V+L’ orbit estimation of SU Cyg.

Reference	BJD (d)	ϵv_γ (km s^{-1})	$\sigma \epsilon v_\gamma$ (km s^{-1})	Reference	BJD (d)	ϵv_γ (km s^{-1})	$\sigma \epsilon v_\gamma$ (km s^{-1})	Reference	BJD (d)	ϵv_γ (km s^{-1})	$\sigma \epsilon v_\gamma$
Ba87	43 616.98	-25.28	5.34	Bo19	56 566.33	4.12	2.06	Go92	50 705.31	-14.31	0.74
Ba87	43 617.98	-29.49	5.34	Bo19	56 898.52	-55.52	0.39	Go92	50 707.32	-16.54	0.81
Ba87	43 618.97	-18.86	5.34	Bo19	56 899.57	-57.23	0.39	Go92	50 708.35	-21.89	0.88
Ba87	43 620.99	-33.88	5.34	Bo19	56 900.44	-56.70	0.39	Go92	50 708.35	-21.97	0.79
Ba87	43 622.96	-36.96	5.34	Bo19	56 901.57	-57.04	0.39	Go92	50 709.29	-16.26	0.76
Ba87	43 683.86	-44.62	4.50	Go92	50 236.43	-31.47	1.11	Go92	50 711.25	-15.71	0.78
Ba87	43 683.86	-38.26	4.50	Go92	50 238.40	-31.79	1.11	Go92	50 713.28	-16.36	0.75
Ba87	43 684.84	-41.70	4.50	Go92	50 245.48	-36.12	1.15	Go92	50 714.38	-16.70	0.77
Ba87	43 684.84	-36.56	4.50	Go92	50 246.51	-36.22	1.20	Go92	50 715.25	-13.86	0.81
Ba87	43 684.85	-37.22	4.50	Go92	50 247.50	-32.82	1.22	Go92	50 716.29	-20.98	0.87
Ba87	43 685.77	-39.75	4.50	Go92	50 248.47	-35.83	1.16	Go92	50 718.27	-16.77	0.77
Ba87	43 686.81	-41.03	4.50	Go92	50 255.42	-38.30	0.78	Go92	50 719.24	-13.29	0.80
Ba87	43 688.84	-39.13	4.50	Go92	50 257.46	-36.84	0.79	Go92	50 719.25	-13.31	0.75
Ba87	43 713.94	-54.46	4.50	Go92	50 259.41	-38.76	0.76	Go92	50 720.34	-17.83	0.81
Ba87	43 821.58	-31.42	4.14	Go92	50 261.41	-39.11	0.80	Go92	50 726.33	-20.37	0.81
Ba87	43 822.57	-29.65	4.14	Go92	50 264.48	-40.48	0.78	Go92	50 727.29	-16.22	0.87
Ba87	43 825.67	-28.00	4.14	Go92	50 265.41	-40.77	0.86	Go92	50 728.33	-21.40	0.80
Ba87	44 044.87	-9.43	4.15	Go92	50 275.46	-45.78	1.29	Go92	50 729.31	-18.55	0.85
Ba87	44 045.89	-5.06	4.15	Go92	50 276.43	-47.12	1.27	Go92	50 730.30	-20.42	0.82
Ba87	44 046.88	-7.48	4.15	Go92	50 277.41	-46.35	1.39	Go92	50 731.25	-22.28	0.79
Ba87	44 059.87	-12.19	4.15	Go92	50 278.42	-47.40	1.30	Go92	50 732.23	-20.55	0.83
Ba87	44 060.89	-8.55	4.15	Go92	50 279.44	-46.92	1.29	Hermes	55 896.32	-21.12	0.60
Ba87	44 063.89	-5.09	4.15	Go92	50 280.41	-48.98	1.33	Hermes	55 896.32	-21.06	0.60
W89	43 378.67	5.42	4.11	Go92	50 281.38	-49.72	1.31	Hermes	55 897.32	-20.75	0.59
W89	43 378.68	-2.60	4.11	Go92	50 284.42	-36.17	1.35	Hermes	55 897.32	-20.72	0.59
W89	43 378.76	-1.49	4.11	Go92	50 285.37	-52.24	1.35	Hermes	55 898.32	-20.20	0.59
W89	43 378.76	2.46	4.11	Go92	50 333.33	-53.54	2.07	Hermes	55 898.32	-20.22	0.59
W89	43 378.82	5.24	4.11	Go92	50 342.26	-50.21	2.05	Hermes	55 900.35	-19.65	0.60
W89	43 378.83	0.78	4.11	Go92	50 345.30	-48.24	2.06	Hermes	55 900.36	-19.76	0.60
W89	43 381.86	2.54	4.11	Go92	50 619.49	1.15	4.76	Hermes	56 091.50	-3.43	0.20
W89	43 381.86	6.49	4.11	Go92	50 621.52	-2.18	4.76	Hermes	56 092.57	-3.58	0.24
W89	43 384.67	3.01	4.11	Go92	50 623.49	-7.05	4.76	Hermes	56 093.48	-3.50	0.22
W89	43 384.67	2.18	4.11	Go92	50 652.37	-6.34	0.95	Hermes	56 097.61	-3.36	0.22
W89	43 384.82	2.26	4.11	Go92	50 653.49	-4.95	0.93	Hermes	56 098.61	-2.52	0.24
W89	43 384.83	1.53	4.11	Go92	50 655.42	-8.75	0.93	Hermes	56 099.60	-2.63	0.25
W89	43 385.65	-1.67	4.11	Go92	50 658.47	-12.37	0.93	Hermes	58 070.37	-32.19	0.54
W89	43 386.65	6.80	4.11	Go92	50 662.39	-9.66	0.98	Hermes	58 071.37	-32.02	0.57
W89	43 387.66	2.96	4.11	Go92	50 663.44	-7.67	0.98	Hermes	58 071.38	-31.40	0.55
W89	43 388.63	0.29	4.11	Go92	50 667.47	-8.53	0.89	Hermes	58 073.34	-31.03	0.55
Bo19	56 500.52	1.37	2.06	Go92	50 668.48	-10.31	0.97				
Bo19	56 501.57	1.52	2.06	Go92	50 669.46	-6.40	0.97				
Bo19	56 504.60	1.61	2.06								
Bo19	56 505.51	2.06	2.06								
Bo19	56 563.32	4.52	2.06								
Bo19	56 565.43	2.33	2.06								

Notes. The column labeled ‘Reference’ lists the sources of various RV datasets, with corresponding abbreviations as follows: , Ba87 for Barnes et al. (1987), W89 for Wilson et al. (1989), Bo19 for Borgniet et al. (2019), Go92 for Gorynya et al. (1992). In column 2 is the Barycentric Julian Date (BJD) of the observation, in column 3 is the residuals between the measurement and the VELOCE template (ϵv_γ) after applying the zero-point offset (shifted according to the phase shift of the epoch) v_γ residuals. Finally, in column 4 we present the uncertainty on the zero-point corrected ϵv_γ .